Mechanistic study of electron transfer at the oil/water interface

堀田，弘樹

(Degree)
博士（理学）

(Date of Degree)
2003-09-30

(Date of Publication)
2008-06-23

(Resource Type)
doctoral thesis

(Report Number)
甲2911

(URL)
https://hdl.handle.net/20.500.14094/D1002911

博士論文

Mechanistic Study of Electron Transfer at the Oil/Water Interface

油水界面電子移動の反応機構に関する研究

平成 15 年 8 月

神戸大学大学院自然科学研究科

堀田　弘樹

Table of Contents

Chapter 1. Introduction

1.1 Overview

The study of electron transfer (ET) at the polarized oil (O)/water (W) (or liquid/liquid) interface is useful for understanding not only certain catalytic reactions in two-phase systems (e.g., liquid membranes, microemulsions, micelles, etc.) but also energy conversion processes occurring at biomembranes (e.g., respiratory chain, photosynthesis, etc.). In 1979, Samec et al. [1,2] reported, as the first example, an ET between ferrocene (Fc) in nitrobenzene (NB) and $Fe(CN)_6^{3-}$ in W:

$$Fc\ (NB) + Fe(CN)_6^{3-}\ (W) \rightleftharpoons Fc^+\ (NB) + Fe(CN)_6^{4-}\ (W) \qquad (1.1)$$

A well-defined voltammetric wave with positive- and negative-current peaks due to the forward and backward ET processes was observed. However, the possibility was suggested [3] that the reaction mechanism for this ET system is not simple, but involves ion transfer (IT) of the product, i.e., Fc^+, as follows

$$Fc\ (NB) \rightleftharpoons Fc\ (W) \qquad (1.2a)$$

$$Fc\ (W) + Fe(CN)_6^{3-}\ (W) \rightleftharpoons Fc^+\ (W) + Fe(CN)_6^{4-}\ (W) \qquad (1.2b)$$

$$Fc^+\ (W) \rightleftharpoons Fc^+\ (NB). \qquad (1.2c)$$

In this so-called ion transfer (IT) mechanism, the ET (1.2b) takes place in homogeneous media (i.e., in W), and the IT (1.2c) is responsible for the current flowing through the interface. However, if all equilibria are quite mobile, the IT mechanism is not distinguishable from that described as a single-step ET (1.1).

In 1988, Schiffrin's group [4] claimed that the use of lutetium biphthalocyanine ($LuPc_2$) complex more hydrophobic than Fc enabled observation and investigation of a "true", or, heterogeneous ET across the O/W interface. A series of subsequent papers reported ET systems by other hydrophobic metal complexes including tin diphthalocyanine [5], iron and ruthenium metalloporphyrin complexes with pyridine [6], and Fc derivatives [7]. These experimental studies then stimulated theoretical studies on the ET kinetics by some researchers [8–16].

On the other hand, Kihara's group reported interesting ET systems for biological molecules including L-ascorbic acid [17], flavin mononucleotide (FMN) [18], and β-nicotinamide adenine dinucleotide (NADH) [19]. While these ET systems are very important from a biological viewpoint, their reaction mechanisms are often complicated by the coupling of ET and proton or ion transfer.

A recent introduction of Scanning Electrochemical Microscopy (SECM) to this field [20–27] has revitalized the study of ET at the O/W interface. In contrast to the conventional, four-electrode cyclic voltammetry at externally polarized O/W interfaces, the SECM measurements not necessarily require supporting electrolytes, and thus can be carried out over a wide range of driving forces without the limitation of the potential

window. It should also be noted that in ordinary SECM measurements, all electrodes are in a single phase, so that it is possible to avoid the problems of *IR* drop and charging current. These advantages of SECM allowed for an experimental verification of the Marcus theory [8–12] in the driving-force dependence of the ET rate constant [22,25].

As another application of microtechnology, a microelectrochemical technique by laser trapping of a single oil droplet was developed by Nakatani et al. [28–30].

Recently, novel interesting ET systems including metal nanoparticles [31,32] and redox enzymes [33,34] have been developed. These ET systems seem important from technological and biological viewpoints. Fundamental studies, as performed in this thesis, are expected to provide guidelines for design of such practically useful ET systems.

1.2 Electron transfer at the polarizable oil/water interfaces

1.2.1 Principles

Let us consider an ET reaction between a hydrophilic redox couple (O1/R1) in the W phase and a hydrophobic redox couple (O2/R2) in the O phase:

$$\mathrm{R2\ (O) + O1\ (W) \rightleftharpoons O2\ (O) + R1\ (W)} \tag{1.3}$$

in which n electrons are involved. If this ET system is in equilibrium, the Galvani potential difference ($\Delta_{\mathrm{O}}^{\mathrm{W}}\phi$) of the O/W interface is given by the Nernst equation:

$$\Delta_{\mathrm{O}}^{\mathrm{W}}\phi = \Delta_{\mathrm{O}}^{\mathrm{W}}\phi_{\mathrm{ET}}^{\circ'} + \frac{RT}{nF}\ln\left(\frac{[\mathrm{R1}]_{\mathrm{W}}[\mathrm{O2}]_{\mathrm{O}}}{[\mathrm{O1}]_{\mathrm{W}}[\mathrm{R2}]_{\mathrm{O}}}\right) \tag{1.4}$$

where the brackets [ ]$_{\mathrm{W}}$ and [ ]$_{\mathrm{O}}$ stand for the equilibrium concentrations of redox species in the W and O phases, respectively; R, T, and F have their usual meanings; and $\Delta_{\mathrm{O}}^{\mathrm{W}}\phi_{\mathrm{ET}}^{\circ'}$ is the formal potential which is determined by

$$\Delta_{\mathrm{O}}^{\mathrm{W}}\phi_{\mathrm{ET}}^{\circ'} = \Delta_{\mathrm{O}}^{\mathrm{W}}\phi_{\mathrm{ET}}^{\circ} + \frac{RT}{nF}\ln\left(\frac{\gamma_{\mathrm{R1}}^{\mathrm{W}}\gamma_{\mathrm{O2}}^{\mathrm{O}}}{\gamma_{\mathrm{O1}}^{\mathrm{W}}\gamma_{\mathrm{R2}}^{\mathrm{O}}}\right) \tag{1.5}$$

Here, γ represents the activity coefficient of a redox species in the indicated phase, and $\Delta_{\mathrm{O}}^{\mathrm{W}}\phi_{\mathrm{ET}}^{\circ}$ is the standard redox potential for the ET system, being given by the difference between the standard potentials of the respective redox couples which are expressed on a same potential scale:

$$\Delta_{\mathrm{O}}^{\mathrm{W}}\phi_{\mathrm{ET}}^{\circ} = E_{\mathrm{O2/R2}}^{\circ} - E_{\mathrm{O1/R1}}^{\circ}\ . \tag{1.6}$$

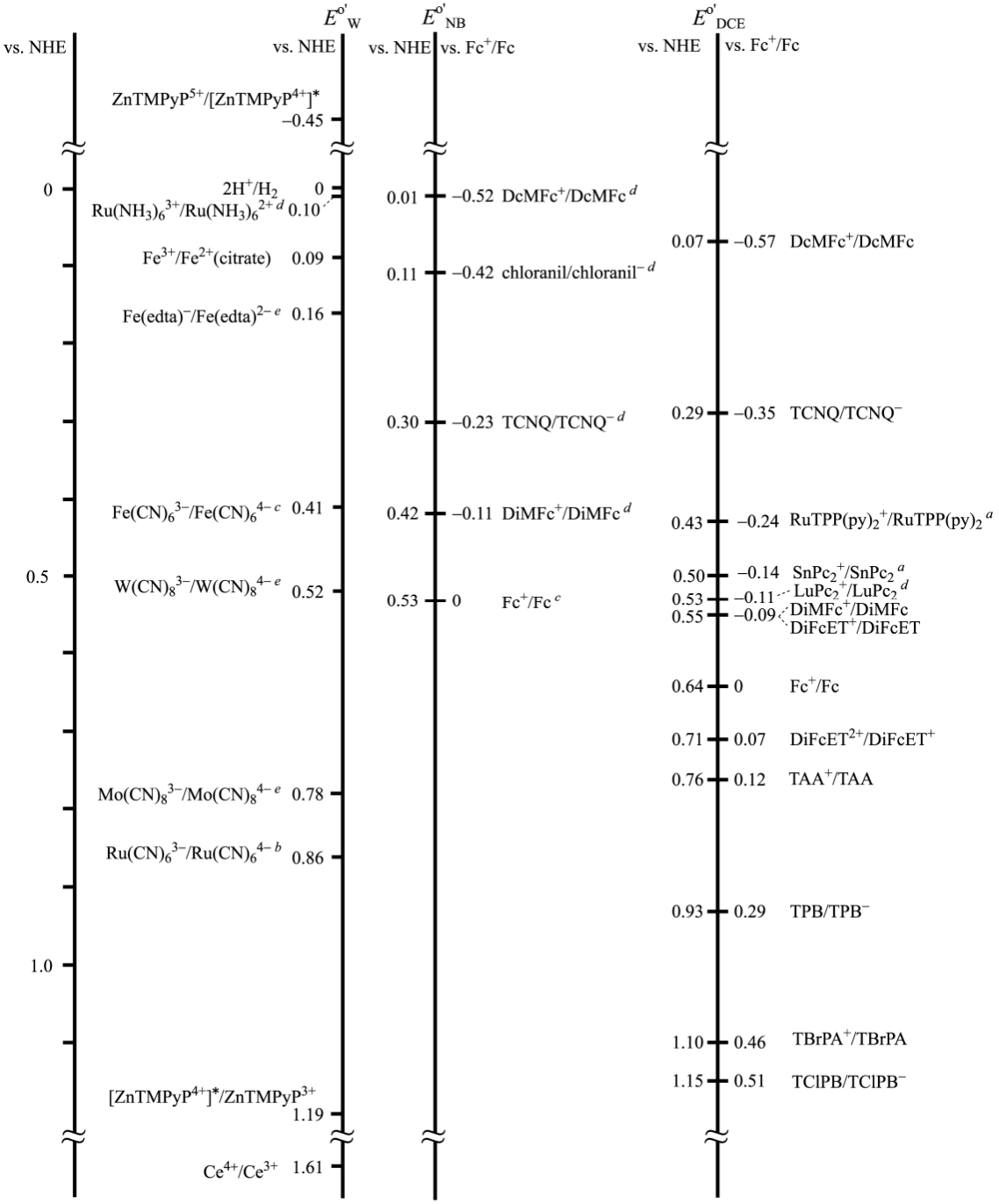

Figure 1.1. Formal potentials of redox species in W, NB, and DCE versus NHE [35]. Abbreviations: ZnTMPyP = zinc tetra-*N*-methyl-4-pyridium porphyrin, DcMFc = deca-methylferrocene, TCNQ = 7,7,8,8-tetracyanoquinodimethane, DiMFc = dimethylferrocene, Fc = ferrocene, $RuTPP(py)_2$ = bis(pyridine) *meso*-tetraphenylporphyrinato ruthenium(II), $SnPc_2$ = tin(IV) diphthalocyanine, $LuPc_2$ = lutetium(III) diphthalocyanine, DiFcET = diferrocenylethane, TAA = tris(4-methoxyphenyl)amine, TPB = tetraphenylborate, TBrPA = tris(4-bromo-phenyl)amine, TClPB = tetrakis(4-chlorophenyl)borate. The data is from Ref. 36, except where otherwise noted: [a] Ref. 6, [b] Ref. 37, [c] Ref. 38, [d] Ref. 39, [e] Ref. 40.

If we choose a proper set of redox couples whose $\Delta_O^W\phi_{ET}^\circ$ lies within the potential window, we can observe the voltammetric wave due to the ET shown in equation (1.3). Figure 1.1 shows the formal potentials, $E^{\circ\prime}$ ($\approx E^\circ$), of various redox species in W, NB, and DCE versus normal hydrogen electrode (NHE) [35].

The ET reaction at the polarizable O/W interface thus described is formally similar to that at a metal electrode surface. This allows us to employ usual electrochemical techniques including cyclic voltammetry (CV), polarography, and a.c. impedance method for the study of ET at O/W interfaces.

1.2.2 Voltammetric behavior

Now let us assume that the redox couple in one phase (e.g., O1, R1 in W) exists in excess. In this case, the interfacial concentrations of O1 and R1 are kept constant even if the ET reaction proceeds. Then, the Nernst equation (1.4), which is valid for reversible ET systems, is reduced to $\Delta_O^W\phi = const. + (RT/nF)\ln([O2]_O/[R2]_O)$. This expression is the same as that for a typical electrode reaction. Thus, the W phase containing O1 and R1 in excess may be regarded as a metal electrode, and the ET reaction is limited by the diffusion of O2 (or R2) in O from the bulk to the interface. The reversible cyclic voltammogram obtained under these conditions has a peak separation of (59/*n*) mV (at 25 °C) in the same manner as that obtained for a typical electrode reaction. Unless one of the redox couples exists in excess, however, the shape of a reversible wave in CV is changed by relative concentrations of the redox species, as claimed by Girault et al. [41]. Figure 1.2 represents reversible cyclic voltammograms (with n = 1) calculated for various concentration conditions. Panel (A) shows the case where the concentration of the redox couple in W is changed (where $[O1]_W = [R1]_W$ is assumed) at constant concentrations of the redox couple in O (i.e., $[O2]_O$ = 0 mM; $[R2]_O$ = 1 mM). When $[O1]_W$, and $[R1]_W$ are high enough (i.e., 100 mM), the peak separation is 59 mV as described above. However, it should be noted that the peak separation becomes larger with decreasing $[O1]_W$, and $[R1]_W$. Thus, for the ET at the O/W interface, the peak separation of a reversible wave is not necessarily (59/*n*) mV. Panel (B) in Figure 1.2 shows the case where $[R2]_O$ is changed at $[O1]_W = [R1]_W$ = 1 mM and $[O2]_O$ = 0 mM. The decrease of $[R2]_O$ from 100 mM to 1 mM leads to a shift of the midpoint potential from 71 mV to 101 mV. Thus, for the ET at the O/W interface, the midpoint potential does not necessarily coincide with the value of $\Delta_O^W\phi_{ET}^{\circ\prime}$, being generally influenced by the concentration conditions for redox species.

1.3 Marcus theory

In the early 1990s, Marcus [8–12] presented a general equation for the second-order rate constant of a heterogeneous ET at the "sharp" O/W interface:

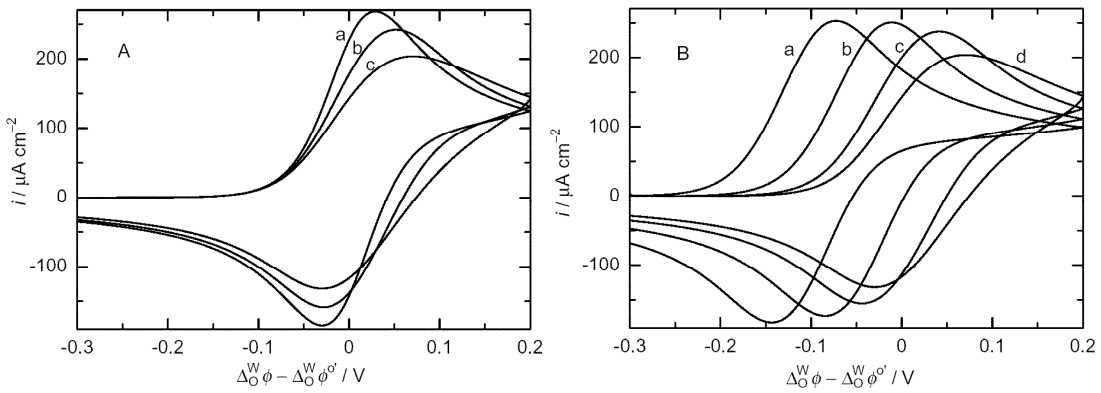

Figure 1.2. Reversible cyclic voltammograms of ET at the O/W interface under various concentration conditions [35]. (A): $[O1]_W = [R1]_W$ = (a) 100, (b) 2, (c) 1 mM; $[O2]_O$ = 0 mM; $[R2]_O$ = 1 mM. (B): $[O1]_W = [R1]_W$ = 1 mM; $[O2]_O$ = 0 mM; $[R2]_O$ = (a) 100, (b) 10, (c) 2, (d) 1 mM. The diffusion coefficients of all redox species are 1×10^{-5} cm^2 s^{-1}. Sweep rate: 0.1 V s^{-1}.

$$k = Z \exp\left(\frac{-\Delta G^{\ddagger}}{RT}\right) \tag{1.7}$$

where Z is the pre-exponential frequency factor, and $\Delta G^{\ddagger}$ is the standard Gibbs energy of the activation of the reaction, which is related to the standard Gibbs energy of ET ($\Delta G°$) with

$$\Delta G^{\ddagger} = w^{r} + \frac{\pi}{4}\left(1 + \frac{\Delta G° + w^{p} - w^{r}}{\lambda}\right)^2 . \tag{1.8}$$

Here, w^r and w^p are the work terms for bringing the reactants from d (the distance between two reactants) = ∞ and for removing the products to d = ∞, respectively. These work terms can be estimated based on a dielectric continuum model, from the size and charge of redox species, dielectric constants of solvents, and locations of the redox species. λ is given by the sum of the reorganization energy of "outer sphere", i.e., the solvents (λ_o) and that of "inner sphere", i.e., the intramolecular ligands (λ_i). The value of λ_i can be obtained experimentally from the normal vibrational analysis, whereas the value of λ_o can be estimated theoretically as the electrostatic energy, in a similar manner to the work terms. For the equations to calculate w^r, w^p, and λ_o, see the original papers by Marcus [8–12].

Marcus proposed that the frequency factor Z for a sharp O/W interface is given by

$$Z = 2\pi(r_A + r_B)\kappa\nu(\Delta R)^3 \tag{1.9}$$

where r_A and r_B are the molecular radii of the reactants in O and W, respectively; κ is the transmission coefficient (κ = 1 for a perfect adiabatic ET); ν is the frequency of molecular

motion; and ΔR is the parameter appearing in an exponent for the dependence of the ET rate on separation distance R ($\propto \exp(-R/\Delta R)$). Marcus also estimated the frequency factor for the case in which both reactants are allowed to penetrate the interfacial region in such a way that their centers can effectively reach the liquid boundary:

$$Z \approx \pi(r_A + r_B)^3 \kappa\nu(\Delta R). \tag{1.10}$$

If we assume that $r_A + r_B = 10$ Å and $\Delta R = 1$ Å, it can be estimated that the Z value given by equation (1.10) is approximately two orders of magnitude larger than the Z value given by equation (1.9) for a sharp O/W interface.

In general, the phenomenological Butler–Volmer expression is assumed for the forward (k_f) and backward (k_b) rate constants of the ET reaction shown by equation (1.3):

$$k_f = k^\circ \exp\left[\frac{(1-\alpha)nF}{RT}\left(\Delta_O^W\phi - \Delta_O^W\phi_{ET}^{\circ'}\right)\right] \tag{1.11a}$$

$$k_b = k^\circ \exp\left[-\frac{\alpha nF}{RT}\left(\Delta_O^W\phi - \Delta_O^W\phi_{ET}^{\circ'}\right)\right] \tag{1.11b}$$

where k° is the standard rate constant at $\Delta_O^W\phi = \Delta_O^W\phi_{ET}^{\circ'}$, and α the transfer coefficient. These kinetic parameters can be evaluated based on Marcus theory as described in chapter 5. There have been a few reports on the application of the Marcus theory to interfacial ET systems. Cheng and Schiffrin [42] employed the a.c. impedance technique to determine the rate constants for some ET systems including the $LuPc_2$ (DCE)–$Fe(CN)_6^{3-}$ (W) system, and then claimed that the Marcus theory can be used to predict the rate constants. Recently, Bard's group [22,25] reported that the rate constants k_{12} (= k) for the heterogeneous ETs between $ZnPor^+$ (the oxidized form of 5,10,15,20-tetraphenylporphyrinato zinc(II)) and various aqueous reductants, being determined by means of SECM, showed the driving-force (ΔG°) dependence in accordance with the Marcus theory. Figure 1.3 shows the plot of log k_{12} against $\Delta E_{1/2}$ (= $\Delta_O^W\phi - \Delta_O^W\phi_{ET}^{\circ} = -\Delta G^\circ/nF$) for three O/W systems [25]. It is expected from equations (1.7) and (1.8) that log k_{12} shows a parabolic dependence on $\Delta E_{1/2}$ (or ΔG°), if the work terms can be neglected. It has been claimed that the decrease in k_{12} at higher driving forces is an evidence of the Marcus inverted region. In this analysis, however, the differences in reorganization energy between aqueous redox couples are neglected, though their influences may not be significant. Further experimental verification is desirable.

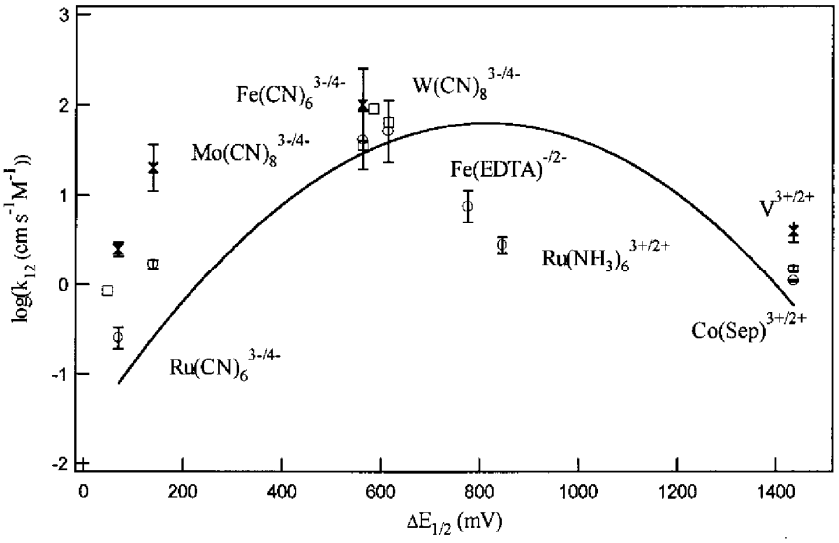

Figure 1.3. Dependence of the bimolecular rate constant, log(k_{12}), on driving force, $\Delta E_{1/2}$, at the BN/water (○), benzene/water (□), and DCE/water (×) interfaces for heterogeneous ET between tip generated organic phase $ZnPor^+$ and aqueous $Ru(CN)_6^{4-}$, $Mo(CN)_8^{4-}$, $Fe(CN)_6^{4-}$, $W(CN)_8^{4-}$, $Fe(EDTA)^{2-}$, $Ru(NH_3)_6^{2+}$, V^{2+}, and $Co(Sep)^{2+}$. The solid line gives the Marcus prediction [8–12]. Data for $Fe(EDTA)^{2-}$ at the BN/W interface are reprinted from Ref. 22. Abbreviations: BN = benzonitrile, DCE = 1,2-dichloroethane, $ZnPor^+$ = Zinc-21H, 23H-tetraphenylporphine, EDTA = ethylendiaminetetraacetic acid, Sep = sepulchrate.

1.4 Objective of this study

In this dissertation, I have introduced some new methodologies in order to clarify the mechanism of ET at O/W interfaces, especially focusing on the discrimination of IT and ET mechanisms.

In chapter 2, a new measurement system in which the O and W phases are separated by an electron conductor (EC; e.g., Pt) has been devised. In this electron conductor separating O/W (ECSOW) system, no IT across the EC phase can be taken place. Therefore, the ECSOW system is useful for discrimination between ET and IT occurring at the O/W interface. In chapter 3, a microflow coulometric cell has been developed, in which complete electrolysis can be accomplished. This microflow cell allows not only for determination of the number of electrons required for a ET reaction (chapter 4) but also spectrophotometric detection of reaction products (chapter 5). In chapter 4, the reaction mechanism of the oxidation of ascorbic acid in W by chloranil added to NB has been studied by means of cyclic voltammetry, polarography, and the above-mentioned new

methods. The results have shown that the ET process can be elucidated in terms of the IT mechanism. In chapter 5, the ET reaction between Fc in NB and $Fe(CN)_6^{3-}$ in W has been clarified as the IT mechanism by means of cyclic voltammetry with a digital simulation analysis. A direct evidence for the production of Fc^+ in the W phase has been given by the spectrophotometric detection with the microflow cell, supporting the validity of the proposed IT mechanism. In the last chapter, a theoretical consideration on the diffusion-controlled rate constant of heterogeneous ET at the O/W interface has been made in the analogy of the Smoluchowski theory [43–45].

References

[1] Z. Samec, V. Marecek, and J. Weber, J. Electroanal. Chem. 96 (1979) 245.

[2] Z. Samec, V. Marecek, and J. Weber, J. Electroanal. Chem. 103 (1979) 11.

[3] J. Hanzlík, Z. Samec, and J. Hovorka, J. Electroanal. Chem. 216 (1987) 303.

[4] G. Geblewicz and D.J. Schiffrin, J. Electroanal. Chem. 244 (1988) 27.

[5] V.J. Cunnane, D.J. Schiffrin, C. Beltran, G. Geblewicz, and T. Solomon, J. Electroanal. Chem. 247 (1988) 203.

[6] Y. Cheng and D.J. Schiffrin, J. Electroanal. Chem. 314 (1991) 153.

[7] V.J. Cunnane, G. Geblewicz, and D.J. Schiffrin, Electrochim. Acta 40 (1995) 3005.

[8] R.A. Marcus, J. Phys. Chem. 94 (1990) 1050.

[9] R.A. Marcus, J. Phys. Chem. 64 (1990) 4152.

[10] R.A. Marcus, J. Phys. Chem. 94 (1990) 7742 (corrections).

[11] R.A. Marcus, J. Phys. Chem. 95 (1991) 2010.

[12] R.A. Marcus, J. Phys. Chem. 99 (1995) 5742 (corrections).

[13] H.H. Girault, J. Electroanal. Chem. 388 (1995) 93.

[14] Y.I. Kharkats and A.M. Kuznetsov, *Liquid-Liquid Interfaces, Theory and Methods,* Ed. A.G. Volkov and D.W. Deamer, CRC Press, Boca Raton, 1996, p. 139.

[15] W. Schmickler, J. Electroanal. Chem. 428 (1997) 123.

[16] I. Benjamin and Y. I. Kharkats, Electrochim. Acta 44 (1998) 133.

[17] M. Suzuki, S. Umetani, M. Matsui, and S. Kihara, J. Electroanal. Chem. 420 (1997) 119.

[18] M. Suzuki, M. Matsui, and S. Kihara, J. Electroanal. Chem. 438 (1997) 147.

[19] H. Ohde, K. Maeda, Y. Yoshida, and S. Kihara, Electrochim. Acta 44 (1998) 23.

[20] C. Wei, A.J. Bard, and M.V. Mirkin, J. Phys. Chem. 99 (1995) 16033.

[21] T. Solomon and A.J. Bard, J. Phys. Chem. 99 (1995) 17487.

[22] A.L. Barker, P.R. Unwin, S. Amemiya, J. Zhou, and A.J. Bard, J. Phys. Chem. 103 (1999) 7260.

[23] S. Amemiya, Z. Ding, J. Zhou, and A.J. Bard, J. Electroanal. Chem. 483 (2000) 7.

[24] J. Zhang, A.L. Barker, and P.R. Unwin, J. Electroanal. Chem. 483 (2000) 95.

[25] Z. Ding, B. M. Quinn, and A. J. Bard, J. Phys. Chem. 105 (2001) 6367.

[26] J. Zhang and P. R. Unwin, Phys. Chem. Chem. Phys. 4 (2002) 3820.
[27] Z. Zhang, Yi Yuan, P. Sun, B. Su, J, Guo, Y. Shao, and H.H. Girault, J. Phys. Chem. 106 (2002) 6713.
[28] K. Nakatani, T. Uchida, H. Misawa, N. Kitamura, and H. Masuhara, J. Electroanal. Chem. 367 (1994) 109.
[29] K. Nakatani, K. Chikama, H.-B. Kim, and N. Kitamura, Chem. Phys. Lett. 237 (1995) 133.
[30] K. Chikama, K. Nakatani, and N. Kitamura, Bull. Chem. Soc. Jpn. 71 (1998) 1065.
[31] C. Johans, R. Lahtinen, K. Kontturi, and D.J. Schiffrin, J. Electroanal. Chem. 488 (2000) 99.
[32] C. Johans, K. Kontturi, and D.J. Schiffrin, J. Electroanal. Chem. 526 (2002) 29.
[33] D.G. Georganopoulou, D.J. Caruana, J. Strutwolf, and D.E. Williams, Faraday Discuss. 116 (2000) 109.
[34] G.C. Lillie, S.M. Homes, and R.A. W. Dryfe, J. Phys. Chem. B 106 (2002) 12101.
[35] H. Hotta and T. Osakai, Rev. Polarogr. (Kyoto) 49 (2003) 15.
[36] D.J. Fermín and R. Lahtinen, *Liquid Interfaces in Chemical, Biological, and Pharmaceutical Applications*; Ed. A.G. Volkov; Marcel Dekker, New York, 2001; Chapter 8.
[37] *Standard Potentials in Aqueous Solution*; Eds. A.J. Bard, R. Parsons, and J. Jordan; Marcel Dekker, New York, 1985.
[38] H. Hotta, S. Ichikawa, T. Sugihara, and T. Osakai, J. Phys. Chem. B, in press.
[39] H. Hotta and T. Osakai, unpublished results (2003).
[40] K. Kano, Rev. Polarogr. (Kyoto) 48 (2002) 29.
[41] A.A. Stewart, J.A. Campbell, H.H. Girault, and M. Eddowes, Ber. Bunsenges. Phys. Chem. 94 (1990) 83.
[42] Y. Cheng and D.J. Schiffrin, J. Chem. Soc. Faraday Trans. 89 (1993) 199.
[43] M. von Smoluchowski, Z. Phys. Chem. 92 (1917) 129.
[44] P. Debye, Trans. Electrochem. Soc. 82 (1942) 265.
[45] G.K. Vemulapalli, *Physical Chemistry*; Prentice-Hall, Englewood Cliffs, NJ, 1993.

Chapter 2. Electron Conductor Separating Oil/Water (ECSOW) System

2.1 Introduction

As mentioned in chapter 1, it is not necessarily easy to distinguish heterogeneous and homogeneous ET processes at O/W interfaces (i.e., the ET and IT mechanisms). If all equilibria in the IT mechanism (as shown in equations (1.2a)–(1.2c)) are quite mobile, the IT mechanism is not distinguishable from the ET mechanism described as a single-step ET (equation (1.1)). Certain efforts have been devoted to the study of the Fc (O)–$Fe(CN)_6^{3-}$ (W) system by means of convolution potential step voltammetry [1], a.c. impedance method [2], current scan polarography [3], SECM [4], voltammetry with micro O/W interfaces [5], and microelectrochemical measurement at expanding droplets [6]. However, no definitive conclusion regarding the reaction mechanism seems to be drawn.

In this study we have devised a new electrochemical method, in which the O- and W-phases are separated by an electron conductor (EC; e.g., Pt) and the ET across the EC phase is observed voltammetrically in a similar manner to the O/W interface. In the EC separating O–W (ECSOW) system, however, no IT across the EC phase can be taken place. Therefore, the ECSOW system would be useful for discrimination between ET and IT occurring at the O/W interface. In this study, we have applied the ECSOW system to the Fc (NB)–$Fe(CN)_6^{3-}$ (W) system, and have verified the validity of this measurement system.

2.2 Experimental

2.2.1 Chemicals

Analytical grade ferrocene (Aldrich), $K_3Fe(CN)_6$ (Wako Pure Chemical Industries, Ltd.), and $K_4Fe(CN)_6$ (trihydrate, Wako) were used as received. Tetrapentylammonium tetraphenylborate (TPnATPB) were prepared as described previously [7]: by mixing equimolar ethanolic solutions of *n*-tetrapentylammonium bromide (Tokyo Kasei Industry Co., Ltd.) and sodium tetraphenylborate (NaTPB, Dojindo Laboratories); the precipitate was washed five times with distilled water and further purified by recrystallization from acetone. An aqueous solution of TPnACl was treated with silver chloride to remove a trace amount of iodide ion; the concentration of TPnACl was determined by potentiometric titration with a standard silver nitrate solution. Analytical grade NB (Wako) was treated with activated alumina for column chromatography (Wako; 200 mesh) before use. Tetrapenthylammonium tetrakis(4-chlorophenyl)borate (TPnATClPB) was synthesized by mixing an acetone solution of tetrapenthylammonium bromide

(Tokyo Kasei) with a reaction mixture containing sodium tetrakis(4-chlorophenyl)borate prepared by using *p*-chlorophenyl Grignard reagent [8]. The resultant white precipitate was washed by 1 : 1 (v/v) water–ethanol mixture and then recrystallized more than three times from 1 : 1 (v/v) acetone–ethanol mixture. All other reagents were of analytical grade and used as received.

2.2.2 Electrochemical measurements

Cyclic voltammetry with the ECSOW system was performed using a four-electrode system with the following cell:

	(W)	(NB)	(EC)	(W)	
Ag/AgCl	0.02 M TPnACl 0.1 M $MgSO_4$	0.1 M TPnATPB *x* mM Fc		0.1 M LiCl *y* mM $K_3Fe(CN)_6$ (*y*/5) mM $K_4Fe(CN)_6$	Pt
(RE1)					(RE2)

Cell 2A

where RE1 and RE2 are the reference electrodes immersed in the NB and W phases by means of Luggin capillaries whose tips were located near the respective boundaries of the EC phase. Two platinum coil electrodes were immersed in the respective phases and served as counter electrodes. Figure 2.1 shows the scheme of the electrolytic cell. As is seen in the figure, the EC phase which separates the O and W phases can be feasibly realized by connecting two platinum disk electrodes (each surface area, 0.02 cm^2) with an electric wire. For each measurement, the electrode surfaces were fleshly polished with a 0.25 μm diamond slurry and rinsed with distilled water or acetone in an ultrasonic field. The O and W phases were purged with N_2 gas prior to voltammetric measurements. The electrolytic cell was immersed in a water bath thermostatted at 25.0 ± 0.1 °C.

In cyclic voltammetry with ECSOW system, the Galvani potential difference $\Delta\phi_O^W$ ($\equiv \phi^W - \phi^O$) between the O and W phases was controlled by means of a four-electrode potentiostat (Hokuto Denko, HA1010mM1A) equipped with a positive feedback circuit for ohmic drop compensation [9]. The solution resistance between the tips of the Luggin capillaries was about 3 kΩ, being usually compensated for by 95%.

Cyclic voltammetric measurements with stationary O/W interfaces were also performed in a similar manner to the ECSOW system. The four-electrode electrolytic cell described elsewhere [9] was employed. For each measurement, the test interface was renewed by pouring an aqueous solution from a reservoir. Unless noted otherwise, all electrochemical measurements were performed using a computer assisted system [9].

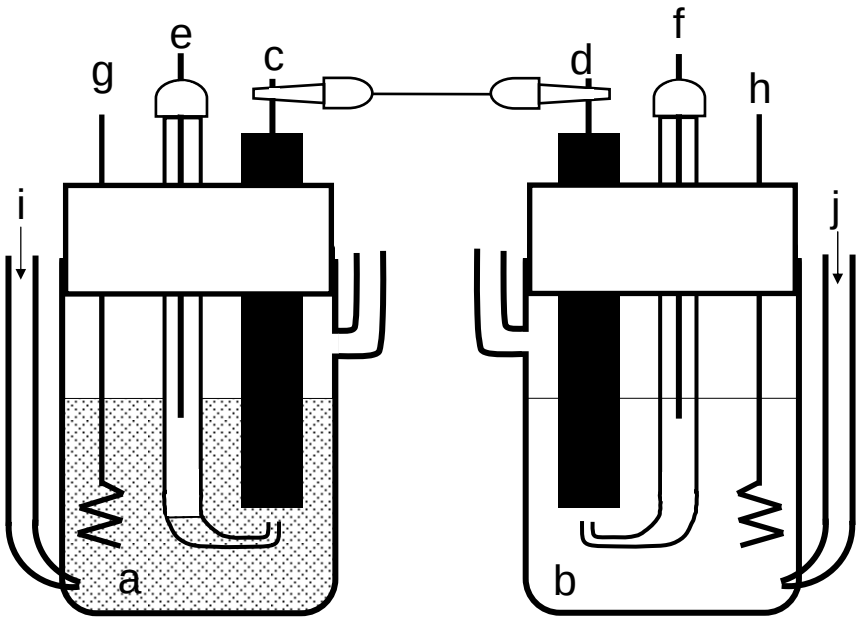

Figure 2.1. Electrolytic cell for the ECSOW system: (a) O phase; (b) W phase; (c), (d) platinum disk electrodes connected with an electric wire; (e), (f) reference electrodes with Luggin capillaries; (g), (h) platinum coil counter electrodes; (i), (j) N_2 gas inlet.

The calculation of cyclic voltammograms was performed by a normal explicit finite difference digital simulation technique [10,11]. A simulation program was written in Microsoft Visual Basic and used for the manual curve-fitting analysis. The validity of the program was checked by referring to the previous numerical analysis [12].

2.3 Results and discussion

Fc (NB)–$Fe(CN)_6^{3-}$ (W) system

In Figure 2.2, curve A shows the voltammogram observed with the ECSOW system in the presence of 100 mM Fc in NB and 0.5 mM $Fe(CN)_6^{3-}$ and 0.1 mM $Fe(CN)_6^{4-}$ in W. A well-defined voltammogram having a pair of current peaks was obtained. The anodic (positive-current) peak corresponds to the ET from Fc to $Fe(CN)_6^{3-}$, whereas the cathodic (negative-current) peak corresponds to the back ET. Such ET processes should occur through redox reactions at the platinum electrode surfaces in the NB and W phases:

$$Fc\ (NB) \rightleftharpoons Fc^+\ (NB) + e^- \qquad (2.1a)$$

$$Fe(CN)_6^{3-}\ (W) + e^- \rightleftharpoons Fe(CN)_6^{4-}\ (W) \qquad (2.1b)$$

where e^- represents an electron in the EC phase. Conventional cyclic voltammetric measurements have revealed that these redox reactions are very fast, i.e., electrochemically reversible. Under these conditions, the ET process in the ECSOW system cannot be discriminated from a postulated reversible ET (equation (1.1)) at the

O/W interface. In practice, the corresponding O/W interface gave totally the same voltammogram, as shown by curve B in Figure 2.2. This result clearly shows that the

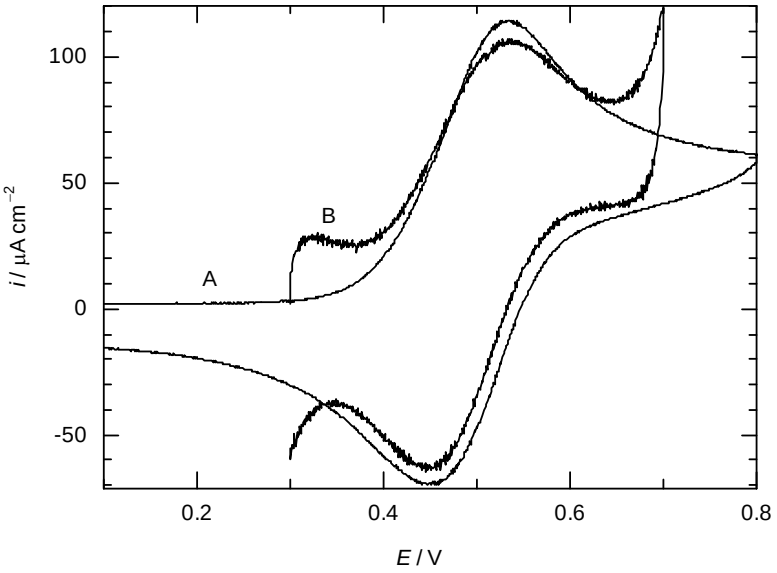

Figure 2.2. Cyclic voltammograms observed with (A) the ECSOW system and (B) the corresponding O/W interface in the presence of 100 mM Fc in NB and 0.5 mM $Fe(CN)_6^{3-}$ and 0.1 mM $Fe(CN)_6^{4-}$ in W. Scan rate: 0.1 V s^{-1}.

ECSOW system is thermodynamically equivalent with the corresponding O/W interface. Accordingly, the equilibrium electromotive force of Cell 2A is given by the Nernst equation:

$$E = E^\circ + \frac{RT}{nF} \ln\left(\frac{a_{\mathrm{R1}}^{\mathrm{W}} a_{\mathrm{O2}}^{\mathrm{O}}}{a_{\mathrm{O1}}^{\mathrm{W}} a_{\mathrm{R2}}^{\mathrm{O}}} \right) \tag{2.2}$$

where a_i^{O} or a_i^{W} is the activity of redox species i (= R1 or O1 in W; R2 or O2 in O), n is the number of electrons involved in the interfacial redox reaction, R, T, and F have their usual meanings, and the standard potential $E°$ is determined by

$$E^\circ = \Delta_{\mathrm{O}}^{\mathrm{W}}\phi^\circ + \Delta E_{\mathrm{ref}} = \left(E_{\mathrm{O2/R2}}^\circ - E_{\mathrm{O1/R1}}^\circ \right) + \Delta E_{\mathrm{ref}} \tag{2.3}$$

Here, $E_{\mathrm{O1/R1}}^\circ$ and $E_{\mathrm{O2/R2}}^\circ$ are the standard redox potentials of the O1/R1 and O2/R2 couples in respective phases, which are expressed on a same potential scale, and ΔE_{ref} is a constant which is determined only by the reference electrodes used.

Under the conditions where the Nernst equation is valid for the activities of the redox species on the EC-phase boundaries, the current flowing through the EC phase should be determined by the diffusion of the redox species in O and/or in W. In practice, the anodic peak current of the voltammogram (curve A) in Figure 2.2 was proportional to the square root of the voltage sweep rate in the range of 20 to 200 mV s^{-1}.

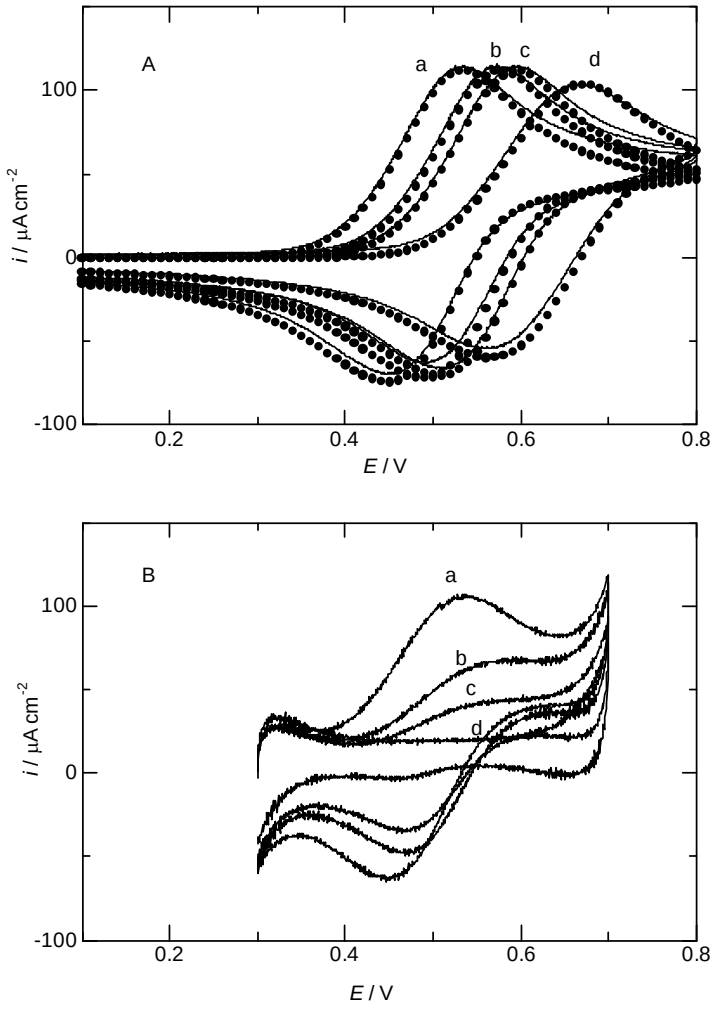

Figure 2.3. Cyclic voltammograms observed with (A) the ECSOW system and (B) the corresponding O | W interface in the presence of (a) 100, (b) 20, (c) 10, and (d) 1 mM Fc in NB and 0.5 mM $Fe(CN)_6^{3-}$ and 0.1 mM $Fe(CN)_6^{4-}$ in W. Scan rate: 0.1 V s^{-1}. The solid circles in (A) show the regression data calculated by using E° = 0.625 V as the sole adjusting parameter; the diffusion coefficients of Fc in the NB phase and of $Fe(CN)_6^{3-}$ and $Fe(CN)_6^{4-}$ in the W phase were independently determined as 0.56×10^{-5}, 0.90×10^{-5}, and 0.57×10^{-5} cm^2 s^{-1}, respectively, by conventional cyclic voltammetry (for Fc) or normal pulse voltammetry using a platinum disk electrode.

When the concentration of Fc, [Fc], was much higher than that of hexacyanoferrate, either the ECSOW system or the O/W interface usually gave a “reversible” wave, as represented in Figure 2.2. However, it was found that when [Fc] was decreased, kinetic features appeared in the voltammograms obtained with the O/W interface. Figure 2.3 shows the voltammograms for (A) the ECSOW system and (B) the corresponding O/W interface. For the ECSOW system, the voltammetric wave was only moved to more

Table 2.1.

The observed and calculated values of the anodic and cathodic peak potentials (E_{pa} and E_{pc}), the peak separation (ΔE_p), the midpoint potential (E_{mid}), and the anodic and cathodic peak currents (i_{pa} and i_{pc}) for the cyclic voltammograms observed with the ECSOW system in the presence of different concentrations of Fc in NB and 0.5 mM $Fe(CN)_6^{3-}$ and 0.1 mM $Fe(CN)_6^{4-}$ in W. [a]

[Fc] / mM	E_{pa} / V		E_{pc} / V		ΔE_p / V		E_{mid} / V		i_{pa} / μA cm^{-2}		i_{pc} / μA cm^{-2}	
	Obs.	Calc.	Obs.	Calc.	Obs.	Calc.	Obs.	Calc.	Obs.	Calc.	Obs.	Calc.
100	0.532	0.532	0.451	0.449	0.081	0.083	0.492	0.491	0.114	0.112	–0.0693	–0.0745
20	0.570	0.575	0.491	0.491	0.079	0.084	0.531	0.533	0.114	0.112	–0.0623	–0.0720
10	0.593	0.592	0.510	0.508	0.083	0.084	0.552	0.550	0.114	0.112	–0.0668	–0.0706
1	0.663	0.669	0.562	0.564	0.101	0.105	0.613	0.617	0.104	0.104	–0.0543	–0.0599

[a] Scan rate: 0.1 V s^{-1}.

positive potentials by decreasing [Fc] from 100 mM to 1.0 mM. Such a change of the voltammogram is in accord with a former theoretical expectation for the reversible ET at the O/W interface [12]. Then, we have performed a digital simulation, in which the reversible ETs, i.e., equations (2.1a) and (2.1b), are assumed. As can be seen in Figure 2.3A, the regression data (solid circles) fit the experimental data (solid lines) very well. In Table 2.1 are shown the observed and calculated values of the anodic and cathodic peak potentials (E_{pa} and E_{pc}), the peak separation (ΔE_p), the midpoint potential ($E_{mid} \equiv (E_{pa} + E_{pc})/2$), and the anodic and cathodic peak currents (i_{pa} and i_{pc}). Thus, the cyclic voltammograms in the ECSOW system can be elucidated in terms of a simple, reversible ET across the EC phase (see equation (1.1)).

On the other hand, however, the voltammograms observed with the O/W interface showed quite different features. As shown in Figure 2.3B, the cathodic peak was depressed significantly by lowering [Fc], suggesting the existence of a kinetically controlled process. Such "kinetic" waves could be tentatively elucidated by assuming the transfer coefficient (α) is close to unity in the Butler–Volmer formalism, as suggested by Samec [13]. Although the set of voltammograms in Figure 2.3B could be simulated on the assumption, another set of voltammograms obtained under the reverse concentration conditions (i.e., when the concentration of hexacyanoferrate was higher) could not be simulated by using the same fitting parameters. Then, we assumed the above-mentioned IT mechanism (equations (1.2a)–(1.2c)), and successfully simulated the voltammograms in Figure 2.3B and also those obtained with any other concentration conditions by using a single parameter set. The detailed results will be described in chapter 5.

Thus, it has been shown that the EC phase can be regarded as an electrocatalyst for the ET process and that the ECSOW system may easily provide the voltammograms that correspond to the true ET across the O/W interface. Their comparison of the voltammograms obtained with the corresponding O/W interface is very useful for clarifying the reaction mechanism of the heterogeneous ET at the O/W interface.

In the last part of this section, we would like to address a frequently asked question as to how the internal potential of the EC phase is changed during the voltammetric measurements. In the ECSOW system, the EC phase is not connected to the potentiostat, so its internal potential is electrically "floated". Nevertheless, the electric currents flowing through the two electrode surfaces should be identical, and simultaneously, the sum of the potential differences across the electrode surfaces equals to the applied potential between the two reference electrodes. These conditions would regulate the voltammetric current observed in the ECSOW system, in a similar manner to that for the ion transport across a liquid or polymer membrane [14–18]. In order to verify this, we have employed an electrometer (Advantest, TR8652) to monitor the potential change of the EC phase (i.e., the platinum electrodes) during cyclic voltammetry with the ECSOW system. In Figure 2.4, curves (a) and (b) show the electrode potentials measured against

the reference electrodes in O and W, respectively (the curves have been corrected for the ohmic drop). In the figure are shown the cyclic voltammograms that were obtained with a platinum working electrode in (1) NB and (2) W, each being recorded by using the same reference electrode as in the ECSOW system. The respective voltammetric waves are due to the reversible redox reactions, equations (2.1a) and (2.1b), at the platinum electrode. As is seen in Figure 2.4, the potential changes shown by curves (a) and (b) clearly show the oxidation of Fc and the reduction of $Fe(CN)_6^{3-}$, respectively. Then, the sum of the electrode potentials (a)+(b), being shown by a dashed line, was in good agreement with the triangular wave (c) applied across the EC phase.

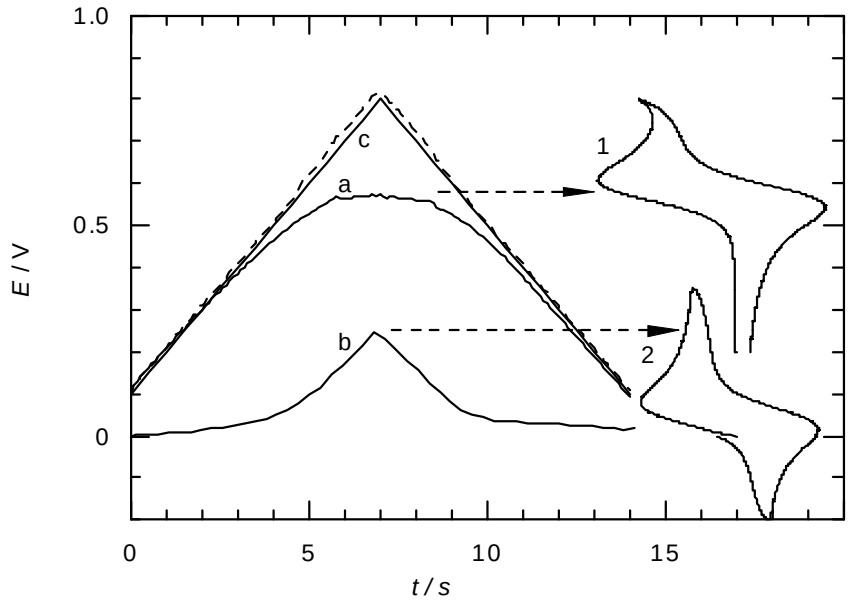

Figure 2.4. Potential change of the EC phase measured against the reference electrodes in (a) NB and (b) W in the presence of 1.0 mM Fc in NB and 0.5 mM $Fe(CN)_6^{3-}$ and 0.1 mM $Fe(CN)_6^{4-}$ in W. Curve (c) shows the applied triangular wave, and the dashed line shows the sum of the electrode potentials (a)+(b). Voltammograms (1) and (2) were recorded using a platinum working electrode in the NB and W phases, respectively. The scan rate was usually 0.1 V s^{-1}.

Furthermore, the currents flowing through the respective EC-phase boundaries have been calculated from the measured potential changes (a) and (b) in Figure 2.4, by means of a digital simulation technique [10,11]. In Figure 2.5, the current–time curves calculated from the measured potential changes (a) and (b) are compared with the observed current–time curve (c). As is seen in the figure, there are good agreements between the calculated and observed curves, although some deviations due to experimental errors are recognized.

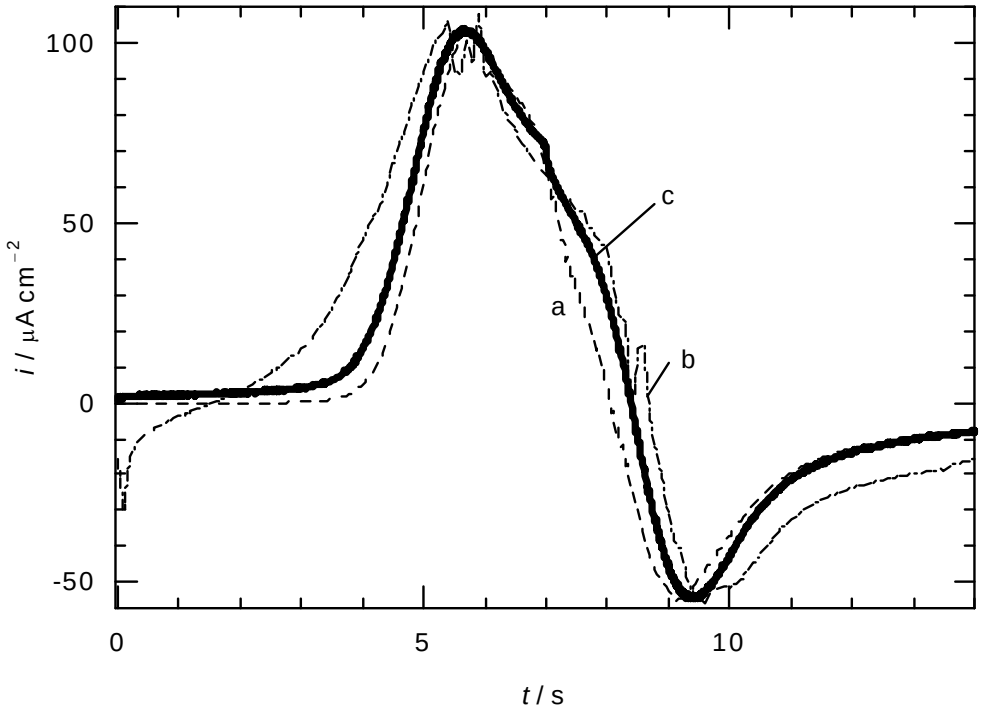

Figure 2.5. Current–time curves calculated from the measured potential changes (a) and (b) in Figure 2.4. Curve (c) shows the observed current–time curve.

Thus, the ECSOW system has been shown to be promising for clarification of the mechanism of ET at the O/W interface.

References

[1] Z. Samec, V. Marecek, J. Weber, and D. Homolka, J. Electroanal. Chem. 126 (1981) 105.

[2] Q.Z. Chen, K. Iwamoto, and M. Seno, Electrochim. Acta 36 (1991) 291.

[3] S. Kihara, M. Suzuki, K. Maeda, K. Ogura, M. Matsui, and Z. Yoshida, J. Electroanal. Chem. 271 (1989) 107.

[4] C. Wei, A.J. Bard, and M.V. Mirkin, J. Phys. Chem. 99 (1995) 16033.

[5] B. Quinn, R. Lahtinen, L. Murtomäki, and K. Kontturi, Electrochim. Acta 44 (1998) 47.

[6] J. Zhang, C.J. Christopher, J. Slevin, and P.R. Unwin, Chem. Commun. (1999) 1501.

[7] T. Osakai, S. Himeno, and A. Saito, J. Electroanal. Chem. 332 (1992) 169.

[8] F.P. Cassaretto, J.J. McLafferty, and C.E. Moore, Anal. Chim. Acta 32 (1965) 376.

[9] S. Aoyagi, M. Matsudaira, T. Suzuki, H. Katano, S. Sawada, H. Hotta, S. Ichikawa, T. Sugihara, and T. Osakai, Electrochemistry 70 (2002) 329.

[10] S.W. Feldberg, *Electroanalytical Chemistry*, Vol. 3, Ed. A.J. Bard; Marcel Dekker, New York, FL, 1969; pp. 199–296.

[11] A.J. Bard, and L.F. Faulkner, *Electrochemical Methods, Fundamentals and Applications*; Wiley, New York, 2001; pp. 785.
[12] A.A. Stewart, J.A. Campbell, H.H. Girault, and M. Eddowes, Ber. Bunsenges. Phys. Chem. 94 (1990) 83.
[13] Z. Samec, personal communication, 2000.
[14] S. Kihara, and K. Maeda, Prog. Surf. Sci. 47 (1994) 1.
[15] K. Maeda, W. Hyogo, S. Nagami, and S. Kihara, Bull. Chem. Soc. Jpn. 70 (1997) 1505.
[16] Z. Samec, A. Trojánek, and P. Vanysek, J. Electroanal. Chem. 332 (1992) 349.
[17] Z. Samec, A. Trojánek, and E. Samcová, J. Electroanal. Chem. 388 (1995) 25.
[18] Z. Samec, A. Trojánek, J. Langmaier, and E. Samcová, J. Electroanal. Chem. 481 (2000) 1.

Chapter 3. Complete Electrolysis Using a Microflow Cell with the Oil/Water Interface

3.1 Introduction

In recent years, much attention has been paid to amperometric (or voltammetric) detection of ions with the O/W interface [1–4]. The amperometric detection is based on measurement of ion-transfer current which is directly proportional to ion concentration, and is therefore very suitable for flow injection analysis (FIA). So far, a variety of amperometric flow cells with the O/W interface have been reported [5–12]. However, they are all designed to detect ion-transfer current due to *partial* electrolysis of the sample aqueous solution. To the best of our knowledge, there has been reported no O/W-type flow cell that can accomplish *complete* electrolysis [13] of the sample solution. If such a flow cell is realized, it will enable us to perform coulometric analysis of ions in a similar manner to conventional flow column electrodes utilizing glassy carbon granule or carbon fiber [14,15]. From the viewpoint of the mechanistic study of interfacial ETs, the flow cell would also be useful for the product analysis (see chapter 5).

In this study, we have constructed a microflow cell [16,17] using the hydrophobic-membrane stabilized O/W interface [18], which is formed over a thin channel (0.1 mm thick, 48 cm long) on a silver plate. By using the microflow cell, we have accomplished complete electrolysis for the interfacial transfer of a representative ion (tetramethylammonium ion, TMA^+ [19]).

3.2 Experimental

3.2.1 Chemicals

Tetrabutylammonium tetraphenylborate [19] (TBATPB) and tetrapentylammonium tetraphenylborate [20] (TPnATPB) were prepared as described previously. Analytical grade tetrabutylammonium chloride (TBACl) or tetrapentylammonium chloride (TPnACl) was occasionally contaminated by a trace amount of iodide ion, which was removed by metathesis with silver chloride in the aqueous solution; the concentration of TBACl or TPnACl was determined by potentiometric titration with a standard silver nitrate solution. Analytical grade nitrobenzene (NB), which was treated as shown in chapter 2, was used as the oil-phase solvent. The other reagents were of analytical grade.

3.2.2 Construction of a microflow cell

A silver plate (30 × 41 × 5 mm) was employed as the electrode for the aqueous mobile phase, which served as both the reference and counter electrodes. As seen in Figure 3.1, the silver plate was provided with two small orifices (0.9-mm diameter) for a

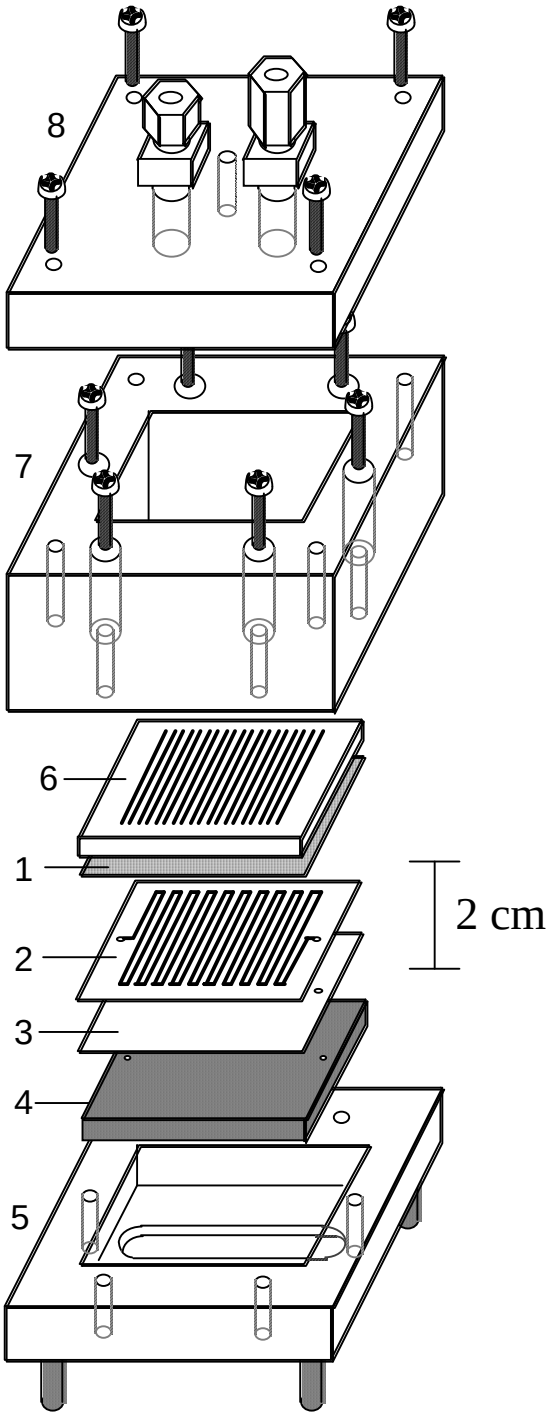

Figure 3.1. Cell construction: (1) PTFE membrane filter, (2) polyester gasket with a channel (1 mm wide; 48 cm long), (3) dialysis membrane, (4) silver plate, (5) Teflon pedestal with steel legs, (6) Teflon draining board (3 mm thick) with 19 slots (each being 1 mm wide and 23 mm long), (7) Teflon block with a square hole, (8) Teflon lid with orifices for counter and reference electrodes and an air vent.

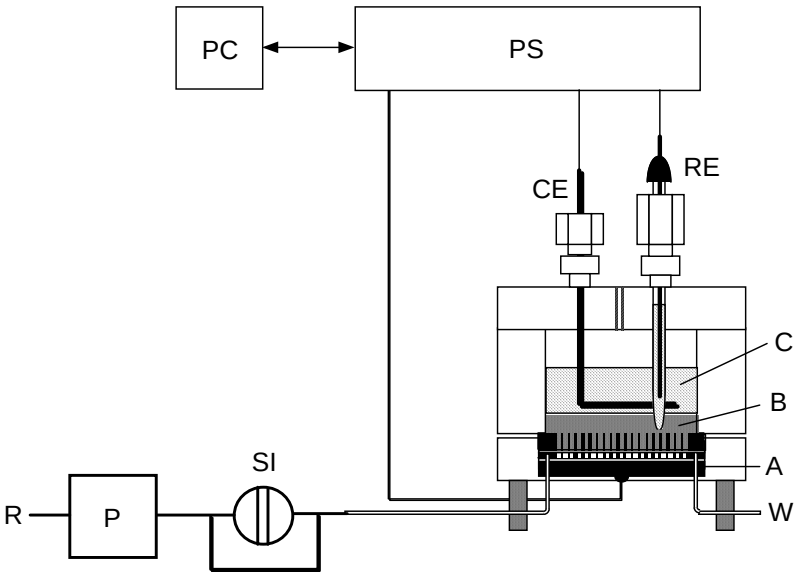

Figure 3.2. Scheme of the microflow electrolysis system: (A) silver plate, (B) NB phase, (C) 0.1 M LiCl aqueous solution, (RE) reference electrode, (CE) silver counter electrode, (SI) sample injector, (P) pump, (R) solution reservoir containing a 0.1 M LiCl aqueous solution, (W) waste, (PS) potentiostat, and (PC) personal computer.

solution inlet and outlet, into which Teflon tubes (0.86-mm outer diameter, 0.38-mm inner diameter) were inserted. The surface of the silver plate was polished in advance by using a 0.3-μm aluminum-oxide lapping film (Sumitomo 3M, #15,000), and then preelectrolysed to form a AgCl layer on it (see below). When the mobile phase contains redox species, the silver plate needs to be covered with a dialysis membrane (Viskase, 20 μm thick). On this silver plate, a thin channel (1 mm wide, 48 cm long) was formed by using a polyester gasket (an OHP film of 0.1-mm thickness), on which a poly(tetrafluoroethylene) (PTFE) membrane filter (Advantec, T010A047A, 70 μm thick, with 0.10-μm pore size) and a Teflon draining board were piled up as shown in Figure 3.1. These laminated plates were pressed into a Teflon pedestal by using a Teflon block and six screws. After necessary solutions were supplied to the flow cell, a Teflon lid furnished with counter and reference electrodes was screwed down.

The NB/W interface was prepared in the microflow cell by pouring a 5-mL NB solution containing a supporting electrolyte (0.1 M TBATPB or 0.1 M TPnATPB) onto the PTFE membrane filter through the Teflon draining board (Figure 3.2). Because NB is toxic, its handling should be made under the hood by using safety groves. Since the PTFE membrane is hydrophobic, the NB/W interface is formed at the lower surface of the membrane. Next, a 0.1 M LiCl aqueous solution was gently applied onto the NB solution. In this aqueous solution, a square-spiral silver counter electrode (1-mm diameter, 10 cm

long) was immersed. The reference electrode was an Ag/AgCl electrode immersed in a TBACl or TPnACl aqueous solution held in a Luggin capillary; the tip of the capillary was located in the NB solution.

The pretreatment of the silver plate was performed as follows: The flow cell was constructed in the same manner as illustrated in Figure 3.1, except that the silver plate was not covered with the dialysis membrane and the PTFE membrane was replaced by a dialysis membrane (Viskase, 20-μm thick). A 2% KCl aqueous solution was then poured onto the dialysis membrane, and the same solution was made to flow through the channel by using a peristaltic pump (flow rate: 180 μL min^{-1}). Under these conditions, the surface of the silver plate, being in contact with the flow channel, was electrolyzed in the dark for several hours by using a 3 V dry battery that was connected in series to a 1 kΩ resistor. This electrolysis formed a brownish AgCl layer on the silver plate, which served as an Ag/AgCl electrode.

3.2.3 Electrochemical cell systems

The microflow cell for the coulometric detection of TMA^+ is expressed as

	(W)	(NB)	(NB)	(W) (mobile phase)	
Ag/AgCl (RE1)	0.1 M TBACl	0.1 M TBATPB	PTFE membrane	0.1 M LiCl	AgCl/Ag (RE2,CE2)

Cell 3A

Here the silver counter electrode is omitted, which was immersed in a 0.1 M LiCl aqueous solution contacting with the NB phase. A 20 to 200-μL aliquot of a 0.5–2.0 mM TMACl aqueous solution was injected into the mobile phase. The left-side Ag/AgCl electrode serves as the reference electrode for the NB phase, while the right-side Ag/AgCl electrode (i.e., the electrolyzed silver plate) serves as both reference and counter electrodes for the W phase.

If we assume that the ohmic drop is correctly compensated in potentiostatic measurements and that the Ag/AgCl electrode for the W phase functions as an ideal non-polarizable electrode (i.e., its potential remains unchanged during the current flow), the applied potential (E) between the two Ag/AgCl electrodes is related to the Galvani potential difference ($\Delta_O^W\phi$) between the NB/W interface by

$$E = \Delta_O^W\phi + \Delta E_{ref} \quad (3.1)$$

where ΔE_{ref} is a constant which depends only on the reference electrode system. Supposing that liquid-junction potentials of the PTFE and dialysis membranes are

negligible, ΔE_{ref} can be regarded as identical with that for the cell used previously, [20] i.e., 323 mV at 25 °C.

3.2.4 Apparatus

Figure 3.2 shows the scheme of the microflow electrolysis system, which comprised a peristaltic pump (Iuchi, CTP-1), a sample injector (Rheodyne, model 7125), and the microflow cell. The flow rate was usually set at 180 μL min^{-1}. A homemade potentiostat was used in order to control the $\Delta_O^W\phi$ of the NB/W interface and detect the ion-transfer current. A positive feedback circuit mounted in the potentiostat was employed with the intention of compensating the solution resistance (*ca*. 90 Ω). The coulometric and voltammetric data acquisition was controlled by means of a 16-bit personal computer (NEC, PC9801VM) equipped with a 12-bit analog-to-digital converter and a 16-bit digital-to-analog converter.

3.3 Results and discussion

3.3.1 Preliminary experiments

In our initial experiments, a dialysis membrane was used instead of the PTFE membrane in order to prepare a NB/W interface in a microflow cell. However, a complete electrolysis was not accomplished, the electrolysis efficiency not going up to over 30%. Since a dialysis membrane is hydrophilic, an O/W interface is usually formed on the membrane surface adjacent to the O phase [21,22]. Accordingly, an ion in the mobile W phase should cross the dialysis membrane until it transfers across the O/W interface. In the preliminary experiments, some of the transferring ions were supposed to pass through the flow channel without transferring across the O/W interface. Then, we changed the dialysis membrane to a porous hydrophobic PTFE membrane to form an O/W interface on the membrane surface adjacent to the mobile W phase. Hundhammer and Wilke [18] employed a similar porous hydrophobic membrane (polyethylene terephthalate membrane) to stabilize a NB/W interface.

3.3.2 Voltammetric responses

Figure 3.3 shows cyclic voltammograms recorded after providing 0.1 M LiCl aqueous solutions containing several concentrations of TMACl to the microflow cell. The voltammetric measurements were carried out under quiescent conditions. As seen in Figure 3.3, well-developed voltammetric waves for the transfer of TMA^+ at the NB/W interface were obtained in a similar manner as reported [19]. The positive-current peak is due to the transfer of TMA^+ from W to NB, whereas the negative-current peak is due to its transfer back to W. Thus, it was shown that the NB/W interface formed by using a PTFE membrane in the microflow cell could function as a polarizable interface in the same manner as ordinary NB/W interfaces.

Nevertheless, the peak separation was found to increase with the TMA^+-ion

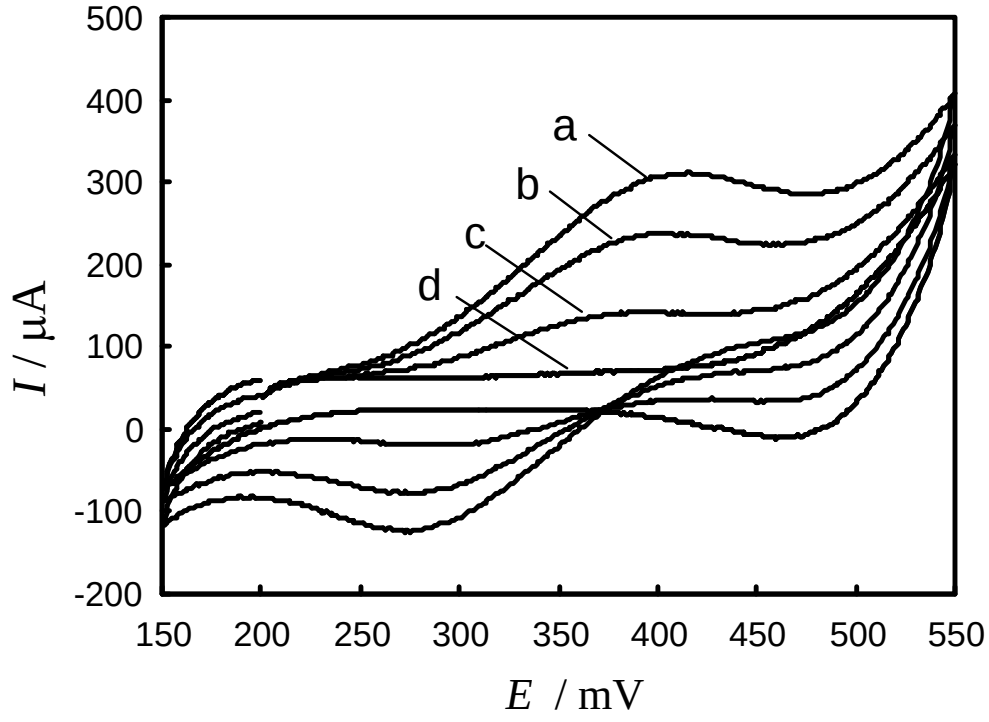

Figure 3.3. Cyclic voltammograms for the transfer of TMA^+ at the NB/W interface, which were recorded by using the microflow cell (Figure 3.1) under quiescent conditions; 0.1 M LiCl aqueous solutions containing (a) 0.6, (b) 0.4, (c) 0.2, (d) 0 mM TMACl were provided in advance to the microflow cell. The potential scan was applied from 200 mV to 550 mV in the positive direction, followed by the negative to 150 mV, and then back to the initial potential. Scan rate: 50 mV s^{-1}.

concentration, being much larger than the value of *ca.* 60 mV for a reversible wave of the transfer of a univalent ion. Since the transfer of TMA^+ at the NB/W interface is known to be very fast (i.e., electrochemically reversible) [19,23], the large peak separation may be ascribed in part to polarization of the Ag/AgCl electrode for the W phase due to the current flow. Also, it seems likely that an unequal potential distribution over the NB/W interface formed on the long channel arose from imperfect compensation of the ohmic drop. Such incompleteness in the voltammetric measurements, however, affected hardly the coulometric measurements described below.

3.3.3 Coulometry of TMA^+

Figure 3.4 shows the coulometric curves obtained with the microflow cell to which a 100 μL aliquot of a sample solution containing several concentrations of TMACl was injected. The electrode potential (*E*) was set at 500 mV where TMA^+ ions in the mobile W phase would be completely “electrolyzed”, or, thoroughly transported to the NB phase (cf.

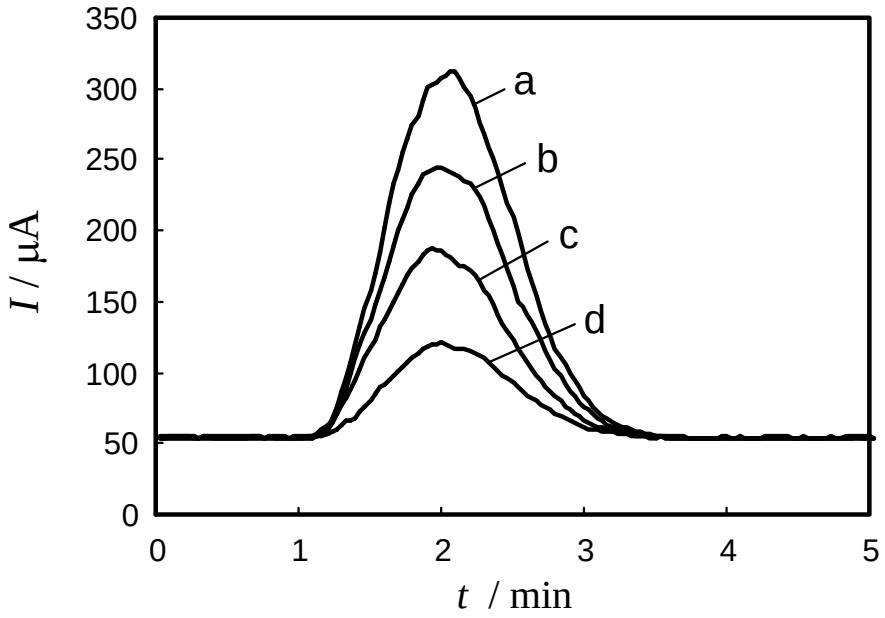

Figure 3.4. Coulometric curves obtained with the microflow cell (cell 3A) to which a 100-μL aliquot of a sample solution containing (a) 2.0, (b) 1.5, (c) 1.0, or (d) 0.5 mM TMACl was injected. Applied potential: 500 mV.

Figure 3.3). Immediately after the potentiostatic operation was started, a positive current probably due to transfer of supporting-electrolyte ions (TPB^- and/or Li^+) was observed, but rapidly reduced to a constant value, which seems to be due to the transfer of Li^+ being constantly provided from the mobile phase. After then a sample solution was provided to the flow cell to record a coulometric curve as shown in Figure 3.4. As seen in the figure, an almost symmetrical current peak due to the TMA^+-ion transfer was obtained for every concentration. When the injection volume was increased up to 200 μL, however, a slight deformation of the current peak, i.e., "tailing", was observed (not shown).

Provided that complete electrolysis is accomplished, the quantity of electricity, being obtained from the peak area, should be proportional to the mole number of the transferring ion in the sample solution. In Table 3.1, the electrolysis efficiencies evaluated from the peak areas are shown for different concentrations of TMA^+ (0.5–2.0 mM) and injection volumes (20–200 μL). Under these conditions, the electrolysis efficiency was over 90%, showing the accomplishment of almost complete electrolysis. Thus, the present microflow cell appears to be promising for absolute quantitative analysis of ions. We would like to add that the present technique has great potentialities for the determination of non-redox species such as ionic and ionizable drugs, ionic surfactants, or some metal ions (alkali/alkaline earth metals).

In the reported O/W-type flow cell [9,10], a four-electrode configuration has been adopted, in which the Galvani potential difference between the O/W interface can be controlled more accurately than in a three- or two-electrode configuration. However, a four-electrode configuration is cumbersome and unsuitable for designing a thin-layer cell for complete electrolysis. In the present flow cell, the electrolyzed silver plate serves as both reference and counter electrodes. Hence, some polarization of the electrode due to current flow is inevitable, so that the concentration of a transferring ion should be kept lower than millimolar level. However, we would like to stress that a simpler three-electrode configuration has effectively functioned to realize a thin-layer flow cell for complete electrolysis. In subsequent chapters, we would like to demonstrate the utilities of this measurement system for determination of number of electrons (chapter 4), and for the product analysis of ET at O/W interface (chapter 5).

Table 3.1.
Electrolysis efficiency (%)[a] for the Transfer of TMA^+ at the NB/W Interface

	TMA^+ concentration, mM			
injection volume, μL	0.5	1.0	1.5	2.0
20	91 ± 0	93 ± 2	99 ± 1	93 ± 3
50	94 ± 4	90 ± 4	99 ± 1	99 ± 0
100	98 ± 2	92 ± 1	91 ± 1	91 ± 1
200	96 ± 1	91 ± 0	92 ± 0	90 ± 1

[a] Mean of four repeat measurements.

References and notes

[1] M. Senda, T. Osakai, T. Kakutani, and T. Kakiuchi, Nippon Kagaku Kaishi (1986) 956.

[2] M. Senda, T. Kakiuchi, and T. Osakai, Electrochim. Acta 36 (1991) 253.

[3] M. Senda, and Y. Yamamoto, *Liquid–Liquid Interfaces, Theory and Methods*; Eds. A.G. Volkov, D.W. Deamer; CRC Press, Boca Raton, FL, 1996; Chapter 12.

[4] F. Reymond, D. Fermín, H.J. Lee, and H.H. Girault, Electrochim. Acta 45 (2000) 2647.

[5] V. Marecek, H. Jänchenová, M.P. Colombini, and P. Papoff, J. Electroanal. Chem. 217 (1987) 213.

[6] H. Ji, and E. Wang, Analyst 113 (1988) 1541.

[7] E. Wang, and H. Ji, Electroanalysis 1 (1989) 75.

[8] E. Wang, H. Ji, and W. Hou, Electroanalysis 3 (1991) 1.

[9] S. Wilke, H. Franzke, and H. Müller, Anal. Chim. Acta 268 (1992) 285.
[10] S. Wilke, H. Wang, M. Muraczewska, and H. Müller, Fresenius J. Anal. Chem. 356 (1996) 233.
[11] H.J. Lee, and H.H. Girault, Anal. Chem. 70 (1998) 4280.
[12] S. Sawada, H. Torii, T. Osakai, and T. Kimoto, Anal. Chem. 70 (1998) 4286.
[13] Although the term “electrolysis” is not very suitable for representing ion-transfer processes at the oil/water interface, it has been customary to use “electrolysis” even for ion-transfer reactions since 1976, when the late Prof. Koryta published a paper entitled “Electrolysis with an Electrolyte Dropping Electrode” (J. Koryta, P. Vanysek, and M. Brezina, J. Electroanal. Chem. 37 (1976) 263).
[14] T. Fujinaga, and S. Kihara, CRC Crit. Rev. Anal. Chem. 6 (1977) 223.
[15] A.J. Bard, and L.R. Faulkner, *Electrochemical Methods, Fundamentals and Applications*, 2nd Ed.; Wiley, New York, 2001; pp 441–452.
[16] M. Maruo, N. Nakayama, K. Kamiyama, and T. Kimoto, In Proceedings of the 2nd Symposium on Micro Total Analysis Systems, Analytical Methods and Instrumentation, Special Issue 1996, Widmer, H.M. Ed.; AMI Editorial Office: Basel, 1996; p 233.
[17] M. Maruo, E. Nakayama, H. Obata, K. Kamiyama, and T. Kimoto, Field Anal. Chem. Tech. 5 (2001) 29.
[18] B. Hundhammer, and S. Wilke, J. Electroanal. Chem. 266 (1989) 133.
[19] T. Kakutani, T. Osakai, and M. Senda, Bull. Chem. Soc. Jpn. 56 (1983) 991.
[20] T. Osakai, S. Himeno, and A. Saito, J. Electroanal. Chem. 332 (1992) 169.
[21] B. Hundhammer, S.K. Dhawan, A. Bekele, and H.J. Seidlitz, J. Electroanal. Chem. 217 (1987) 253.
[22] S. Sawada, T. Osakai, and M. Senda, Bunseki Kagaku 39 (1990) 539.
[23] T. Osakai, T. Kakutani, and M. Senda, Bull. Chem. Soc. Jpn. 57 (1984) 370.

Chapter 4. Reaction Mechanism of the Oxidation of L–Ascorbic Acid by Chloranil at the Oil/Water Interface

4.1 Introduction

Electron transfer at the O/W interface is fundamentally important for understanding the energy conversion in biomembranes [1]. So far, heterogeneous redox reactions for organic compounds of biological significance which include L-ascorbic acid [2], flavin mononucleotide (FMN) [3], and β-nicotinamide adenine dinucleotide (NADH) [4] had been studied.

This chapter focuses on the redox reaction between L-ascorbic acid (AH_2) in W and chloranil (2,3,5,6-tetrachloro-1,4-benzoquinone; denoted by Q) added in NB, in which a one-electron transfer was claimed to occur between AH_2 (W) and Q (NB) based on current-controlled polarography with an ascending water electrode [2]. In this study we have reexamined the reaction mechanism in detail using various techniques including cyclic voltammetry, potential-controlled polarography, coulometry with a microflow cell, ECSOW system, etc. The results have clearly shown that two electrons per AH_2 molecule participate in the redox reaction that includes an IT process due to a reduction product of Q (i.e., the semiquinone radical ion; $Q^{\bullet -}$).

4.2 Experimental

4.2.1 Chemicals

L-ascorbic acid (Wako Pure Chemical Industries, Ltd.; analytical grade) and chloranil (Tokyo Kasei Industry Co., Ltd.) were used as received. The tetra-*n*-pentylammonium salt of 12-tungstophosphate, $(TPnA)_3[PW_{12}O_{40}]$, which can be used as the supporting electrolyte in NB, was prepared by the equimolar addition of an aqueous solution of 12-tungstophosphoric acid *n*-hydrate (Wako; analytical grade) and an aqueous solution of *n*-tetrapentylammonium chloride (TPnACl; Wako's practical grade); the precipitate was washed five times with distilled water and recrystallized from acetone. The preparation of tetrapentylammonium tetraphenylborate (TPnATPB) salt and aqueous TPnACl solution and the purification of NB are described in chapter 2. All other reagents were of the highest grade available and used as received.

4.2.2 Electrochemical measurements

In cyclic voltammetry and polarography with NB/W interfaces the following electrochemical cell was used:

	I	II	III	IV	
	(W)	(NB)	(W)	(W)	
			0.1–0.5 mM AH_2		
Ag/AgCl	0.1 M $MgSO_4$	20 mM Q	0.1 M NaCl	0.5 M Na_2SO_4	AgCl/Ag
	0.02 M TPnACl	0.035 M $(TPnA)_3[PW_{12}O_{40}]$	0.5 M Na_2SO_4		
			0.05 M phosphate buffer		
(RE1)					(RE2)

Cell 4A

The NB/W interface denoted by || is to be tested. The pH (= 5.7–7.9) of the aqueous phase (III) was adjusted with 0.05 M phosphate buffer. Phases III and IV were separated by means of a glass sinter.

For the cyclic voltammetry with a stationary NB/W interface, the previous three-electrode electrolytic cell [6] was used, but partly modified so as to deaerate the NB and W phases with N_2 gas. The surface area of the NB/W interface to be tested was 0.049 cm^2.

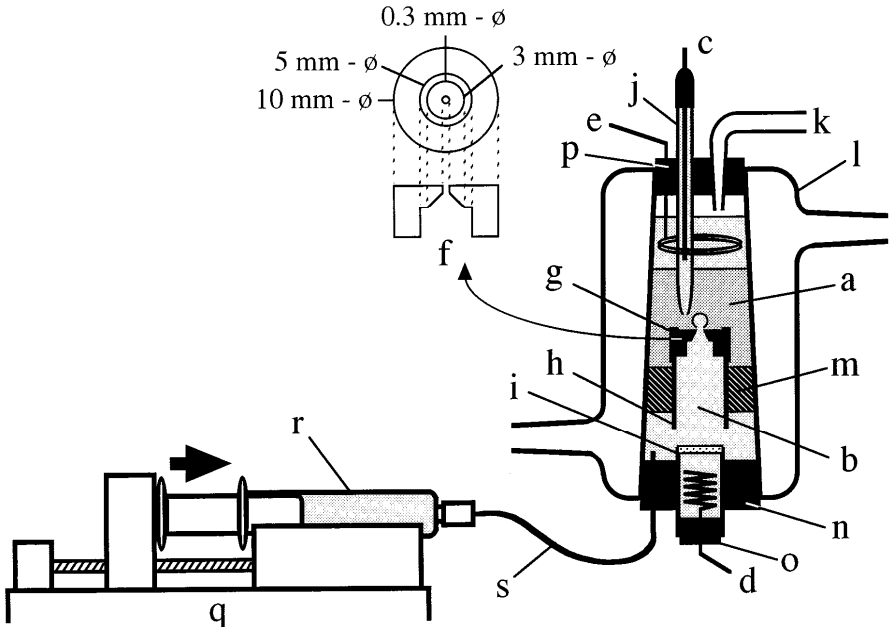

Figure 4.1. Three-electrode type electrolytic cell with an ascending water electrode: (a) NB solution for phase II in cell 4A; (b) aqueous solution for phase III; (c) Ag/AgCl rod electrode for potential control; (d) Ag/AgCl spiral electrode for potential control and current detection; (e) spiral platinum electrode for current detection; (f) Teflon tip; (g) Teflon heat-shrink tubing; (h) glass tube; (i) glass tube with a glass sinter; (j) Luggin capillary; (k) glass capillary connected to an aspirator to suck off excess solution; (l) glass ware with a water jacket; (m) elastic silicone+Teflon rubber distributed by Nippon Rikagaku Kikai Co., Ltd.; (n), (o), (p) silicone rubber; (q) infusion pump; (r) 10 ml syringe; (s) Teflon tubing (0.5 mm i.d.).

For the polarography with an ascending water electrode, a modified three-electrode cell [7] was used. As shown in Figure 4.1, a Teflon tip with a small orifice of 0.3 mm diameter, which was supported on a glass tube with Teflon heat-shrink tubing, was incorporated into glassware like a Liebig condenser (85 mm length, 45 mm o.d., 20 mm (upper) and 25 mm (lower) i.d.). In place of the solution reservoir with a glass capillary [7], an infusion pump (World Precision Instruments, SP100i) equipped with a 10 ml syringe (Hamilton 1010 model) was used to send an aqueous solution to the cell at a constant rate. The aqueous solution in the syringe, as well as the NB solution in the cell, was deaerated in advance.

For the cyclic voltammetry with the ECSOW system, the Galvani potential difference $\Delta_{\mathrm{O}}^{\mathrm{W}}\phi$ ($\equiv \phi^{\mathrm{W}} - \phi^{\mathrm{O}}$) between the O and W phases was controlled by means of a four-electrode potentiostat (Hokuto Denko, HA1010mM1A) equipped with a positive feedback circuit for ohmic drop compensation [8]. The electrochemical cell used is:

	(W)	(NB)	(EC)	(W)	
	0.004 M TPnACl	0.02 M TPnATClPB		0.1 M LiCl 0.5 mM AH_2	
Ag/AgCl	0.02 M $MgSO_4$	15 mM Q		0.05 M phosphate buffer (pH 7.0)	Ag/AgCl
(RE1)					(RE2)

Cell 4B

where the counter electrodes are omitted. The details of the electrolytic cell are as described in chapter 2. The temperature of the electrolytic cells was always set at 25 ± 0.1 °C.

The number (n) of electrons required for the oxidation of one molecule of AH_2 by Q was determined by coulometry with the microflow cell as shown in Figures 3.1 and 3.2. The microflow cell is expressed as:

	I	II	III	IV	V	
	(W)	(NB)	(NB)	(W) (mobile phase)	(W)	
	0.02 M TPnACl	0.1 M TPnATPB	PTFE membrane	0.1 M LiCl	dialysis membrane	AgCl/Ag
Ag/AgCl	0.1 M $MgSO_4$	20 mM Q				
(RE1)						(RE2)

Cell 4C

Here the silver counter electrode is omitted, which was immersed in a 0.1 M LiCl aqueous solution contacting with the NB phase. A 100-μL aliquot of a 0.2 mM AH_2 aqueous solution was injected into the mobile phase (flow rate = 180 μl min^{-1}), whose pH was adjusted to 7.0 with 0.05 M phosphate buffer. As described in chapter 3, the ohmic drop can be compensated by a positive feedback circuit mounted in the potentiostat. This experiment was carried out under room temperature (25 ± 5 °C).

These electrochemical measurements were all performed using a laboratory-constructed computer assisted system.

4.2.3 Spectrophotometric measurements

As shown in Figure 4.2, an interface between a 2.0 ml aqueous solution of 0.5 mM AH_2 (containing 0.05 M phosphate buffer) and a 0.2 ml NB solution of 20 mM Q was formed in a 10 mm quartz cell. While stirring the aqueous phase with a direct-mixing motor (SpectroCell, Inc. MTR-11D), the absorbance of the aqueous phase was monitored by means of a photodiode array spectrophotometer (Shimadzu MultiSpec-1500). This experiment was carried out under room temperature (25 ± 5 °C).

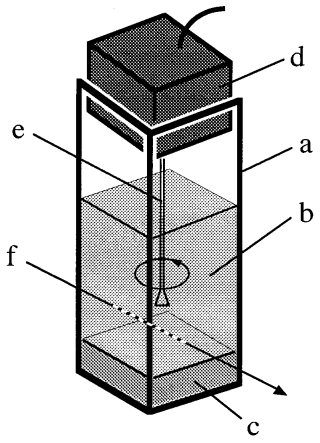

Figure 4.2. Spectrophotometric cell for monitoring a redox reaction at the NB/W interface: (a) 10 mm quartz cell; (b) 2 ml aqueous solution; (c) 0.2 ml NB solution; (d) direct-mixing motor; (e) Teflon propeller; (f) light pass through the aqueous phase.

4.3 Results

4.3.1 Cyclic voltammetry

Figure 4.3 shows cyclic voltammograms for stationary NB/W interfaces. Curve A represents the voltammogram which was recorded in the presence of 0.5 mM AH_2 in W. Because no peaks were observed in the absence of AH_2 (curve B), it was suggested that the cathodic (negative-current) peak should be due to the oxidation of AH_2 by Q. The peak separation (ΔE_p) increased with the voltage scan rate (v); under the same conditions as in Figure 4.3, ΔE_p = 65, 70, 95, and 110 mV at v = 10, 20, 50, and 100 mV s^{-1}, respectively. However, the midpoint potential (E_{mid}) between the cathodic and anodic peaks was practically independent of v in the range of 10 to 100 mV s^{-1}. This may be a consequence of the comparatively slow charge-transfer process (equation (4.3)) as described later. In this way, the present system was shown to be a quasi-reversible system. As shown in Figure 4.4, a plot of E_{mid} against pH (= 5.7–7.9) showed a straight line with a slope of 59 mV/pH.

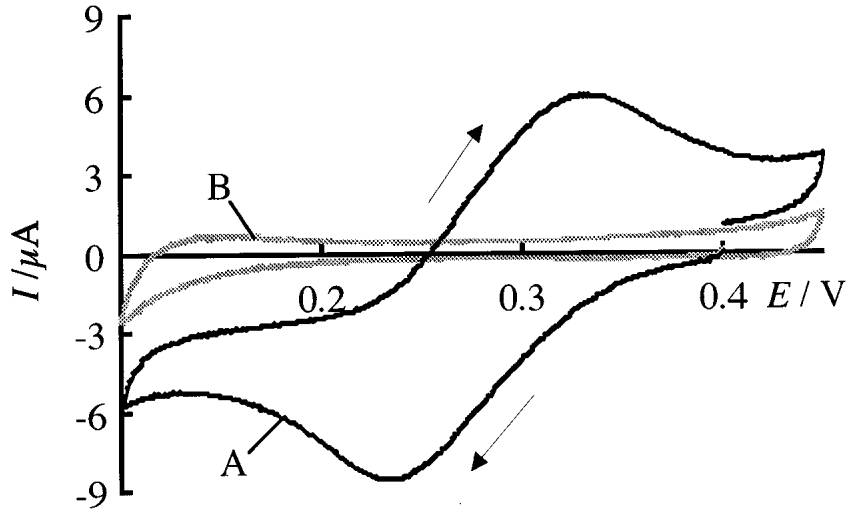

Figure 4.3. Cyclic voltammograms of the stationary NB/W interface in the (A) presence and (B) absence of 0.5 mM AH_2 in W (pH 7.3). The NB phase contained 20 mM Q. For supporting electrolytes, see cell 4A. Scan rate: 50 mV s^{-1}.

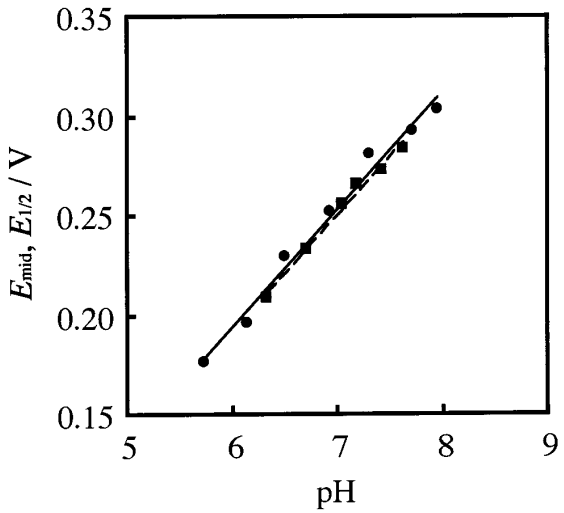

Figure 4.4. Plots of E_{mid} (●) and $E_{1/2}$ (■) against pH for the redox reaction between 0.5 mM AH_2 in W and 20 mM Q in NB. The solid and dashed lines show regression lines with the slopes of 59 and 58 mV/pH, respectively, for E_{mid} and $E_{1/2}$.

Except for a reversible wave due to a simple charge transfer, it is generally difficult to determine the number (n) of electrons involved in the charge transfer from the voltammetric peak current. We then employed a polarographic technique with an ascending water electrode to determine the value of n from the limiting current.

4.3.2 Polarography

Figure 4.5 shows the polarograms which were recorded in the (A) presence and (B) absence of AH_2 in W. Since the concentration of AH_2 in W was much lower than that of Q in NB, the limiting current (I_d) would be determined by the diffusion of AH_2 in W, depending linearly on the AH_2 concentration in the range of 0.1–0.5 mM. It was also found that I_d was practically independent of the Q concentration in the range of 5–20 mM. Therefore, I_d [μA] should be given by the Ilkovič equation [9]:

$$I_d = 3850 n (D_{AH_2})^{1/2} m^{2/3} \tau^{1/6} C^* \qquad (4.1)$$

where D_{AH_2} is the diffusion coefficient ($cm^2\ s^{-1}$) of AH_2 in W, m the flow rate ($mg\ s^{-1}$), τ the drop time (s), and C^* the AH_2 concentration ($mol\ dm^{-3}$). The coefficient of the r.h.s of equation (4.1) was obtained using the measured density (= 1.068 $g\ cm^{-3}$) of the aqueous phase (i.e., an aqueous solution containing 0.1 M NaCl and 0.5 M Na_2SO_4). The previous study [6] showed that the Ilkovič equation could be employed to evaluate the limiting current for transfer of tetramethylammonium ion at the NB/W interface. On the basis of the preliminary examination, we employed equation (4.1) to calculate the n value for the present system. The n values obtained at various pH values are shown in Table 4.1. In this calculation, we used the value of D_{AH_2} (= $5.0\times10^{-6}\ cm^2\ s^{-1}$) which was determined from the diffusion current due to the oxidation of AH_2 on a glassy carbon electrode in an aqueous solution of the same composition as phase III in cell 4A; the diffusion current was measured by potential-step chronoamperometry with a conventional three-electrode electrolytic cell (the applied potential was carefully set at a sufficiently positive potential, +0.9 V vs. Ag/AgCl(sat. KCl), where the current should be limited only by the diffusion of AH_2). The values of τ (e.g., 11.4 s for Figure 4.5) for the calculation of D_{AH_2} were accurately evaluated by recording current–time curves during some drops at the potential where the limiting current was observed. As seen in Table 4.1, the n values thus determined are about 2 or slightly lower, suggesting that the present system should be a two-electron reaction rather than a one-electron reaction.

Figure 4.4 shows the pH dependence of the half-wave potential ($E_{1/2}$), which was very close to E_{mid} in cyclic voltammetry. In the range of pH 6.3–7.6, $E_{1/2}$ as well as E_{mid} showed a straight line with the slope of 58 mV/pH.

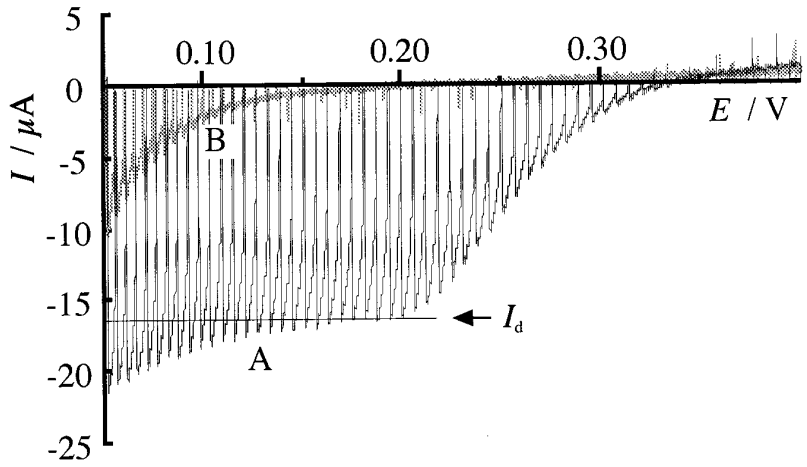

Figure 4.5. Polarograms recorded with an ascending water electrode in the (A) presence and (B) absence of 0.5 mM AH_2 in W (pH 7.3). The NB contained 20 mM Q. *m*: 1.55 mg s^{-1}.

4.3.3 Determination of the number of electrons

Figure 4.6 shows the coulometric curves obtained with the microflow electrolytic cell to which a 100-μL aliquot of a sample solution containing 0.1, 0.2, 0.3, or 0.4 mM AH_2 was injected. The electrode potential (E) was set at 100 mV, where AH_2 in the mobile W phase (pH 7.0) would be completely electrolyzed (cf. Figure 4.3). As seen in Figure 4.6, a well-defined current peak was observed for every AH_2 concentration. The quantity of electricity required for the oxidation of AH_2 was evaluated from the peak area, and then the n value was calculated by using the relation:

$$n = Q/(F[AH_2]V) \qquad (4.2)$$

where Q is the quantity of electricity (C), F the Faraday constant (= 96 485 C mol^{-1}), $[AH_2]$ is the concentration of AH_2 (mol dm^{-3}), and V the injection volume (dm^3). The n value determined was 1.91, 1.98, 2.06, or 2.05 (for one molecule of AH_2) at 0.1, 0.2, 0.3, or 0.4 mM AH_2, respectively. The average of n value was 2.00 ± 0.07.

Table 4.1.
The values of I_d and n at various pH valus

pH	I_d [a] /μA	n
6.12	–18.02	2.1
6.32	–14.14	1.7
6.69	–15.03	1.7
7.03	–15.91	1.8
7.17	–15.25	1.8
7.41	–15.80	1.8
7.62	–15.36	1.8

[a] Obtained for 0.5 mM AH_2 in W and 20 mM Q in NB; m = 1.55 mg s^{-1}.

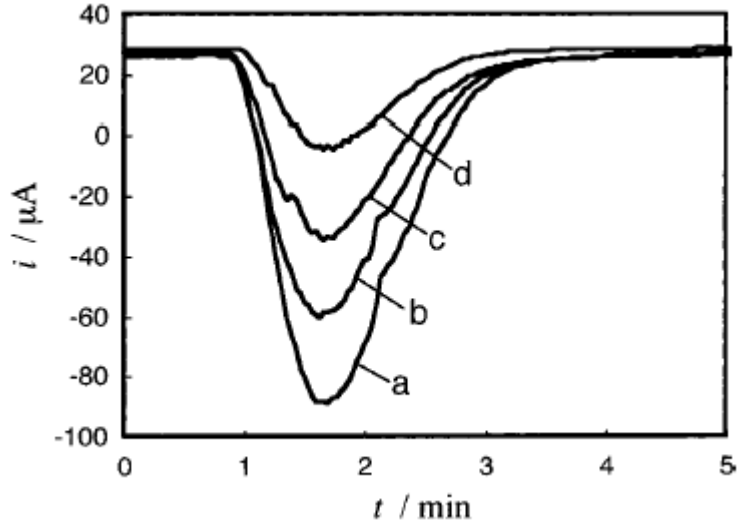

Figure 4.6. Coulometric curves obtained with the microflow cell (cell 4B) to which a 100-μL aliquot of a sample solution containing (a) 0.4, (b) 0.3, (c) 0.2, or (d) 0.1 mM AH_2 was injected. Applied potential: 100 mV.

4.3.4 ECSOW system

In Figure 4.7, the cyclic voltammogram obtained with the ECSOW system is compared with that obtained with the corresponding O/W interface. For the ECSOW system, only a cathodic peak most probably due to the irreversible oxidation of AH_2 in W on the platinum electrode was observed (curve a). For the corresponding O/W interface,

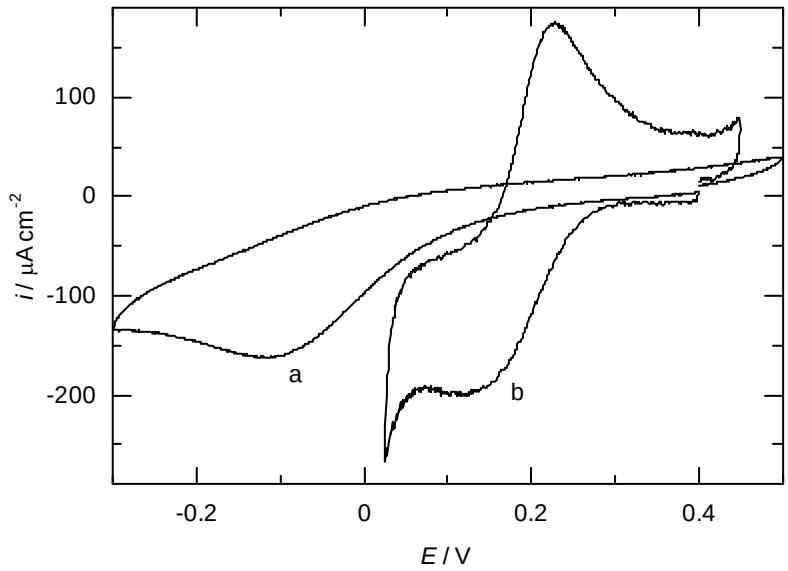

Figure 4.7. Cyclic voltammograms observed with (a) the ECSOW system and (b) the corresponding O/W interface in the presence of 15 mM Q in NB and 0.5 mM AH_2 in W (pH 7.0). Scan rate: 0.1 V s^{-1}.

however, a “reversible” voltammetric wave having a pair of cathodic and anodic peaks (curve b) was observed at a more positive potential (around 0.2 V). It should be noted here that the “reversible” wave appeared at a more positive potential where no redox wave was observed in the ECSOW system. This result strongly suggests that the “reversible” wave for the O/W interface is not due to such a simple heterogeneous ET.

4.3.5 Spectrophotometric measurements without electrochemical control

The redox reactions between 0.5 mM AH_2 in W and 20 mM Q in NB were observed under no electrochemical control using the spectrophotometric cell shown in Figure 4.2. The spectrum changes were monitored while stirring constantly the aqueous phase (with pH = 6.5, 7.2, or 7.8). Figure 4.8 shows the absorption spectrum for pH 7.2 which was recorded at 90 min after the stirring was started. The absorption peaks at around 450 nm and 425 nm show that the semiquinone radical anion ($Q^{\bullet -}$) [10–12] was produced in the aqueous phase from Q initially added to NB. Furthermore, the broad peak around 550 nm suggested the formation of chloranilic acid (ε_{550} = 183 at pH 7.4).

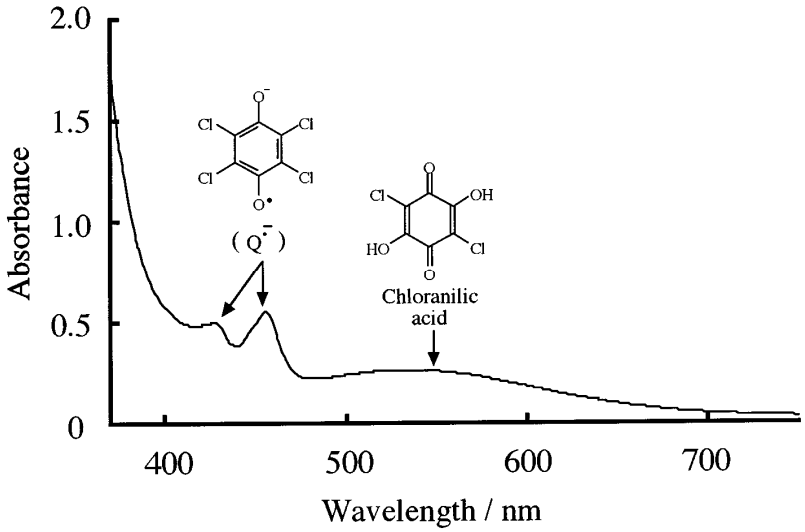

Figure 4.8. Absorption spectrum recorded at 90 min after the stirring was started. The aqueous phase (pH 7.2) contained 0.5 mM AH_2, while the NB phase contained 20 mM Q.

Figure 4.9 shows the time dependence of the absorbances at (A) 456 nm and (B) 600 nm, which correspond to $Q^{\bullet -}$ and chloranilic acid, respectively; the wavelength (600 nm) for monitoring the formation of chloranilic acid was chosen as fairly long to minimize the interference from $Q^{\bullet -}$ by tailing. As seen in the figure, although no absorbance was observed at either wavelength for the first several ten minutes, a sudden increase in the absorbance at 456 nm was observed, followed by a gradual increase in the absorbance at

600 nm. These absorbance changes showed that chloranilic acid was formed through $Q^{\bullet -}$ as the final product. At the present stage, we cannot declare what the trigger of this redox reaction is. However, we can conclude that if a necessary condition is given, a certain redox reaction can occur between AH_2 and Q added to the respective phases, even without electrochemical control. This shows the possibility that neutral molecules of Q were partly distributed to the aqueous phase and then reacted with AH_2.

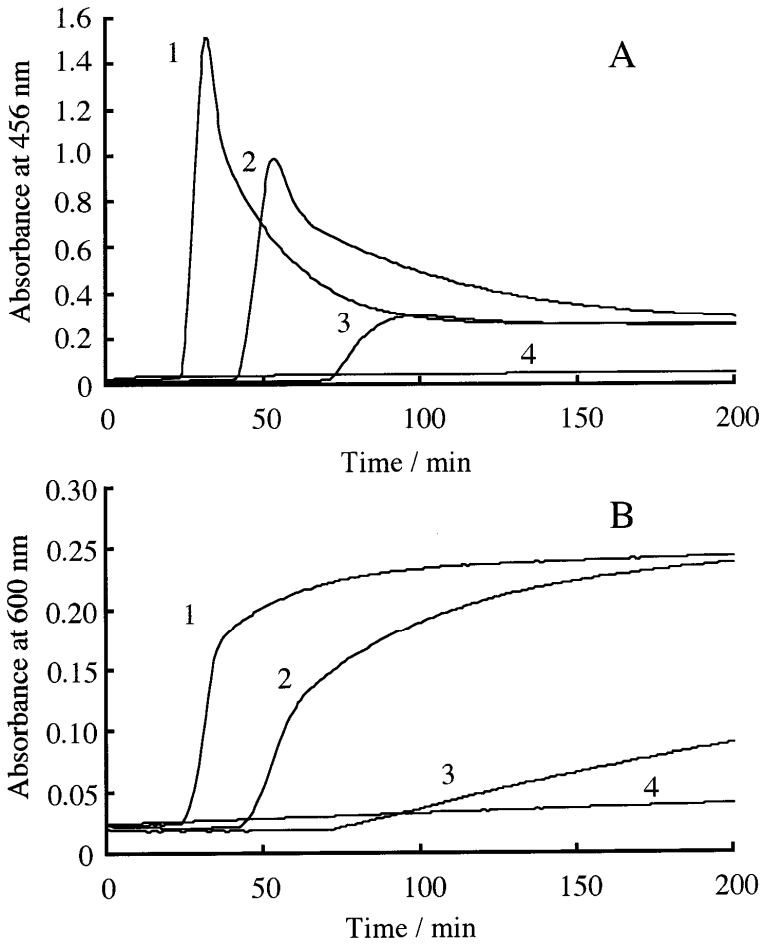

Figure 4.9. Time dependences of the absorbances at (A) 456 nm and (B) 600 nm. The concentrations of AH_2, and Q are as in Figure 4.8, but the pH of the aqueous phase was (1) 7.8, (2) 7.2, or (3) 6.5. Curve (4) was obtained in the absence of AH_2 in the aqueous phase (pH 7.8).

4.4 Discussion

It is known that AH_2 undergoes an irreversible 2-electron oxidation on a metal electrode to form dehydro-L-ascorbic acid (DHA), which further undergoes an irreversible hydrolysis to 2,3-diketo-L-gulonic acid (DKG) [13,14]. If a similar irreversible 2-electron reaction had occurred at the NB/W interface, i.e.,

$$AH_2\,(W) + Q\,(NB) \rightarrow DHA\,(W) + QH_2\,(NB) \qquad (4.3)$$

the well-developed anodic (positive-current) peak observed in cyclic voltammetry (see Figure 4.3) could not be elucidated. Then, we have proposed a new mechanism as shown in Figure 4.10. The conversion of DHA to DKG is not apparently involved in the proposed mechanism, since it does not need to be addressed in the analysis of electrochemical behaviors of interest.

In the range of pH 6–8, AH_2 dissociates into ascorbate (AH^-) in the aqueous phase (for the first dissociation, $pK_a = 4.10$ [15]). In the proposed mechanism, AH^- undergoes an irreversible 2-electron oxidation by Q being only partly distributed to the aqueous phase:

$$AH^- + H^+ + Q \rightarrow DHA + QH_2 \quad \text{(in W)} \qquad (4.4)$$

In this way, AH^- is irreversibly transformed into DHA, whereas Q is reduced to QH_2. The resultant QH_2 and Q should lead to produce the semiquinone radical anion ($Q^{\bullet -}$):

$$QH_2 + Q \rightleftharpoons 2\,Q^{\bullet -} + 2H^+ \quad \text{(in W)} \qquad (4.5)$$

It can be thought that the interfacial transfers of $Q^{\bullet -}$ from W to NB and vice versa can be observed as the IT current under electrochemical control. In this mechanism, the oxidation of 1 mole of AH_2 leads to the interfacial transfer of 2 moles of monovalent $Q^{\bullet -}$. This is consistent with the *n* value of 2 determined from the polarographic coulometric measurements.

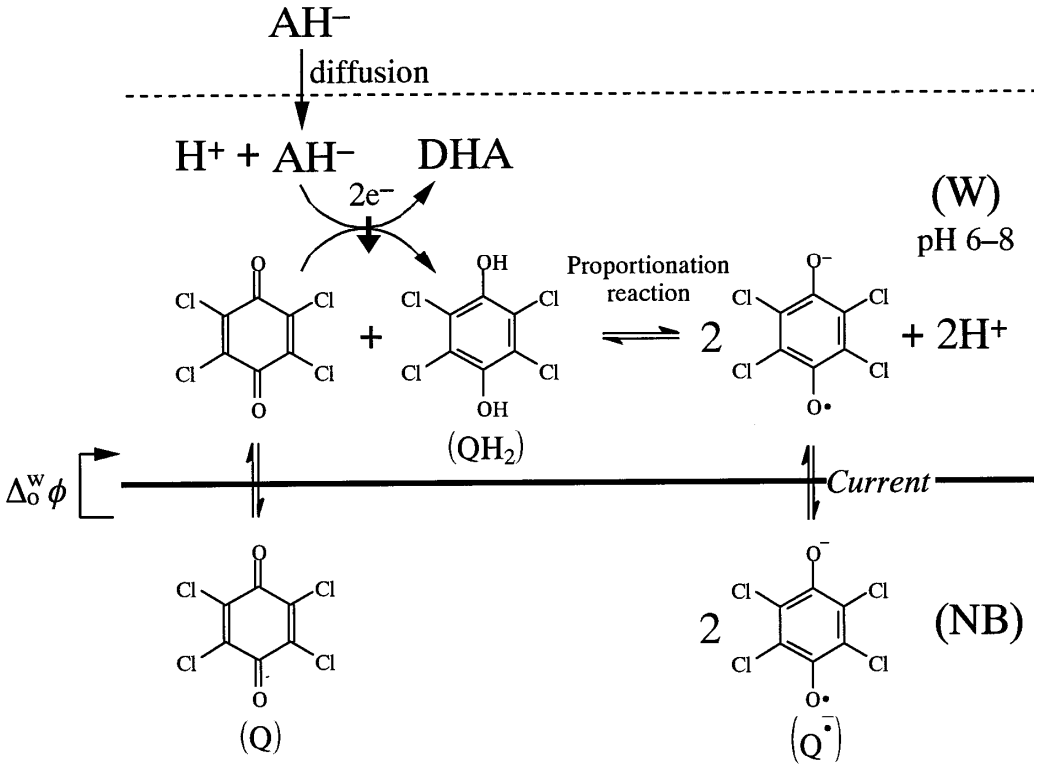

Figure 4.10. Proposed mechanism for the redox reaction between AH_2 ($\rightarrow AH^- + H^+$) added to the aqueous phase (pH 6–8) and Q added to the NB phase. For details, see the text.

Although a series of reactions up to the formation of $Q^{\bullet -}$ may occur without electrochemical control, these reactions seems to be difficult carry out, since Q is hydrophobic to be abundantly distributed to W. However, once the transfer of $Q^{\bullet -}$ to NB is raised by electrochemical control, a series of reactions is facilitated by the IT. Thus, the reaction of interest can be regarded as a homogeneous ET reaction facilitated by a heterogeneous IT.

For examining the validity of reaction (4.4), it is essential to know the standard redox potential of Q in the aqueous solution. Despite of the low solubility of Q in water, we could obtain voltammetric waves for Q with a plastic formed carbon (PFC) electrode in the aqueous test solution, which was prepared by addition of 0.2 ml of a stock solution (10 mM) of Q in acetonitrile to 20 ml of a 0.1 M NaCl aqueous buffer solution (pH 7.0), followed by mixing for 10 min (Q seemed to be only slightly dissolved, but mostly suspended). As shown in Figure 4.11A, Q gave a well-defined wave at a relatively rapid scan rate (1.0 V s^{-1}); the potential scan was made from +0.15 V (around the rest potential) to –0.20 V in the cathodic direction, followed by the anodic to +0.30 V, then the cathodic back to the initial potential. In this case, the cathodic and anodic peaks were small, and the wave shape resembled an adsorption wave. At scan rates < 1.0 V s^{-1}, we could obtain only ill-defined waves which seemed to be affected by possible adsorption–desorption processes. However, when the potential scan was initiated at 0 V where Q can be reduced

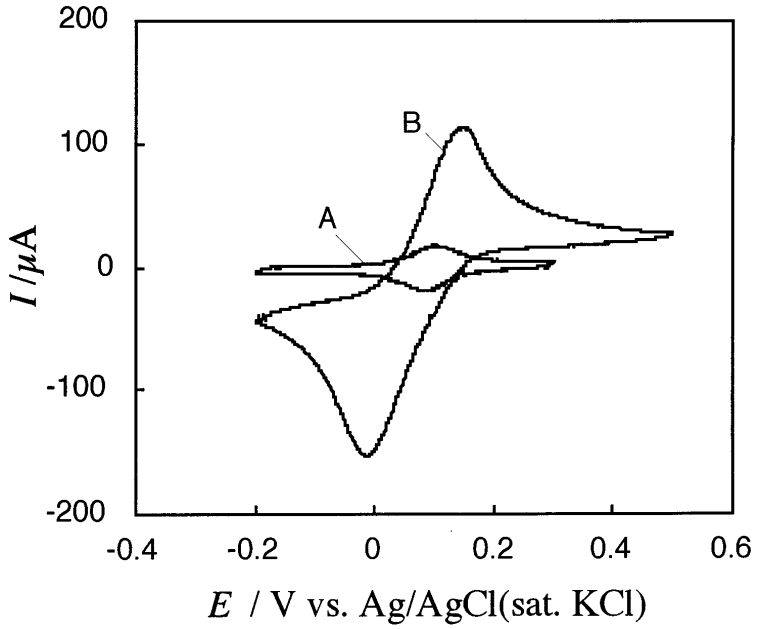

Figure 4.11. Cyclic voltammograms for a saturated solution of Q in a 0.1 M NaCl aqueous solution (containing 0.05 M phosphate buffer; pH 7.0) at the PFC electrode (BAS Inc.; surface area = 0.071 cm^2). For the preparation of the test solution, see the text. The potential scan was made as: (A) +0.2 V → –0.2 V → +0.3 V → +0.2 V; (B) 0 V → +0.5 V → –0.2 V → 0 V. Scan rate: 1.0 V s^{-1}.

to QH_2, a well-developed wave could be obtained at 1.0 V s^{-1}, as shown in Figure 4.11B. This suggests that QH_2, being more soluble than Q, was produced electrolytically in good amount at the electrode surface, and electrolyzed reversibly under the conditions, hardly suffering from adsorption–desorption processes. From the midpoint potential of the quasi-reversible wave, we then estimated the apparent redox potential of Q to be +0.08 V vs. Ag/AgCl(sat. KCl) at pH 7.0. This potential shows a high probability of Q oxidizing AH_2 in the aqueous solution.

In practice, we could observe the oxidation of AH_2 by Q (i.e., reaction (4.4)), as shown in Figure 4.12. The cyclic voltammograms were recorded using the PFC electrode 10 min after the addition of different amounts of Q to a 0.1 M NaCl aqueous solution (pH 7.0) containing 0.5 mM AH_2. The anodic peak around +0.25 V observed in the absence of Q (curve a) shows the irreversible oxidation of AH_2. As seen in Figure 4.12, the addition of Q made the anodic peak shift negatively to around +0.13 V corresponding to the oxidation peak of QH_2, even if the added concentration was lower than the equivalent point, i.e., 0.5 mM (curve d). This suggests that QH_2 produced by the reaction with AH_2 should function as an electron mediator for the oxidation of AH_2 remaining unreacted. It should also be noted that the anodic peak current was not very dependent on the added concentration of Q, probably being limited by the initial concentration of AH_2. On the other hand, the cathodic peak current due to the rereduction of Q increased remarkably with an increase in the added concentration of Q, showing that Q certainly reacted with

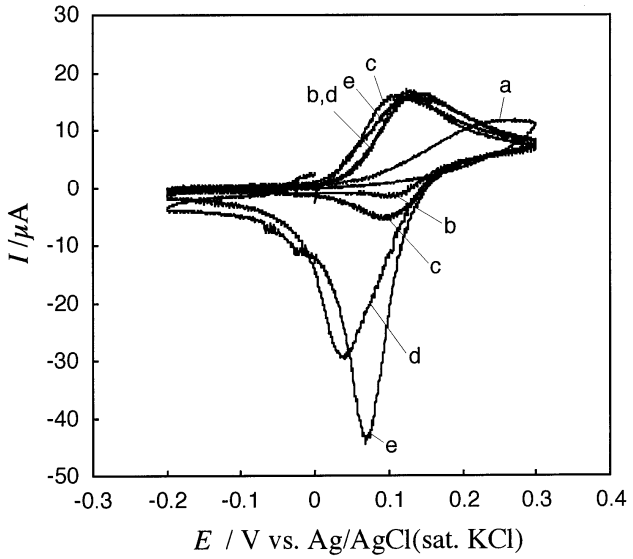

Figure 4.12. Cyclic voltammograms recorded with the PFC electrode 10 min after the addition of different amounts of Q to a 0.1 M NaCl aqueous solution (pH 7.0) containing 0.5 mM AH_2. Q was added as the stock solution in acetonitrile so that the concentration became (a) 0 mM; (b) 0.10 mM; (c) 0.25 mM; (d) 0.5 mM; (e) 0.75 mM (suspension). The potential scan was made as: 0 V $\rightarrow$ +0.3 V $\rightarrow$ –0.2 V $\rightarrow$ 0 V. Scan rate: 0.1 V s^{-1}.

AH_2 and dissolved in the solution as QH_2. Since the cathodic peak showed characteristics of an adsorption wave, we failed to deduce the reaction stoichiometry from the concentration dependence. However, when Q was added at higher concentration than 0.5 mM, the test solution turned turbid owing to unreacted Q, indicating that the mole ratio of AH_2 to Q is 1 : 1. Thus, it has been confirmed that AH_2 undergoes 2-electron oxidation by Q in the aqueous solution, in accordance with reaction (4.4). Similar 2-electron oxidation reactions of AH_2 by stable free radicals were reported [16–18].

On the whole the system of interest could be elucidated by the mechanism shown in Figure 4.10. However, there may be a necessity to take account of some subreaction(s). For example, the distribution of QH_2 formed by the reaction with ascorbic acid cannot be thoroughly excluded, because QH_2 is somewhat hydrophobic. For redox reactions between NADH and quinone derivatives at the 1,2-dichloroethane/water interface [4], it has been reported that a neutral species such as QH_2 is formed in the DCE phase as a reaction product. Supposing that the interfacial transfer of QH_2 occurs in the present system, the faradaic current should be reduced, because the electric charge provided for chloranil by ascorbic acid are transported not only by $Q^{\bullet -}$ but also by neutral QH_2 giving no faradaic current. This may be the reason why the *n* values determined by polarography are a little smaller than 2 (see Table 4.1). In this study, however, we have not made a rigorous theoretical analysis in which the interfacial transfer of QH_2 is also considered, since it seems quite cumbersome or impossible.

In the published paper [19], we tentatively performed a theoretical analysis of the polarographic current–potential curve, which assumed a definite thickness (μ) of the reaction layer (see Figure 4.10). Although the analysis could explain the pH dependence

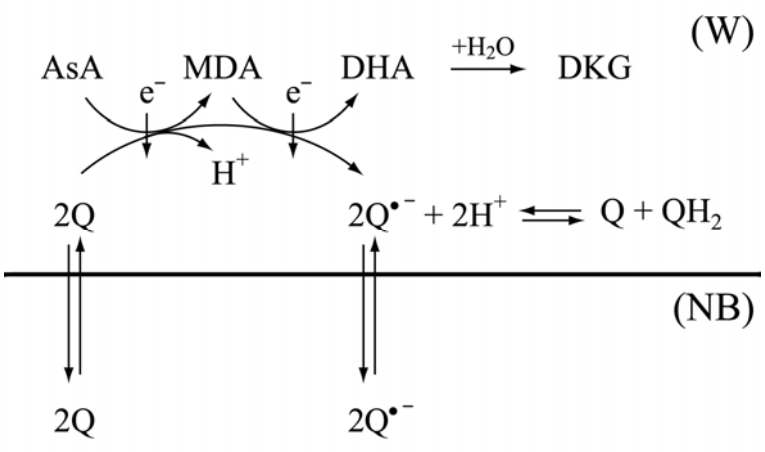

Figure 4.13. Proposed mechanism for the oxidation of AsA by Q at the NB/W interface. In this “2 step” electron transfer mechanism, the two electron oxidation of AsA in the W phase occurs in two one-electron steps. MDA = monodehydro-L-ascorbic acid. DKG = 2,3-diketo-L-gulonic acid.

of $E_{1/2}$ (Figure 4.4), it gave no good explanation for the dependences on the concentrations of AH_2 and Q. Recently, however, the author's coworkers [20] have performed digital simulation analyses of cyclic voltammograms, which requires no vague assumptions. The reaction mechanism shown in Figure 4.10 has been improved significantly providing better explanation on the voltammetric behaviors. In the newly proposed mechanism (Figure 4.13), it is assumed that the homogeneous 2-electron oxidation of AH_2 in W should occur stepwise by one electron.

References

[1] A.G. Volkov, D.W. Deamer, D.L. Tanelian, and V.S. Markin, *Liquid Interfaces in Chemistry and Biology*; Wiley, New York, 1998.

[2] M. Suzuki, S. Umetani, M. Matsui, and S. Kihara, J. Electroanal. Chem. 420 (1997) 119.

[3] M. Suzuki, M. Matsui, and S. Kihara, J. Electroanal. Chem. 438 (1997) 147.

[4] H. Ohde, K. Maeda, Y. Yoshida, and S. Kihara, Electrochim. Acta 44 (1998) 23.

[5] T. Osakai, S. Himeno, and A. Saito, J. Electroanal. Chem. 332 (1992) 169.

[6] T. Osakai, S. Himeno, and A. Saito, Bull. Chem. Soc. Jpn. 64 (1991) 1313.

[7] S. Sawada, T. Osakai, and M. Senda, Bunseki Kagaku 45 (1996) 1045.

[8] S. Aoyagi, M. Matsudaira, T. Suzuki, H. Katano, S. Sawada, H. Hotta, S. Ichikawa, T. Sugihara, and T. Osakai, Electrochemistry 70 (2002) 329.

[9] A.J. Bard, and L.R. Faulkner, *Electrochemical Methods*; Wiley, New York, 1980; p. 148.

[10] J.J. Andre, and G. Weill, Mol. Physics 15 (1968) 97.

[11] K. Kawai, Y. Shirota, H. Tsubomura, and H. Mikawa, Bull. Chem. Soc. Jpn. 45 (1972) 77.

[12] R. Gschwind, and E. Haselbach, Helv. Chim. Acta. 62 (1979) 941.

[13] J.J. Ruiz, A. Aldaz, and M. Domínguez, Can. J. Chem. 55 (1977) 2799.

[14] P. Karabinas, and D. Jannakoudakis, J. Electroanal. Chem. 160 (1984) 159.

[15] *CRC Handbook of Chemistry and Physics*, 80th ed.; Ed. D.R. Lide; CRC Press, Boca Raton, 1999.

[16] M.S. Blois, Nature 181 (1958) 1199.

[17] M. Ohnishi, H. Morishita, H. Iwahashi, S. Toda, Y. Shirataki, M. Kimura, and R. Kido, Phytochemistry 36 (1994) 579.

[18] M. B. Arnao, A. Cano, J. Hernández-Ruiz, F. García-Cánovas, and M. Acosta, Anal. Biochem. 236 (1996) 255.

[19] T. Osakai, N. Akagi, H. Hotta, J. Ding, and S. Sawada, J. Electroanal. Chem. 490 (2000) 85.

[20] T. Sugihara, H. Hotta, and T. Osakai, Bunseki Kagaku 52 (2003) in press.

Chapter 5. Electron Transfer between Ferrocene and Hexacyanoferrate(III) at the Oil/Water Interface

5.1 Introduction

Samec et al. [1] first employed cyclic voltammetry to observe an interfacial redox reaction between ferrocene (Fc) in nitrobenzene (NB) and $Fe(CN)_6^{3-}$ in W:

$$Fc\ (O) + Fe(CN)_6^{3-}\ (W) \rightleftharpoons Fc^+\ (O) + Fe(CN)_6^{4-}\ (W) \qquad (5.1)$$

However, a possible complicated mechanism has been discussed [2]:

$$Fc\ (O) \rightleftharpoons Fc\ (W) \qquad (5.2a)$$

$$Fc\ (W) + Fe(CN)_6^{3-}\ (W) \rightleftharpoons Fc^+\ (W) + Fe(CN)_6^{4-}\ (W) \qquad (5.2b)$$

$$Fc^+\ (W) \rightleftharpoons Fc^+\ (O) \qquad (5.2c)$$

In this so-called IT mechanism, the interfacial transfer of ferricenium ion (Fc^+) being generated by a homogeneous ET reaction in W is responsible for the current passage across the interface. However, if all equilibria are quite mobile, the IT mechanism is not distinguishable from that described as a single-step ET (equation (5.1)). Accordingly, kinetic behavior is essential for clarification of the ET reaction mechanism.

So far, certain efforts have been devoted to study the Fc–$Fe(CN)_6^{3-}$ system using cyclic voltammetry [3–5], convolution potential sweep voltammetry [6], current scan polarography [7], a.c. impedance method [8], voltammetry with micro liquid/liquid interfaces [9], scanning electrochemical microscopy (SECM) [10], and laser trapping of a single oil droplet [11], etc. Noteworthy kinetic behaviors were observed, particularly when the concentration of Fc was lower [1,7], but were discussed mainly in terms of a simple heterogeneous ET such as equation (5.1). On the other hand, a recent microelectrochemical study with expanding droplets suggested an IT of Fc^+ generated in the Fc (DCE)–$IrCl_6^{2-}$ (W) system [12]. This seems to support the IT mechanism shown by equations 5.2a–5.2c, but no definitive conclusion has been drawn for the reaction mechanism.

Recently, we have devised a new electrochemical system for characterizing ET processes at the O/W interface; this is named “electron conductor separating oil–water (ECSOW) system” (see chapter 2). It should be noted that in the ECSOW system, no IT occurs through the EC phase. The ECSOW system is thermodynamically equivalent to the corresponding O/W interface, as far as only a simple ET as shown in equation (5.1) occurs either at the O/W interface or via the electron-conductor phase in the ECSOW system. Nevertheless, they may be different from a kinetic viewpoint. In practice, cyclic voltammograms of the Fc–$Fe(CN)_6^{3-}$ system at the NB/W interface showed different features from those obtained with the ECSOW system, especially when the concentrations of the redox species in both phases were lower. While the

voltammograms for the ECSOW system could be elucidated in terms of a simple, reversible ET catalyzed by the EC phase, those for the NB/W interface suggested the existence of a kinetically controlled process. In this study, I have employed a digital simulation technique to show that the kinetic voltammograms with the NB/W interface can be elucidated in terms of the IT mechanism. Although the presently-used, four-electrode cyclic voltammetry might be conventional, its combination with the digital simulation technique allows us to obtain no less information about the reaction mechanism than the recently-introduced modern techniques. Furthermore, the validity of the IT mechanism has been confirmed by spectrophotometric detection of Fc^+ in the W phase with a conventional spectrophotometric cell and the microflow cell developed in chapter 3. We have also attempted a discussion as to why heterogeneous ET did not occur at the interface, based on a theoretical estimation of the diffusion-controlled rate constant at the O/W interface (chapter 6).

5.2 Experimental

5.2.1 Chemicals

Analytical grade reagents of ferrocene (Aldrich), $K_3Fe(CN)_6$ (Wako Pure Chemical Industries, Ltd.), $K_4Fe(CN)_6$ (trihydrate; Wako), and $Na_4Fe(CN)_6$ (Wako) were used as received. An aqueous solution of $Na_3Fe(CN)_6$ was prepared by electrolysis of an aqueous solution of $Na_4Fe(CN)_6$ with a flow column electrolytic cell (Hokuto Denko Co., HX-203); the electrolysis potential was +0.40 V vs. Ag/AgCl (saturated KCl). The synthesis of tetrapentylammonium tetraphenylborate (TPnATPB), the preparation of an aqueous solution of tetrapentylammonium chloride (TPnACl; Tokyo Kasei Industry Co., Ltd.), and the purification of analytical grade nitrobenzene (Wako) were described in chapter 2. All other reagents were of analytical grade and used as received.

5.2.2 Electrochemical measurements

Cyclic voltammetric measurements with stationary NB/W interfaces were performed using a microcomputer controlled four-electrode potentiostat (Hokuto Denko, HA1010mM1A) which was equipped with a positive feedback circuit for ohmic drop compensation [14]. The electrolytic cell used can be expressed as:

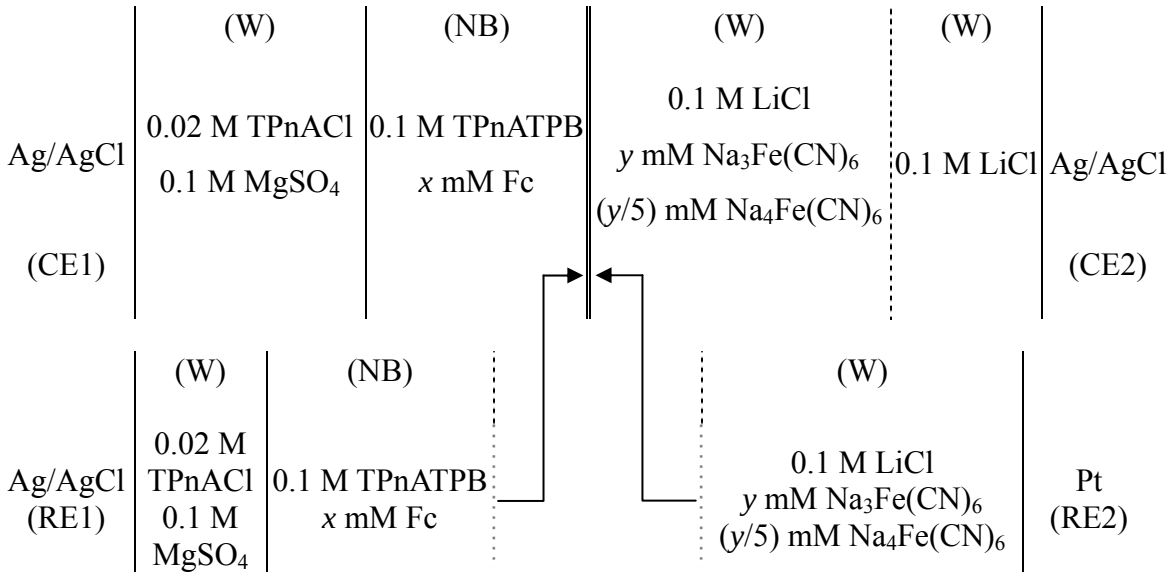

Cell 5A

where || represents the test NB/W interface (geometric area, 0.074 cm^2), the potential difference of which was controlled using the two reference electrodes (RE1 and RE2) immersed in the respective phases by means of Luggin capillaries whose tips were located near the NB/W interface. The solution resistance (~3.5 kΩ) between the tips of the Luggin capillaries was usually compensated for by 95% [13]. The current flowing through the test interface was detected by means of the two counter electrodes (CE1 and CE2). For each voltammetric scan, the test interface was renewed by pouring an aqueous solution from a reservoir.

For measurements with the ECSOW system, an EC phase was inserted between the NB and W phases (i.e., at the NB/W interface indicated by || in Cell 5A). This system can be feasibly realized by immersing in the NB and W phases two Pt disk electrodes connected by an electric wire, as shown in Figure 2.1. Prior to each measurement, the electrode surfaces (area, 0.020 cm^2) were freshly polished with a 0.25 μm diamond slurry and rinsed with distilled water or acetone in an ultrasonic field. Voltammetric measurements with the ECSOW system were performed in a similar manner to those with the above NB/W interface, except that potassium salts of the hexacyanoferrates were used instead of the sodium salts.

Determination of the standard ion-transfer potential of Fc^+ at the NB/W interface was made by using the following cell:

	(W)	(NB)	(W)	(W)	
Ag/AgCl (RE1)	0.02 M TPnACl 0.1 M $MgSO_4$	0.1 M TPnATPB 10 mM Fc	0.1 M LiCl	0.1 M LiCl	Ag/AgCl (RE2)

Cell 5B

The counter electrode for the NB phase was a Pt coil electrode directly immersed in the phase, whereas that for the W phase was also a Pt coil electrode, which was immersed in a 0.1 M LiCl solution connected with the W phase through a glass sinter. Fc^+ was generated in the NB phase by electrolysis with a Pt disk electrode (surface area, 0.071 cm^2) which was located as close as 1 mm from the NB/W interface. The electrode potential of the Pt disk electrode was controlled in a three-electrode configuration with RE1 and the above Pt coil counter electrode immersed in NB. After 10-min electrolysis at +0.70 V, the transfer of Fc^+ across the NB/W interface was voltammetrically observed using Cell 5B in a four-electrode configuration.

It has been claimed that the organic supporting-electrolyte anion used in the above measurements (i.e., TPB^-) had a catalytic influence on the reduction of Fc^+ in 1,2-DCE [3,14]. In our preliminary study, however, no distinct influence was observed in a voltammetric oxidation of Fc at Pt electrode in the NB solution containing 0.1 M TPnATPB. A supplementary experiment where TPnATPB was changed with the tetrakis(4-chlorophenyl)borate salt (known as a more stable electrolyte) was also performed for a typical case as shown later in Figure 5.2A. However, no marked difference was observed, and the validity of the use of TPnATPB as the organic supporting electrolyte in NB was shown.

For all the electrochemical measurements, test solutions were purged with N_2 gas, and electrolytic cells were thermostatted at 25.0 ± 0.1 °C.

5.2.3 Digital simulation of cyclic voltammograms

Calculations of cyclic voltammograms were performed by a normal explicit finite difference (EFD) digital simulation technique [15,16] with an exponentially expanding space grid method [16,17] (see Appendix). Simulation programs were written in Microsoft Visual Basic and used for manual curve-fitting analyses. Generally in digital simulation for a system including chemical reaction(s), the calculation interval of potential, ΔE, should be made small enough that the calculated voltammogram is not dependent on ΔE. In this study, ΔE was set at 5–100 nV. Validity of a program for the reversible ET mechanism was checked by referring to the previous numerical analysis

[18].

In the calculation of cyclic voltammograms, the initial concentrations of redox species were regarded as their "added" concentrations. However, these conditions are not necessarily met for practical voltammetric measurements. For the IT mechanism (equations (5.2a)–(5.2c)), the transfer of the electrically neutral redox species (i.e., Fc) into W can proceed spontaneously, or, even without electrochemical control, until an equilibrium is attained. Nevertheless, the cyclic voltammograms calculated by using the equilibrium concentrations for the initial conditions were practically the same as those calculated by using the added concentrations. Also in experiments, the cyclic voltammograms for the Fc–$Fe(CN)_6^{3-}$ system were not affected by the standing time before starting a voltage sweep.

5.2.4 Distribution experiment

The NB–W partition coefficient of Fc was determined by a solvent extraction experiment. Fc was initially added to 20 mL of NB so that the concentration became 0.05–0.5 M and then distributed to 70 mL of W. After standing overnight at 25 ± 0.1 °C, Fc in the W phase was back-extracted into 20 mL of *n*-hexane. Almost the whole solvent was evaporated using a rotary vacuum evaporator; to the resultant condensed Fc solution, 2 mL of NB was then added. Finally, the concentration of Fc in the NB solution was determined spectrophotometrically (molar absorption coefficient: $\varepsilon = 342$ at 450 nm).

5.2.5 Spectrophotometric measurements without electrochemical control

A spontaneous redox reaction between Fc (NB) and $Fe(CN)_6^{3-}$ (W) under no electrochemical control was monitored by means of a photodiode array spectrophotometer (Shimadzu, MultiSpec-1500). The experimental setup was similar to that described in Figure 4.2. An interface between a 0.8 mL NB solution of 100 mM Fc and 1.4 mL pure water was formed in a 1 cm quarts cell, and both the phases were stirred. After an hour, an aliquot of a condensed hexacyanoferrate(III)/(II) aqueous solution was injected to the W phase so that the concentrations became $[K_3Fe(CN)_6]_W = 5 \times [K_4Fe(CN)_6]_W = 10$ mM, and then absorption spectra of the W phase were recorded at a time interval of 15 s.

5.2.6 Spectrophotometric measurements under potentiostatic conditions

The spontaneous reaction between Fc and $Fe(CN)_6^{3-}$ was also observed under potentiostatic conditions using the microflow cell. The experimental setup is shown in Figure 5.1. The microflow cell shown in Figures 3.1 and 3.2 was slightly modified by changing the positions of solution inlet and outlet ports. As shown in the figure, the microflow cell was combined on-line with the photodiode assay spectrophotometer.

The microflow cell was operated in a three-electrodes configuration:

	(W)	(NB)	(NB)	(W) (mobile phase)	(W)	
Ag/AgCl (CE1)	0.1 M LiCl	0.1 M TBATPB 100 mM Fc	PTFE membrane	0.1 M LiCl	dialysis membrane	Ag/AgCl (CE2)

	(W)	(NB)
Ag/AgCl (RE1)	0.02 M TBACl 0.1 M $MgSO_4$	0.1 M TBATPB *x* mM Fc

Cell 5C

A 50 μL aliquot of a 2.0 mM $Fe(CN)_6^{3-}$ aqueous solution was injected into the mobile phase (0.1 M LiCl aqueous solution; flow rate = 100 μL min^{-1}) from a sample injector (Rheodyne 7725).

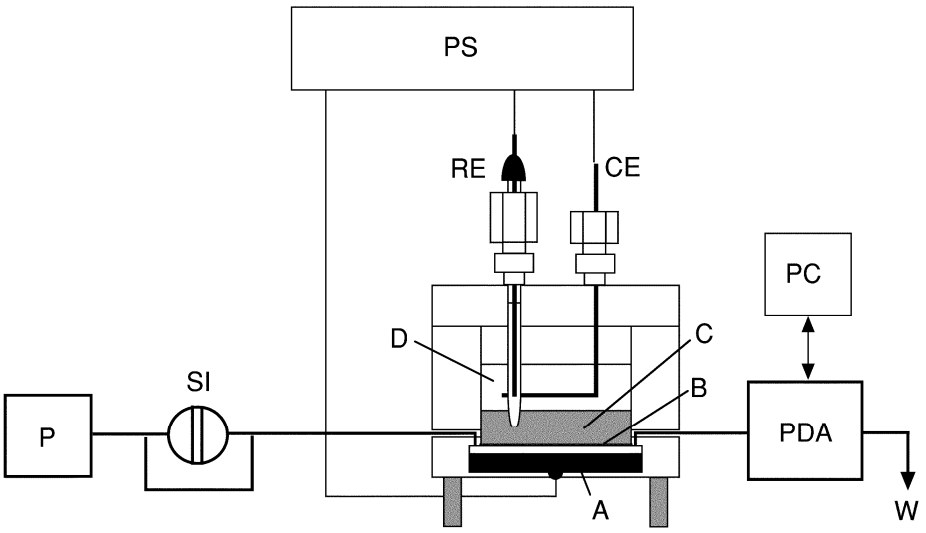

Figure 5.1. Scheme of the microflow electrolysis system with on-line spectrophotometric detection of the electrolysis product: (A) Ag/AgCl plate electrode covered with a dialysis membrane, (B) Teflon membrane, (C) NB phase containing 0.1 M Fc, (D) 0.1 M LiCl aqueous solution, (RE) reference electrode, (CE) counter electrode, (PS) potentiostat (Hokuto Denko, HA1010mM1S), (P) syringe pump (World Precision Instruments, Inc., SP100i), (SI) sample injector, (PDA) photodiode array spectrophotometer (Shimadzu MultiSpec 1500), (PC) personal computer, (W) waste.

5.3 Results

5.3.1 Kinetic behaviors of the cyclic voltammograms

Figure 5.2 shows the cyclic voltammograms for (A) the O/W interface and (B) the ECSOW system in the presence of various concentrations (1–100 mM) of Fc in NB and 0.5 mM $Fe(CN)_6^{3-}$ + 0.1 mM $Fe(CN)_6^{4-}$ in W. At the highest Fc concentration (i.e., $[Fc]_O$ = 100 mM), the voltammetric waves observed with both the systems were almost identical in appearance (see Figure 2.2). This clearly shows that these two systems are thermodynamically equivalent. Under such conditions, one cannot discuss the reaction mechanism.

As shown in chapter 2 the voltammetric behavior observed for the ECSOW system

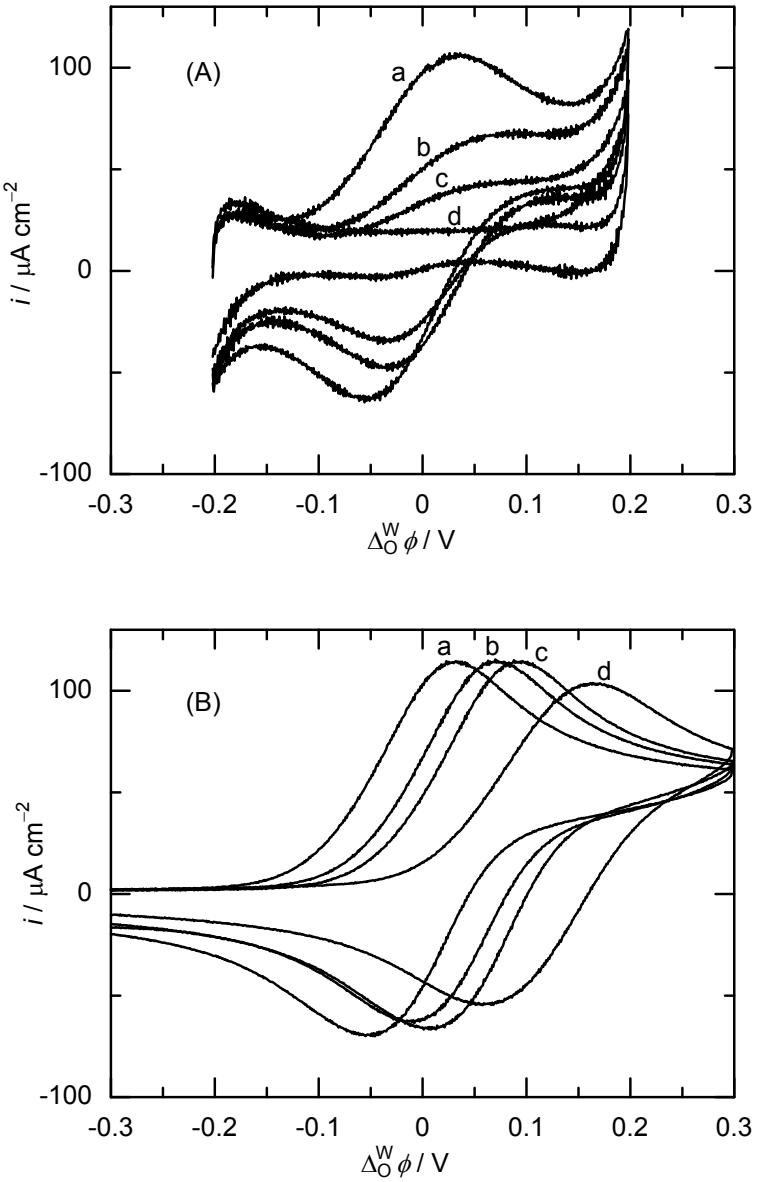

Figure 5.2. Cyclic voltammograms observed with (A) the O/W interface and (B) the corresponding ECSOW system in the presence of (a) 100, (b) 20, (c) 10, and (d) 1 mM Fc in NB and 0.5 mM $Fe(CN)_6^{3-}$ + 0.1 mM $Fe(CN)_6^{4-}$ in W. Sweep rate: 0.1 V s^{-1}.

can be well elucidated by assuming reversible redox reactions at the Pt electrode surfaces in the O and W phases:

$$\mathrm{Fc\,(O)} \rightleftharpoons \mathrm{Fc^{+}\,(O)} + \mathrm{e^{-}} \tag{5.3a}$$

$$\mathrm{Fe(CN)_6^{3-}\,(W)} + \mathrm{e^{-}} \rightleftharpoons \mathrm{Fe(CN)_6^{4-}\,(W)} \tag{5.3b}$$

The voltammograms shown in Figure 5.2B could be completely reproduced by digital simulation in which the equilibrium electromotive force of the ECSOW system is given by the Nernst equation:

$$E = E_{\mathrm{ET}}^{\circ'} + \frac{RT}{nF} \ln\left(\frac{[\mathrm{R1}]_{\mathrm{W}}[\mathrm{O2}]_{\mathrm{O}}}{[\mathrm{O1}]_{\mathrm{W}}[\mathrm{R2}]_{\mathrm{O}}}\right) \tag{5.4}$$

where O1 = $Fe(CN)_6^{3-}$, R1 = $Fe(CN)_6^{4-}$, R2 = Fc, and O2 = Fc^+; the brackets [ ]$_W$ and [ ]$_O$ denote the equilibrium concentrations of the redox species in the W and O phases, respectively; n is the number of electrons involved in the interfacial redox reaction (here, n = 1); R, T, and F have their usual meanings; and $E_{\mathrm{ET}}^{\circ'}$ is the formal potential determined by

$$\begin{aligned} E_{\mathrm{ET}}^{\circ'} &= \left(E_{\mathrm{O2/R2}}^{\circ'} - E_{\mathrm{O1\,/\,R1}}^{\circ'}\right) + \Delta E_{\mathrm{ref}} \\ &= \Delta_{\mathrm{O}}^{\mathrm{W}}\phi_{\mathrm{ET}}^{\circ'} + \Delta E_{\mathrm{ref}} \\ &= \Delta_{\mathrm{O}}^{\mathrm{W}}\phi_{\mathrm{ET}}^{\circ} + \frac{RT}{nF}\ln\left(\frac{\gamma_{\mathrm{R1}}^{\mathrm{W}}\gamma_{\mathrm{O2}}^{\mathrm{O}}}{\gamma_{\mathrm{O1}}^{\mathrm{W}}\gamma_{\mathrm{R2}}^{\mathrm{O}}}\right) + \Delta E_{\mathrm{ref}} \end{aligned} \tag{5.5}$$

Here, $E_{\mathrm{O2/R2}}^{\circ'}$ and $E_{\mathrm{O1/R1}}^{\circ'}$ are the formal potentials of the redox couples in the respective phases, which are expressed on a same potential scale; $\Delta_{\mathrm{O}}^{\mathrm{W}}\phi_{\mathrm{ET}}^{\circ'}$ and $\Delta_{\mathrm{O}}^{\mathrm{W}}\phi_{\mathrm{ET}}^{\circ}$ are the formal and standard redox potentials for the ET system; γ_i^{α} (α = W or O) is the activity coefficient of redox species i in the α phase; and ΔE_{ref} is a constant which is determined only by the reference electrodes used. In this study, all interfacial potentials refer to the mid-point potential (= 0.546 V in Cell 5A) for the reversible transfer of tetramethylammonium (TMA^+) ion from W to NB, whose standard ion-transfer potential ($\Delta_{\mathrm{O}}^{\mathrm{W}}\phi_{\mathrm{TMA^+}}^{\circ}$) is known to be +0.035 V [19]. Then, ΔE_{ref} for Cell A was evaluated to be 0.502 V in a similar manner as described previously [20]. By fitting the simulation curves into experimental voltammograms in Figure 5.2B, the standard potential of the heterogeneous ET could be determined as $E_{\mathrm{ET}}^{\circ'}$ = 0.625 V in Cell A, i.e., $\Delta_{\mathrm{O}}^{\mathrm{W}}\phi_{\mathrm{ET}}^{\circ'}$ = 0.123 V; the diffusion coefficients of Fc in the NB phase and of $Fe(CN)_6^{3-}$ and $Fe(CN)_6^{4-}$ in the W phase were determined in chapter 2 (see the caption of Figure 2.3).

In contrast to the ECSOW system usually showing the reversible ET, the O/W interface gave kinetically controlled voltammograms under certain conditions; when the

Fc concentration was decreased, the anodic peak current (I_{pa}) was significantly depressed and showed plateau, as seen in Figure 5.2A. This result is essentially the same as reported previously by Samec et al. [1]. Figure 5.3 shows the dependence of I_{pa} on the square root of the voltage sweep rate (v). At higher Fc concentrations (i.e., $[Fc]_O$ = 200 and 100 mM), the I_{pa} vs. $v^{1/2}$ plot shows an almost straight line crossing the origin expected for the diffusion-controlled current, however, at lower Fc concentrations (20 and 10 mM), the plot deviated too much from the straight line even at lower vs.

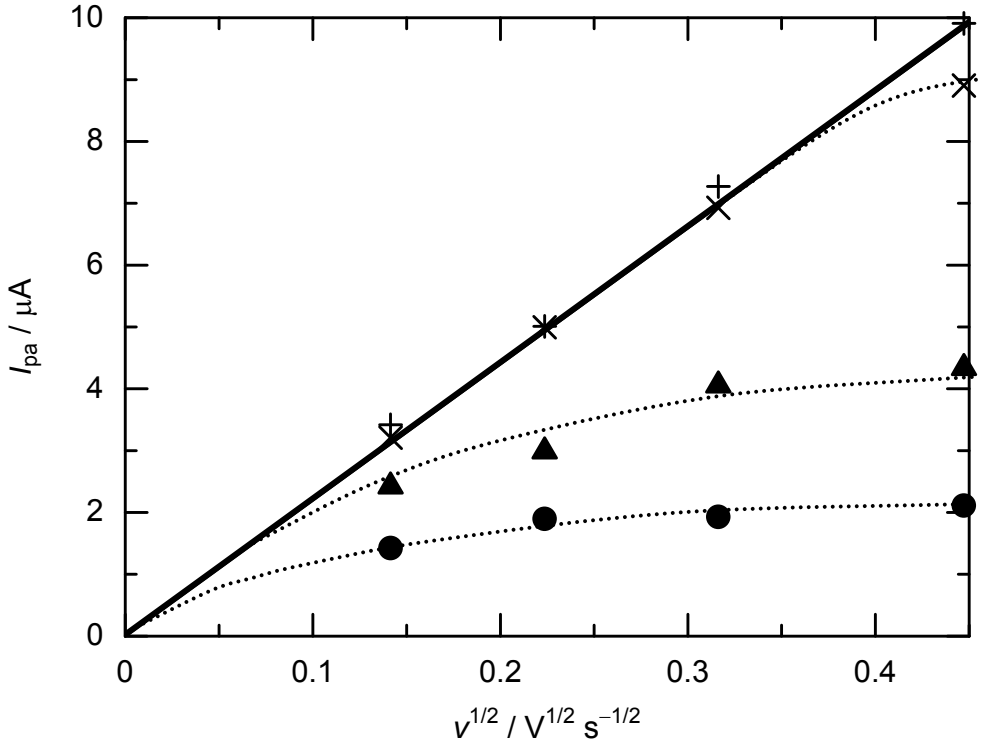

Figure 5.3. Sweep rate dependence of the anodic peak current for the voltammograms observed with the O/W interface in the presence of (+) 200, (×) 100, (▲) 20, and (●) 10 mM Fc in NB and 0.5 mM $Na_3Fe(CN)_6$ + 0.1 mM $Na_4Fe(CN)_6$ in W.

5.3.2 Digital simulation analysis based on the electron transfer mechanism

First, we assumed a simple heterogeneous ET mechanism to simulate cyclic voltammograms using the digital simulation technique [15,16]. In this case, the second-order rate constants of the forward (k_f) and backward (k_b) reactions of equation (5.1) are given by the Butler–Volmer equations:

$$k_f = k^\circ \exp\left[\frac{(1-\alpha)nF}{RT}\left(\Delta_O^W\phi - \Delta_O^W\phi_{ET}^{\circ'}\right)\right] \quad (5.6a)$$

$$k_b = k^\circ \exp\left[-\frac{\alpha nF}{RT}\left(\Delta_O^W\phi - \Delta_O^W\phi_{ET}^{\circ'}\right)\right] \quad (5.6b)$$

where $k°$ is the standard rate constant at $\Delta_O^W\phi = \Delta_O^W\phi_{ET}^{\circ'}$, and α the transfer coefficient. Using $k°$ and α as adjusting parameters and the beforehand-determined standard potential and diffusion coefficients, we performed a manual curve-fitting analysis for the voltammograms shown in Figure 5.2A. Only when α was assumed to be close to unity (with $k° = 0.12$ M^{-1} cm s^{-1} and $\Delta_O^W\phi_{ET}^{\circ'} = 0.123$ V), a satisfactory result was achieved, as

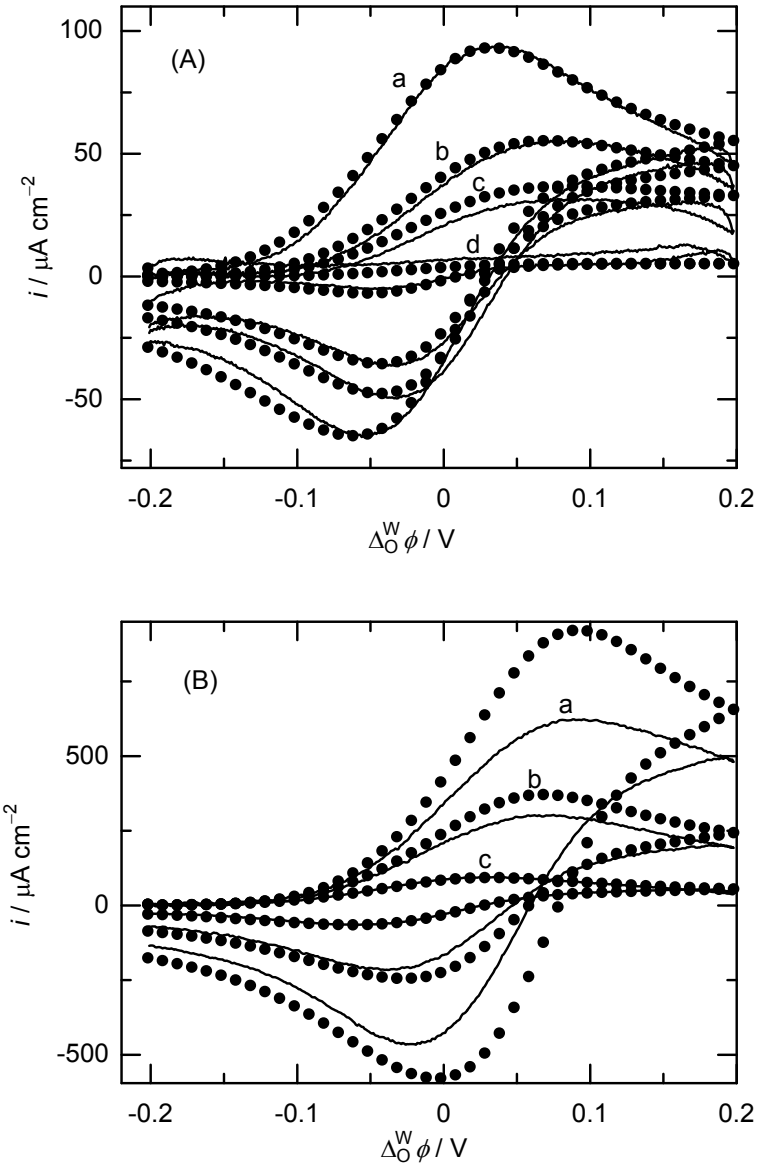

Figure 5.4. Base-line corrected cyclic voltammograms observed with the O/W interface by changing the concentration of (A) Fc in NB or (B) $Na_3Fe(CN)_6$ in W. (A): $[Fc]_O$ = (a) 100, (b) 20, (c) 10, and (d) 1 mM; $[Na_3Fe(CN)_6]_W = 5 \times [Na_4Fe(CN)_6]_W = 0.5$ mM. (B): $[Fc]_O$ = 100 mM; $[Na_3Fe(CN)_6]_W = 5 \times [Na_4Fe(CN)_6]_W$ = (a) 5, (b) 2, and (c) 0.5 mM. Sweep rate: 0.1 V s^{-1}. The solid circles in either (A) or (B) show the simulation data obtained by assuming the Butler–Volmer formalism. The adjusting parameters used are: $k°$ = 0.12 M^{-1} cm s^{-1}; α = 1.0; the others as described in the text.

shown in Figure 5.4A. The α value of 1 is rather different from the value of 0.56 that is expected from the Marcus theory (see Discussion). Furthermore, when the concentration of $Fe(CN)_6^{3-}$ in the W phase was changed in turn from 0.5 to 5 mM at a constant $[Fc]_O$ (= 100 mM), the observed voltammograms could not be simulated using the same parameter set as in Figure 5.4A (see Figure 5.4B which represents large deviations between the simulation and experimental curves). This is the case for the voltammograms recorded under the concentration conditions reverse to those in Figures 5.4A and 5.4B, i.e., $[Fc] < [Fe(CN)_6^{3-}]$ (data not shown). Thus, the interfacial ET mechanism (equation (5.1)) could not give a good explanation for the present system.

5.3.3 Digital simulation analysis based on the IT mechanism

We then employed the IT mechanism (equations (5.2a)–(5.2c)) to perform a digital simulation analysis. The IT mechanism is represented schematically in Figure 5.5. In the present analysis, the distribution of Fc at the O/W interface was assumed to be always in equilibrium, i.e.,

$$\frac{[Fc]_O}{[Fc]_W} = K_D(\text{constant}) \tag{5.7}$$

The value of K_D was independently determined to be 6×10^3 by the solvent extraction experiment described above. This value is somewhat larger than a literature value of 1.2×10^3 [21], but in good agreement with another value of 7×10^3 [22]. Because the interfacial IT reaction is generally very fast, the IT of Fc^+ (= O2) across the O/W interface was assumed to obey the Nernst equation:

$$\begin{aligned}\Delta_O^W\phi &= \Delta_O^W\phi^\circ_{Fc^+} + \frac{RT}{F}\ln\left(\frac{\gamma^O_{Fc^+}}{\gamma^W_{Fc^+}}\right) + \frac{RT}{F}\ln\left(\frac{[Fc^+]_O}{[Fc^+]_W}\right) \\ &= \Delta_O^W\phi^{\circ'}_{Fc^+} + \frac{RT}{F}\ln\left(\frac{[Fc^+]_O}{[Fc^+]_W}\right)\end{aligned} \tag{5.8}$$

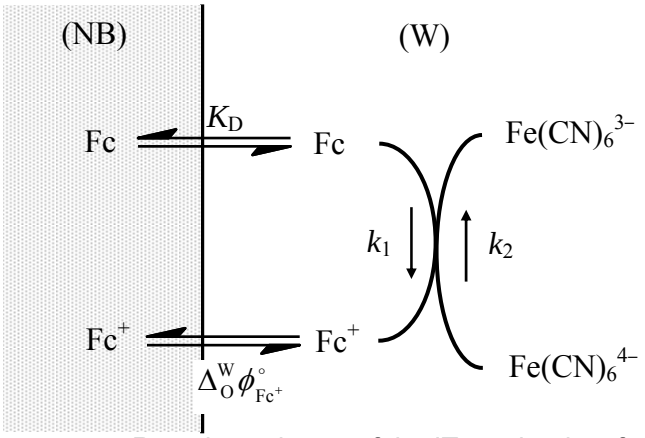

Figure 5.5. Reaction scheme of the IT mechanism for the Fc (NB)–$Fe(CN)_6^{3-}$ (W) system. For details, see the text.

The formal ion-transfer potential of Fc^+ ($\Delta_O^W\phi_{Fc^+}^{\circ'}$) was determined to be –0.096 V as described above. This value is in reasonable agreement with a literature value [2] of –0.075 V. In the digital simulation, equation (5.8) was employed for relating the "interfacial" concentrations of Fc^+ in the two phases (see Appendix; equation (5.A18)), however it should be valid also for the "equilibrium" concentrations.

The kinetically-controlled process in the IT mechanism is the homogeneous ET between Fc and $Fe(CN)_6^{3-}$ in the W phase. The reaction rate (v_{hom}) is expressed as

$$\begin{aligned} v_{hom} &= -\frac{d[R2]_W}{dt} = \frac{d[O2]_W}{dt} = -\frac{d[O1]_W}{dt} = \frac{d[R1]_W}{dt} \\ &= k_1[R2]_W[O1]_W - k_2[O2]_W[R1]_W \end{aligned} \tag{5.9}$$

where t is the time, and k_1 and k_2 are the forward and backward second-order rate constants, respectively. In equilibrium (i.e., $v_{hom} = 0$), we obtain

$$\frac{[R1]_W[O2]_W}{[O1]_W[R2]_W} = \frac{k_1}{k_2} = K_{hom} \tag{5.10}$$

When the overall ET reaction across the O/W interface is in equilibrium, equation (5.4) should be valid regardless of the reaction mechanism adopted. Therefore, we can rewrite equation (5.4) for the present case, by replacing E and $E_{ET}^{\circ'}$ with $\Delta_O^W\phi$ and $\Delta_O^W\phi_{ET}^{\circ'}$, respectively:

$$\Delta_O^W\phi = \Delta_O^W\phi_{ET}^{\circ'} + \frac{RT}{F}\ln\left(\frac{[R1]_W[O2]_O}{[O1]_W[R2]_O}\right) \tag{5.11}$$

We assume for the simplicity that $\gamma_{O1}^W/\gamma_{R1}^W = \gamma_{O2}^O/\gamma_{R2}^O = 1$ and $\gamma_{O2}^O/\gamma_{O2}^W = 1$, and then obtain from equations (5.7), (5.8), (5.10), and (5.11) the following relation:

$$K_D \exp\left[\frac{F}{RT}\left(\Delta_O^W\phi_{Fc^+}^{\circ'} - \Delta_O^W\phi_{ET}^{\circ'}\right)\right] = K_{hom} = \frac{k_1}{k_2} \tag{5.12}$$

By substituting to equation (5.12) the known-values of $\Delta_O^W\phi_{Fc^+}^{\circ'}$ and $\Delta_O^W\phi_{ET}^{\circ'}$, K_{hom} was estimated to be 1.19. This value is in good agreement with that calculated from the redox potential difference between Fc^+/Fc in water (0.40 V vs. NHE [2]) and $Fe(CN)_6^{3-}$/$Fe(CN)_6^{4-}$ (0.41 V vs. NHE; in this study). As seen in equation (5.12), k_1 and k_2 are related with each other, therefore the unknown parameter is only k_1 (or, alternatively, k_2). The diffusion coefficients of Fc and Fc^+ in W required for the digital simulation were assumed to be identical and estimated to be 1.2×10^{-5} cm^2 s^{-1} from the diffusion coefficient of Fc in NB ($D^{NB} = 0.56 \times 10^{-5}$ cm^2 s^{-1}) on the assumption that $D^W/D^{NB} = 2$ (i.e., the reciprocal of the viscosity ratio of water and NB). In this manner, we carried out

digital simulation using a sole fitting parameter (i.e., k_1). When k_1 was set to be 2.0×10^7 M^{-1} s^{-1}, the curve fitting was successful for the voltammograms observed under any concentration conditions (Figure 5.6A–5.6D). It should be stressed that the same parameter set was employed for the calculation of all sets of voltammograms.

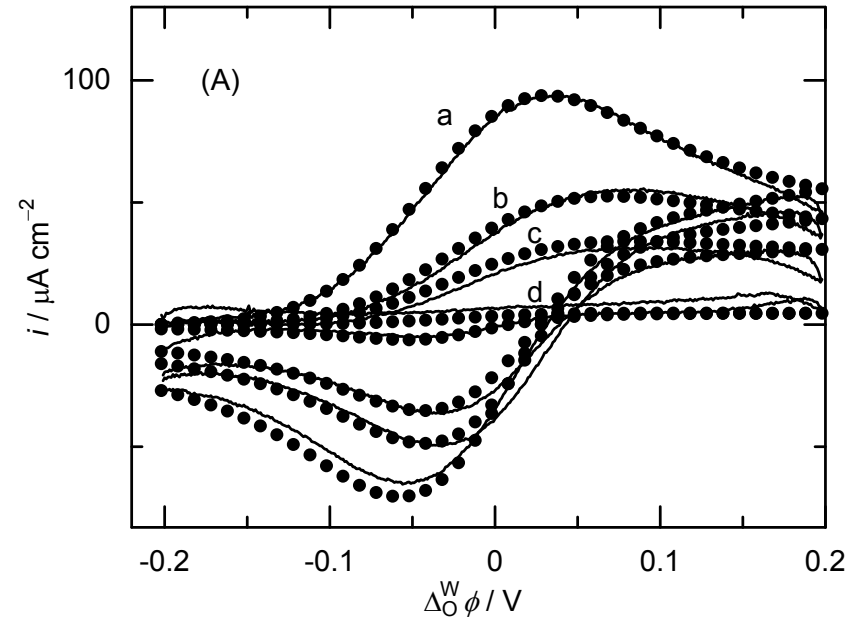

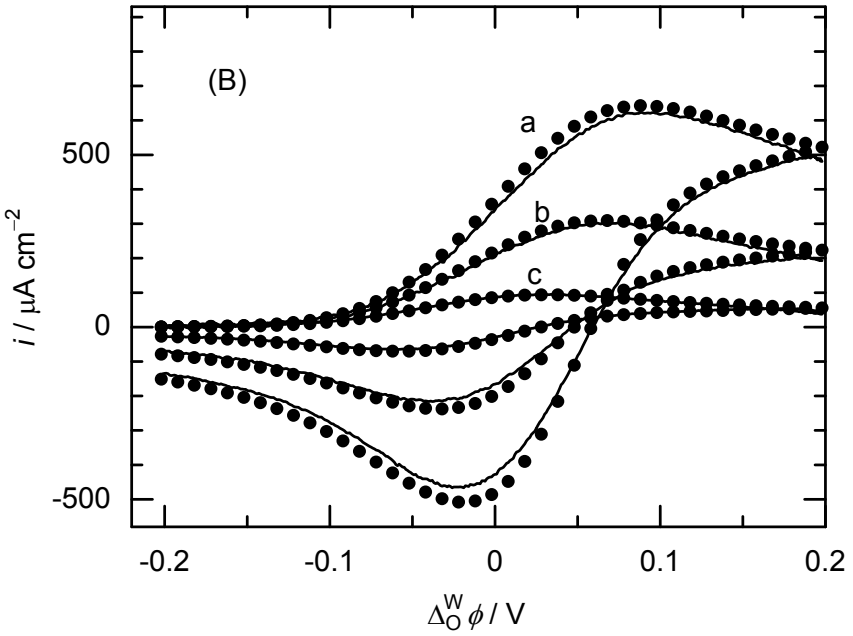

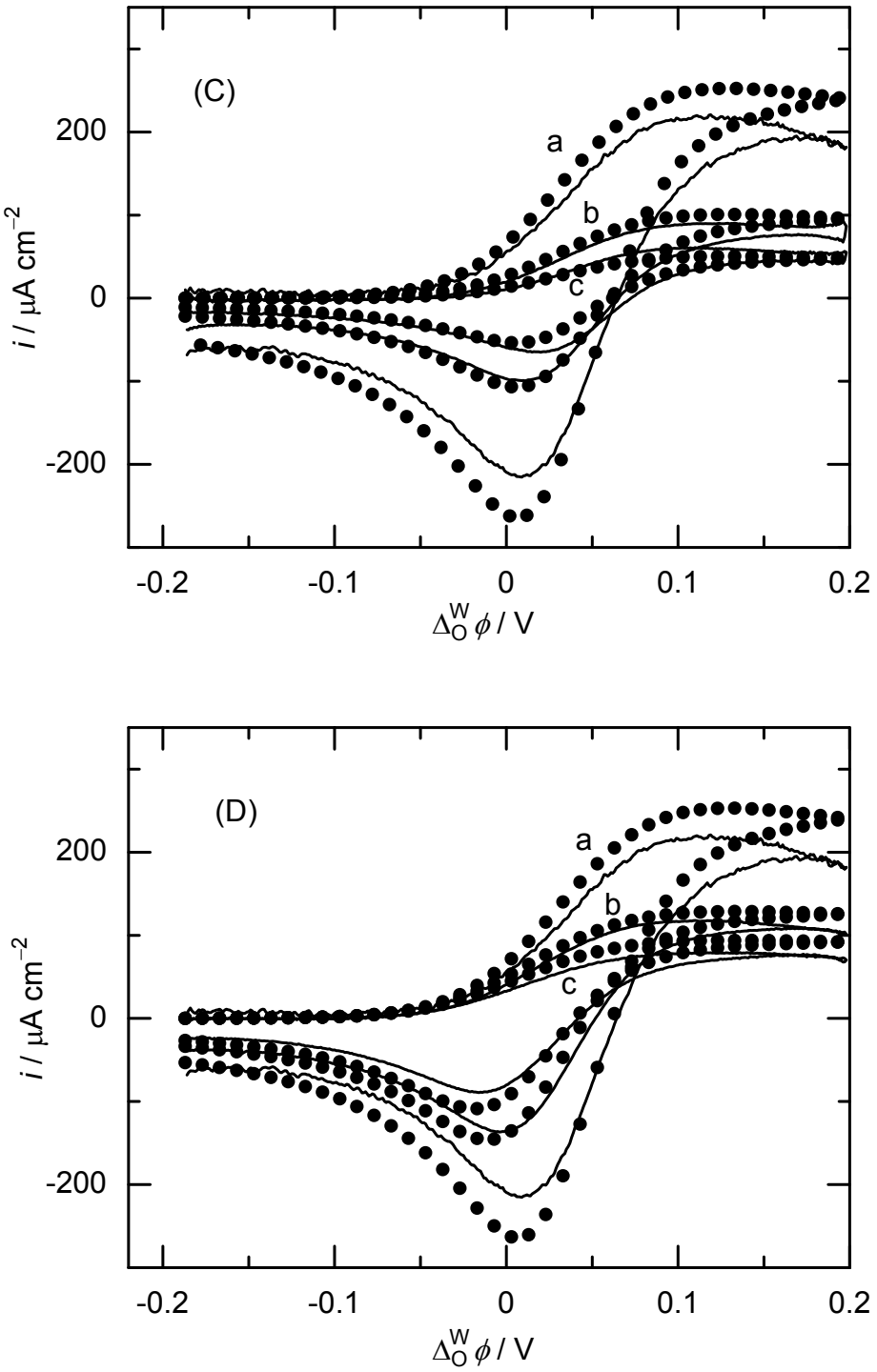

Figure 5.6. Base-line corrected cyclic voltammograms observed with the O/W interface: (A, C) by changing the Fc concentration in NB; (B, D) by changing the $Na_3Fe(CN)_6$ concentration in W. The concentration conditions in (A) and (B) are the same as those in Figure 5.4A and 5.4B, respectively. (C): $[Fc]_O$ = (a) 5, (b) 2, and (c) 1 mM; $[Na_3Fe(CN)_6]_W = 5 \times [Na_4Fe(CN)_6]_W$ = 100 mM. (D): $[Fc]_O$ = 5 mM; $[Na_3Fe(CN)_6]_W = 5 \times [Na_4Fe(CN)_6]_W$ = (a) 100, (b) 20, and (c) 10 mM. Sweep rate: 0.1 V s^{-1}. The solid circles show the regression data obtained by assuming the IT mechanism shown in Figure 5.5.

5.3.4 Spectrophotometric measurement

If the IT mechanism is valid, the reaction steps other than the IT of Fc^+ should occur spontaneously without electrochemical control. In practice, an absorption spectrum change of the W phase could be observed for the use of the conventional spectrophotometric cell, as shown in Figure 5.7. The absorption peak around 620 nm increased with time until it reached an equilibrium value (see the inset of Figure 5.7). This undoubtedly showed the formation of Fc^+ in the W phase, since a flow–column electrolysis of Fc in water–acetone revealed that Fc^+ had an absorption maximum at 620 nm. This result would also support the IT mechanism.

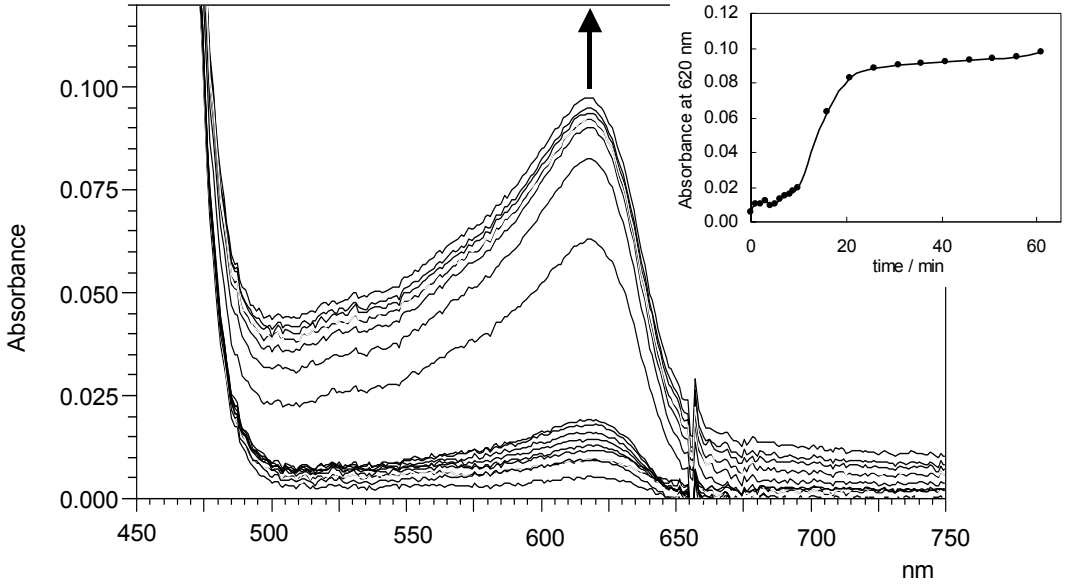

Figure 5.7. Absorption spectrum change of the W phase without electrochemical control. $[Fc]_O$ = 100 mM; $[K_3Fe(CN)_6]_W$ = 5 × $[K_4Fe(CN)_6]_W$ = 10 mM. The absorption spectra were recorded at a time interval of 15 s. The inset shows the time dependence of the absorbance at 620 nm.

Figure 5.8 shows the cyclic voltammogram of the ET between 100 mM Fc in NB and 2 mM $Fe(CN)_6^{3-}$ in W, which was recorded using the microflow cell. Although the separation between anodic and cathodic peak potential was somewhat larger than that expected for an ordinary stationary O/W interface, a well-developed voltammetric wave was obtained. The potential dependence of the electrolysis

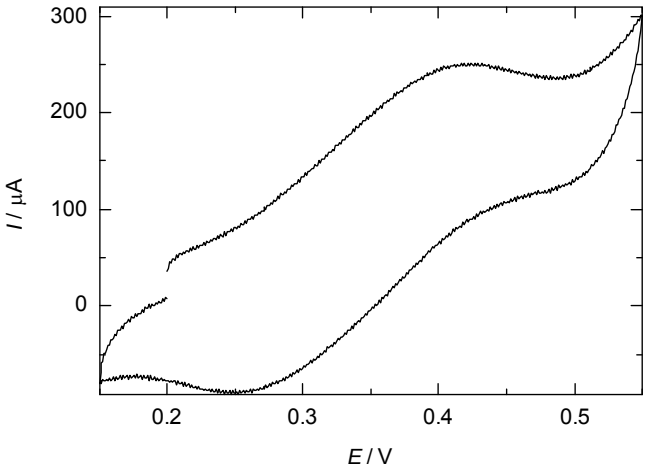

Figure 5.8. Cyclic voltammogram of the ET between 100 mM Fc in NB and 2 mM $Fe(CN)_6^{3-}$ obtained by using microflow cell.

efficiency for this system (at the flow rate of 100 μL min^{-1}) is shown in Figure 5.9. The electrolysis efficiency increased with the applied potential and reached a satisfactory level (~91%) at around 0.55 V. Figure 5.10 shows the potential dependence of the absorption spectrum of the electrolyzed aqueous mobile phase. At a lower potential (e.g., 0.15 V), where the electrical current due to the ET between Fc and $Fe(CN)_6^{3-}$ could not be observed (cf. Figure 5.8), an absorption maximum of ~620 nm was observed. This is the direct evidence for the existence of Fc^+ in the W phase, which would support the IT mechanism. On the other hand, the absorption decreased with the increase of the applied potential. This is because Fc^+, which is probably produced in the W phase, is transferred from W to NB at higher potentials.

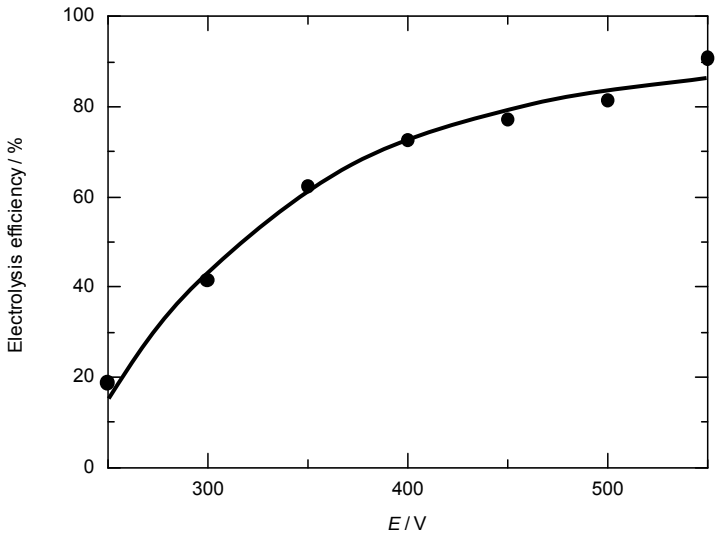

Figure 5.9. Potential dependence of the electrolysis efficiency for the ET between Fc (NB) and $Fe(CN)_6^{3-}$ (W) at the microflow cell. Flow rate: 100 μL min^{-1}.

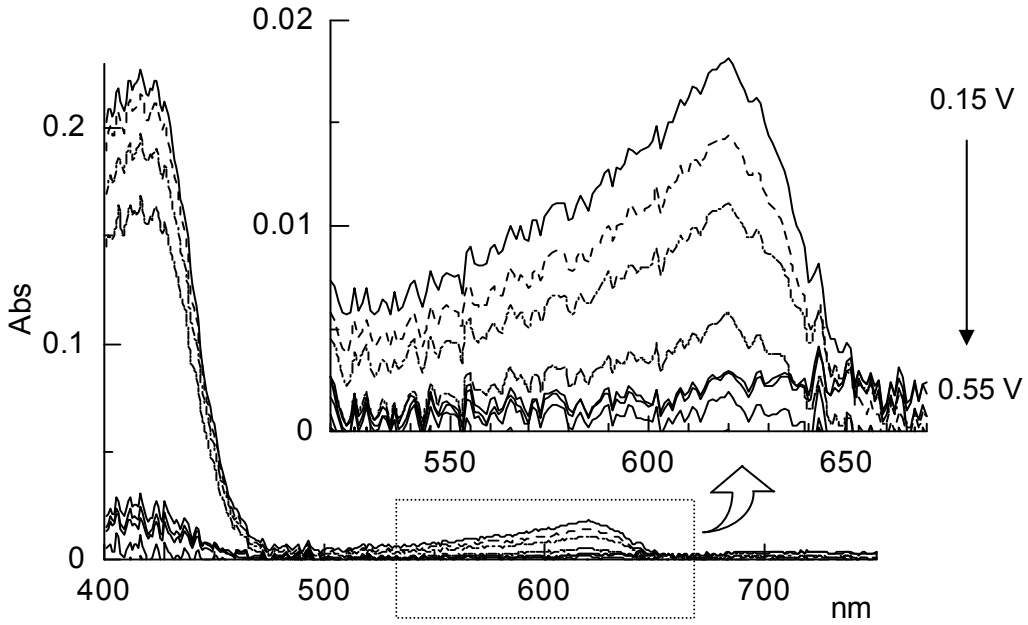

Figure 5.10. Interfacial potential dependence of the absorption spectrum of the aqueous mobile phase for the ET between Fc (NB) and $Fe(CN)_6^{3-}$ (W).

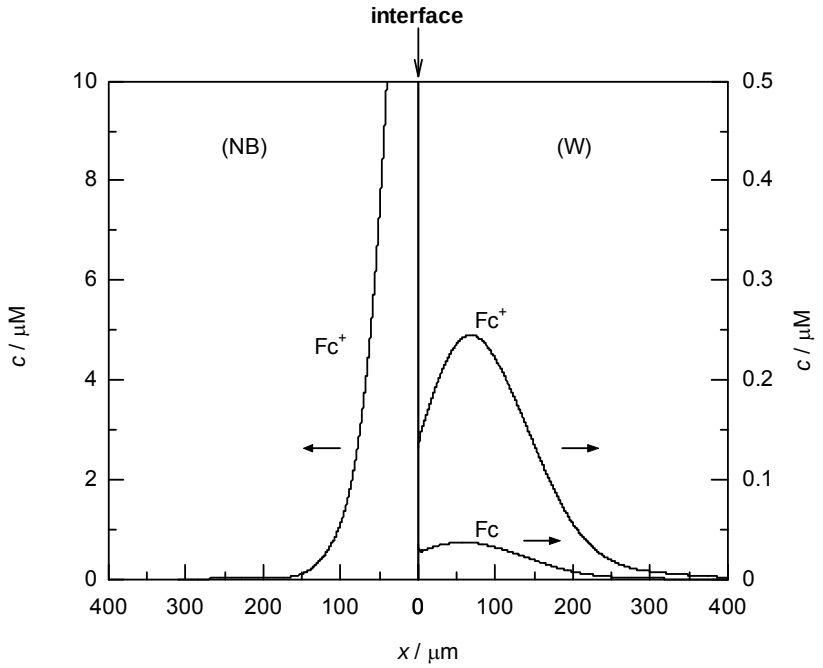

Figure 5.11. A snapshot of concentration profiles of Fc and Fc^+, obtained by the digital simulation based on the IT mechanism, at $\Delta_O^W\phi$ = 0.14 V (i.e., 3.4 s after a voltammetric sweep at 0.1 V s^{-1}). Initial conditions: $[Fc]_O$ = 1.0 mM, $[Fe(CN)_6^{3-}]_W$ = 5 × $[Fe(CN)_6^{4-}]_W$ = 0.5 mM. The concentration profile of Fc in NB is omitted.

5.4 Discussion

The above results clearly showed that in the Fc–$Fe(CN)_6^{3-}$ system, ET should occur not at the O/W interface but in the W phase. In order to verify this, we further calculated the concentration profiles of Fc^+ and Fc, based on the above-mentioned digital simulation of cyclic voltammograms. Figure 5.11 shows a snapshot of the concentration profiles of Fc^+ and Fc at $\Delta_O^W\phi$ = 0.14 V, which was obtained for a typical voltammetric sweep at 0.1 V s^{-1}. As can be seen in the figure, the concentration of either Fc^+ or Fc in the W phase shows a maximum at ca. 80 μm, as a consequence of the competitive ET and diffusion. It should here be noted that the reaction layer in the W phase grows up to ca. 200 μm in the course of the voltammetric sweep of a few seconds. In contrast, the reaction field for the heterogeneous ET should be restricted to an interfacial layer as thin as several Angstroms as shown in Figure 5.12. Therefore, the volume of reaction field for the homogeneous ET would be ~10^6 times larger than that for the heterogeneous ET. Such a large difference in the volume of reaction field leads to the most crucial advantage of the IT mechanism, which would overcome its disadvantage, i.e., the small partition of Fc into the W phase (cf. $K_D = 6 \times 10^3$).

Thus the volume of reaction field is a key factor for determining the reaction pathway or mechanism, but it would be worthwhile to consider theoretically the rate constants of the heterogeneous as well as homogeneous ETs. Recently, we have proposed a theoretical

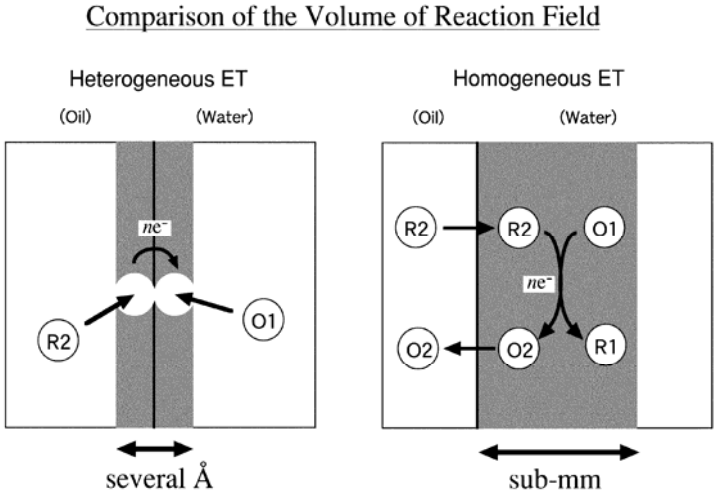

Figure. 5.12. Comparison of the volume of reaction field between the heterogeneous and homogeneous ETs. The thickness of the reaction field for the homogeneous ET was estimated by a digital simulation analysis for the Fc (NB)–$Fe(CN)_6^{3-}$ (W) system.

equation for the diffusion-controlled rate constant of heterogeneous ET at the O/W interface by extension of the Smoluchowski–Debye theory (see chapter 6) for a bimolecular reaction in homogeneous solution (see chapter 6). Using the following parameters: $r_A = 3.8 \times 10^{-8}$ cm [23], $r_B = 4.4 \times 10^{-8}$ cm [24], $D_A^O = 0.56 \times 10^{-5}$ cm^2 s^{-1}, and $D_B^W = 0.90 \times 10^{-5}$ cm^2 s^{-1}, the $k_{D,het}$ value can be estimated for the Fc (NB)–$Fe(CN)_6^{3-}$ (W) system (note here that A = Fc and B = $Fe(CN)_6^{3-}$). The $k_{D,het}$ is calculated to be 114, and 71 M^{-1} cm s^{-1} when the reaction rate is limited by the diffusion of $Fe(CN)_6^{3-}$ and Fc, respectively. Accordingly, the $k_{D,het}$ for the present system is considered as 71 M^{-1} cm s^{-1}.

Previously, Marcus derived an Arrhenius-type general kinetic equation for heterogeneous ET at a sharp O/W interface as described in chapter 1. The pre-exponential frequency factor Z is the "maximum" value of k at $\Delta G^{\ddagger} = 0$ (not necessarily realizable), and it is thus interesting to compare the Z factor with the value of $k_{D,het}$ (71 M^{-1} cm s^{-1}). Using $\kappa\nu = 10^{12}$ s^{-1} and $\Delta R = 1 \times 10^{-8}$ cm, which were adopted by Marcus [25], the Z factor is calculated to be 310 M^{-1} cm s^{-1} for the Fc–$Fe(CN)_6^{3-}$ system. This value is about four times larger than the $k_{D,het}$ value estimated above (i.e., 71 M^{-1} cm s^{-1}).

In the following, we calculate the standard rate constant using equations (1.7)–(1.9). $\Delta G^{\ddagger}$ has been evaluated by substituting into equation (1.8) the following values: $w^r = 3.4$ kJ mol^{-1} [26]; $w^p = -6.8$ kJ mol^{-1} [26]; $\lambda_o = 78.8$ kJ mol^{-1} [27]; $\lambda_i(Fc) = 0.6$ kJ mol^{-1} [28]; $\lambda_i(Fe(CN)_6^{3-/4-}) = 10.6$ kJ mol^{-1} [29]; and $\Delta G° = -F(\Delta_O^W\phi - \Delta_O^W\phi^{\circ}) = 0$ yields $\Delta G^{\ddagger} = 18.5$ kJ mol^{-1} at $\Delta_O^W\phi = \Delta_O^W\phi^{\circ} \approx \Delta_O^W\phi_{ET}^{\circ'}$. Using the value of $\Delta G^{\ddagger}$, $k°$ (i.e., k at $\Delta_O^W\phi = \Delta_O^W\phi_{ET}^{\circ'}$) is estimated to be 0.064 M^{-1} cm s^{-1}. This $k°$ value is enough small than the $k_{D,het}$ value, and

is comparative with the experimental value (0.12 M^{-1} cm s^{-1}) which was tentatively obtained by assuming the ET mechanism. However, we should direct our attention not only to the $k°$ value but also to the α value which will be evaluated based on the Marcus theory as follows: Substituting $-F(\Delta_O^W\phi - \Delta_O^W\phi^\circ)$ for $\Delta G°$ in equation (1.8) yields

$$\Delta G^{\ddagger} = \Delta G^{\circ\ddagger} - \frac{1}{2}F\left(\Delta_O^W\phi - \Delta_O^W\phi^\circ\right) + \frac{1}{4\lambda}\left\{F^2\left(\Delta_O^W\phi - \Delta_O^W\phi^\circ\right)^2 - 2F\left(\Delta_O^W\phi - \Delta_O^W\phi^\circ\right)\left(w^p - w^r\right)\right\} \tag{5.13}$$

where $\Delta G^{\circ\ddagger}$ stands for $\Delta G^{\ddagger}$ at $\Delta_O^W\phi = \Delta_O^W\phi^\circ$. When $F|\Delta_O^W\phi - \Delta_O^W\phi^\circ|/2\lambda \ll 1$, equation (5.13) is reduced to

$$\Delta G^{\ddagger} = \Delta G^{\circ\ddagger} - \frac{1}{2}\left(1 + \frac{w^p - w^r}{\lambda}\right)F\left(\Delta_O^W\phi - \Delta_O^W\phi^\circ\right) \tag{5.14}$$

Comparing this equation with the following relation in the classical Butler–Volmer formalism (note that $\Delta_O^W\phi^\circ \approx \Delta_O^W\phi_{ET}^{\circ'}$),

$$\Delta G^{\ddagger} = \Delta G^{\circ\ddagger} - (1 - \alpha)F\left(\Delta_O^W\phi - \Delta_O^W\phi_{ET}^{\circ'}\right) \tag{5.15}$$

and using the above w^r, w^p, and λ, we can calculate α to be 0.56. As described above, however, the α value obtained by assuming the ET mechanism is unity, being rather different from the theoretically-expected value. This would also imply the invalidity of the ET mechanism (equation (5.1)) for the present system, although the effect of electric double-layer [6] should be considered for a more rigorous discussion.

On the other hand, the homogeneous ET rate constant obtained by the fitting analysis of cyclic voltammograms based on IT mechanism is $k_1 = 2 \times 10^7$ M^{-1} s^{-1}. Although there is no literature about the rate constant for the Fc–$Fe(CN)_6^{3-}$ reaction in W, some rate constants ranging from 10^5 to $>10^8$ M^{-1} s^{-1} were reported for other bimolecular redox reactions in aqueous media in which hexacyanoferrates participate [30]. Also, the k_1 value is three-order lower than the diffusion-controlled rate constant (1.3×10^{10} M^{-1} s^{-1}) calculated by the Smoluchowski–Debye theory [31,32]. Thus, the k_1 value seems reasonable enough to conclude that the Fc (NB)–$Fe(CN)_6^{3-}$ (W) system can be well elucidated in terms of the IT mechanism.

As is evident from the above discussion, however, the reaction mechanism would be affected by hydrophobicity of the redox species in the O phase. The larger the K_D value, the more difficult to occur the homogeneous ET. If we use an extremely hydrophobic redox species in the O phase, the IT mechanism would not occur, and thus a heterogeneous ET would be realized. Further voltammetric studies are now in progress with some Fc derivatives substituted by methyl groups and other metal complexes.

Appendix. Digital simulation of cyclic voltammograms

The EFD method [15,16] was used to calculate cyclic voltammograms for the ET and IT mechanisms. In the calculation, we constructed a discrete model featuring two sequences of volume elements extending away from the O/W interface to the respective bulk phases. To shorten the calculation time, the exponentially expanding grid method [16,17] was used, in which the discretized distance (Δx) for a volume element is given by

$$\Delta x(j) = \Delta x \exp[\beta(j-1)] \tag{5.A1}$$

where j (= 1, 2, 3, · · ·) is the finite difference parameter for distance, and β is an arbitrary parameter (β = 0.5 for the IT mechanism, but β = 0 for the ET mechanism).

If there is no homogeneous ET reaction, the diffusion problem for a redox species, i, in phase X (= O or W) can be written in the finite difference form of Fick's second law: for $j \geq 2$,

$$f_i^{\mathrm{X}}(j,k+1) = f_i^{\mathrm{X}}(j,k) + \mathbf{D}_i^{\mathrm{X}}(j)'\left[f_i^{\mathrm{X}}(j+1,k) - f_i^{\mathrm{X}}(j,k)\right] - \mathbf{D}_i^{\mathrm{X}}(j)''\left[f_i^{\mathrm{X}}(j,k) - f_i^{\mathrm{X}}(j-1,k)\right] \tag{5.A2}$$

and for j = 1,

$$f_i^{\mathrm{X}}(1,k+1) = f_i^{\mathrm{X}}(1,k) + \mathbf{D}_i^{\mathrm{X}}(1)'\left[f_i^{\mathrm{X}}(2,k) - f_i^{\mathrm{X}}(1,k)\right] + J_i(0,k) \tag{5.A3}$$

In these equations, $f_i^{\mathrm{X}}(j,k)$ is the "dimensionless" concentration of species i in the jth element of phase X at the time of $k\Delta t$ (with k = 0, 1, 2, · · · ; Δt being the discretized time), which is defined by the relative concentration of the species with respect to the total concentration (C_{total}) for all the redox species involved in the O/W system; and $\mathbf{D}_i^{\mathrm{X}}(j)'$ and $\mathbf{D}_i^{\mathrm{X}}(j)''$ are defined as follows using the diffusion coefficient of species i in phase X (D_i^{X}), the maximum value among the D_i^{X} values for all species ($D_{\max}$), and the model diffusion coefficient ($\mathbf{D}_{\mathrm{M}}$) [16]:

$$\mathbf{D}_i^{\mathrm{X}}(j)' = \mathbf{D}_{\mathrm{M}} \frac{D_i^{\mathrm{X}}}{D_{\max}} \exp\left[2\beta\left(\frac{3}{4} - j\right)\right] \tag{5.A4}$$

$$\mathbf{D}_i^{\mathrm{X}}(j)'' = \mathbf{D}_{\mathrm{M}} \frac{D_i^{\mathrm{X}}}{D_{\max}} \exp\left[2\beta\left(\frac{5}{4} - j\right)\right] \tag{5.A5}$$

$$\mathbf{D}_{\mathrm{M}} \equiv \frac{D_i^{\mathrm{X}}\Delta t}{(\Delta x)^2} = 0.45 \tag{5.A6}$$

Finally, the remaining term in equation (5.A3), $J_i(0,k)$, is the dimensionless flux of species i across the interface written in the finite difference form of Fick's first law:

$$J_i(0,k) = -2\mathbf{D}_i^{\mathrm{X}}(1)''\left[f_i^{\mathrm{X}}(1,k) - f_i^{\mathrm{X}}(0,k)\right] \tag{5.A7}$$

At the calculation, we first give the calculation interval of potential (ΔE), and then Δx is

set by equation (5.A6) with $\Delta t = \Delta E/v$ (v, voltage sweep rate).

In the ET mechanism, it is assumed that the heterogeneous ET reaction:

$$\mathrm{O1(W) + R2(O)} \rightleftharpoons \mathrm{R1(W) + O2(O)} \tag{5.A8}$$

occurs only at the nearest array to the interface ($j = 0$), and the ET rate constants of the forward and backward reactions are given by the Butler–Volmer equations (equations (5.6a) and (5.6b)). The dimensionless flux of a redox species (e.g. O1) is then given by

$$J_{\mathrm{O1}} = -k_{\mathrm{f}}^{'} f_{\mathrm{O1}}^{\mathrm{W}}(0, k) f_{\mathrm{R2}}^{\mathrm{O}}(0, k) + k_{\mathrm{b}}^{'} f_{\mathrm{R1}}^{\mathrm{W}}(0, k) f_{\mathrm{O2}}^{\mathrm{O}}(0, k) \tag{5.A9}$$

where $k_{\mathrm{f}}^{'}$ and $k_{\mathrm{b}}^{'}$ are the dimensionless rate constants defined by multiplying k_{f} or k_{b} (equations (5.6a) and (5.6b)) by $C_{\mathrm{total}}\Delta t/\Delta x$. Considering the mass balance at the interface, we obtain

$$-J_{\mathrm{O1}}(0, k) = -J_{\mathrm{R2}}(0, k) = J_{\mathrm{R1}}(0, k) = J_{\mathrm{O2}}(0, k) = \frac{I(k)}{nFA} \bullet \frac{\Delta t}{C_{\mathrm{total}} \Delta x} \tag{5.A10}$$

where $I(k)$ is the current at $k\Delta t$. The combination of equations (5.A7), (5.A9), and (5.A10) leads to the following quadratic equation for $J_{\mathrm{O1}}(0,k)$:

$$AJ_{\mathrm{O1}}(0,k)^2 - BJ_{\mathrm{O1}}(0,k) + C = 0 \tag{5.A11}$$

with

$$A = -\frac{k_{\mathrm{f}}^{'}}{4\mathbf{D}_{\mathrm{O1}}^{\mathrm{W}}\mathbf{D}_{\mathrm{R2}}^{\mathrm{O}}} + \frac{k_{\mathrm{b}}^{'}}{4\mathbf{D}_{\mathrm{R1}}^{\mathrm{W}}\mathbf{D}_{\mathrm{O2}}^{\mathrm{O}}} \tag{5.A12}$$

$$B = \frac{k_{\mathrm{f}}^{'}}{2\mathbf{D}_{\mathrm{R2}}^{\mathrm{O}}} f_{\mathrm{O1}}^{\mathrm{W}}(1, k) + \frac{k_{\mathrm{f}}^{'}}{2\mathbf{D}_{\mathrm{O1}}^{\mathrm{W}}} f_{\mathrm{R2}}^{\mathrm{O}}(1, k) + \frac{k_{\mathrm{b}}^{'}}{2\mathbf{D}_{\mathrm{O2}}^{\mathrm{O}}} f_{\mathrm{R1}}^{\mathrm{W}}(1, k) + \frac{k_{\mathrm{b}}^{'}}{2\mathbf{D}_{\mathrm{R1}}^{\mathrm{W}}} f_{\mathrm{O2}}^{\mathrm{O}}(1, k) + 1 \tag{5.A13}$$

$$C = -k_{\mathrm{f}}^{'} f_{\mathrm{O1}}^{\mathrm{W}}(1, k) f_{\mathrm{R2}}^{\mathrm{O}}(1, k) + k_{\mathrm{b}}^{'} f_{\mathrm{R1}}^{\mathrm{W}}(1, k) f_{\mathrm{O2}}^{\mathrm{O}}(1, k) \tag{5.A14}$$

By solving equation (5.A11), we can obtain $J_{\mathrm{O1}}(0,k) = \frac{B - \sqrt{B^2 - 4AC}}{2A}$ and thus $I(k)$ using eq A10.

In the IT mechanism where a homogeneous ET occurs in the W phase, the concentration change of species i due to the chemical reaction, $\Delta f_{i,\mathrm{CR}}^{\mathrm{W}}(j, k+1)$, was calculated by

$$\Delta f_{i,\mathrm{CR}}^{\mathrm{W}}(j, k+1) = k_1^{'} f_{\mathrm{O1}}^{\mathrm{W}}(j, k) f_{\mathrm{R2}}^{\mathrm{W}}(j, k) - k_2^{'} f_{\mathrm{R1}}^{\mathrm{W}}(j, k) f_{\mathrm{O2}}^{\mathrm{W}}(j, k) \quad (\text{for } j \geq 1) \tag{5.A15}$$

where $k_1^{'}$ and $k_2^{'}$ are the dimensionless rate constants which correspond to k_1 and k_2 (cf. equation (5.9)). Independent of the effect of chemical reaction, the concentration change

due to diffusion was treated, i.e.,

$$f_i^{\mathrm{W}}(j,\, k\,+\,1) = f_{i,\mathrm{Diff}}^{\mathrm{W}}(j,\, k\,+\,1) \pm \Delta f_{i,\mathrm{CR}}^{\mathrm{W}}(j,\, k\,+\,1) \tag{5.A16}$$

where $f_{i,\mathrm{Diff}}^{\mathrm{W}}(j,k+1)$ was calculated using equation (5.A2) or (5.A3) for the case where there is no chemical reaction; the + sign corresponds to when i = O2 or R1, while the – sign to when i = O1 or R2.

The following relations were used for the distribution equilibria for Fc (= R2) and Fc^+ (= O2) at the interface (i.e., $j = 0$):

$$K_{\mathrm{D}} = \frac{f_{\mathrm{R2}}^{\mathrm{O}}(0,\, k)}{f_{\mathrm{R2}}^{\mathrm{W}}(0,\, k)} \tag{5.A17}$$

and

$$\frac{f_{\mathrm{O2}}^{\mathrm{O}}(0,\, k)}{f_{\mathrm{O2}}^{\mathrm{W}}(0,\, k)} = \exp\left[\frac{F}{RT}\left(\Delta_{\mathrm{O}}^{\mathrm{W}}\phi(k) - \Delta_{\mathrm{O}}^{\mathrm{W}}\phi_{\mathrm{O2}}^{\circ'}\right)\right] = \theta \tag{5.A18}$$

where $\Delta_{\mathrm{O}}^{\mathrm{W}}\phi(k)$ is the Galvani potential difference of the interface at the time of $k\Delta t$.

Considering the mass balance, we can obtain the following relations for the dimensionless fluxes of Fc and Fc^+ at the interface:

$$J_{\mathrm{R2}}^{\mathrm{W}}(0,\, k) = -J_{\mathrm{R2}}^{\mathrm{O}}(0,\, k) \tag{5.A19}$$

$$J_{\mathrm{O2}}^{\mathrm{O}}(0,\, k) = -J_{\mathrm{O2}}^{\mathrm{W}}(0,\, k) = \frac{I(k)}{FA} \bullet \frac{\Delta t}{C_{\mathrm{total}}\Delta x} \tag{5.A20}$$

Finally, the combination of equations (5.A7), (5.A17), and (5.A19) for R2 leads to

$$J_{\mathrm{R2}}^{\mathrm{O}}(0,\, k) = \frac{-\, f_{\mathrm{R2}}^{\mathrm{O}}(1,\, k) + K_{\mathrm{D}} f_{\mathrm{R2}}^{\mathrm{W}}(1,\, k)}{\dfrac{1}{2\mathbf{D}_{\mathrm{R2}}^{\mathrm{O}}(1)} + \dfrac{K_{\mathrm{D}}}{2\mathbf{D}_{\mathrm{R2}}^{\mathrm{W}}(1)}} \tag{5.A21}$$

and the combination of equations(5.A7), (5.A18), and (5.A20) for O2 leads to

$$J_{\mathrm{O2}}^{\mathrm{O}}(0,\, k) = \frac{-\, f_{\mathrm{O2}}^{\mathrm{O}}(1,\, k) + \theta f_{\mathrm{O2}}^{\mathrm{W}}(1,\, k)}{\dfrac{1}{2\mathbf{D}_{\mathrm{O2}}^{\mathrm{O}}(1)} + \dfrac{\theta}{2\mathbf{D}_{\mathrm{O2}}^{\mathrm{W}}(1)}} \tag{5.A22}$$

This equation with equation (5.A20) allows the calculation of I(k).

References and notes

[1] Z. Samec, V. Mareček, and J. Weber, J. Electroanal. Chem. 103 (1979) 11.

[2] J. Hanzlík, Z. Samec, and J. Hovorka, J. Electroanal. Chem. 216 (1987) 303.

[3] V.J. Cunnane, G. Geblewicz, and D.J. Schiffrin, Electrochim. Acta 40 (1995) 3005.

[4] J. Hanzlík, J. Hovorka, Z. Samec, and S. Toma, Collect. Czech. Chem. Commun. 53 (1988) 903.

[5] B. Quinn, and K. Kontturi, J. Electroanal. Chem. 483 (2000) 124.

[6] Z. Samec, V. Mareček, J. Weber, and D. Homolka, J. Electroanal. Chem. 126 (1981) 105.

[7] S. Kihara, M. Suzuki, K. Maeda, K. Ogura, M. Matsui, and Z. Yoshida, J. Electroanal. Chem. 271 (1989) 107.
[8] Q.Z. Chen, K. Iwamoto, and M. Seno, Electrochim. Acta 36 (1991) 291.
[9] B. Quinn, R. Lahtinen, L. Murtomäki, and K. Kontturi, Electrochim. Acta 44 (1998) 47.
[10] Z. Zhang, Yi Yuan, P. Sun, B. Su, J. Guo, and Y. Shao, J. Phys. Chem. 106 (2002) 6713.
[11] K. Chikama, K. Nakatani, and N. Kitamura, Bull. Chem. Soc. Jpn. 71 (1998) 1065.
[12] J. Zhang, C.J. Slevin, and P.R. Unwin, Chem. Commun. (1999) 1501.
[13] S. Aoyagi, M. Matsudaira, T. Suzuki, H. Katano, S. Sawada, H. Hotta, S. Ichikawa,T. Sugihara, and T. Osakai, Electrochemistry 70 (2002) 329.
[14] V.J. Cunnane, and L. Murtomäki, *Liquid-Liquid Interfaces, Theory and Methods*; Volkov, A.G.; Deamer, D.W., Eds.; CRC Press: Boca Raton, 1996; Chapter 18.
[15] S.W. Feldberg, *Electroanalytical Chemistry*, Vol. 3; Ed. A.J. Bard; Marcel Dekker, New York, 1969; pp. 199–296.
[16] A.J. Bard, and L.F. Faulkner, *Electrochemical Methods, Fundamentals and Applications*; Wiley, New York, 2001; p. 785–806.
[17] S.W. Feldberg, J. Electroanal. Chem. 127 (1981) 1.
[18] A.A. Stewart, J.A. Campbell, H.H. Girault, and M. Eddowes, Ber. Bunsenges. Phys. Chem. 94 (1990) 83.
[19] J. Koryta, P. Vanỳsek, and M. Březina, J. Electroanal. Chem. 75 (1977) 211.
[20] T. Osakai, S. Himeno, and A. Saito, J. Electroanal. Chem. 332 (1992) 169.
[21] C. Wei, A.J. Bard, and M.V. Mirkin, J. Phys. Chem. 99 (1995) 16033.
[22] K. Nakatani, T. Uchida, H. Misawa, N. Kitamura, and H. Masuhara, J. Electroanal. Chem. 367 (1994) 109.
[23] R.M. Nielson, G.E. McManis, M.N. Golovin, and M.J. Weaver, J. Phys. Chem. 92 (1988) 3441.
[24] Y. Marcus, *Ion Properties*; Marcel Dekker, New York, 1997; Chapter 3.
[25] R.A. Marcus, J. Phys. Chem. 95 (1991) 2010.
[26] The values of w^r and w^p were calculated from equation 20 in reference 21 using the static and optical dielectric constants of NB (35.7 and 2.4, respectively) and those of water (78.3 and 1.8).
[27] The value of λ_o was calculated from equation 16 in reference 21.
[28] T. Gennett, D.F. Milner, and M.J. Weaver, J. Phys. Chem. 89 (1985) 2787.
[29] P. Delahay, Chem. Phys. Lett. 99 (1983) 87.
[30] D.E. Pennington, *Coordination Chemistry*, Vol. 2, Ed. A.E. Martell; ACS, Washington, 1978; Chapter 3.
[31] M.V. Smoluchowski, Z. Phys. Chem. 92 (1917) 129.
[32] P. Debye, Trans. Electrochem. Soc. 82 (1942) 265.

Chapter 6. Diffusion Controlled Rate Constant of Electron Transfer at the Oil/Water Interface

6.1 Introduction

In previous chapters, the mechanisms of ET at the O/W interface have been studied, and it showed that the homogeneous ET proceeded more advantageously than the heterogeneous one. In both Q–AH_2 system (chapter 4) and Fc–$Fe(CN)_6^{3-}$ system (chapter 5), these ET reactions occurred homogeneously in the W phase. However, it is expected that the true ET can be obtained when a sufficiently hydrophobic redox species is used in the O phase. From this perspective, the previously reported ET systems involving hydrophobic complexes such as $LuPc_2$ [1–3] might be considered as heterogeneous ETs. Our preliminary study has also shown that some hydrophobic Fc derivatives such as dibutylferrocene and cyclohexenylferrocene may undergo heterogeneous ETs with $Fe(CN)_6^{3-}$ under certain concentration conditions. However, the rate of the heterogeneous ETs would suffer from a geometrical restriction, i.e., the existence of the O/W interface lying between the redox species in the respective phases. In this chapter, we have made a theoretical consideration on the rate of heterogeneous ET at the O/W interface. The diffusion-controlled rate constant of ET has been formulated in the analogy of the Smoluchowski–Debye theory [4–6] for diffusion-controlled reactions in homogeneous solutions. Its contribution to the overall rate constant has also been discussed.

6.2 Bimolecular reaction in homogeneous medium

The diffusion-controlled rate constant for a bimolecular reaction in homogeneous solution was estimated based on Fick's law [4–6]. Let us pay attention to a representative molecule (A) and some molecules (B) which diffuse toward A to react with it. The molar flux of B, j_B' (mol s^{-1}), across a spherical surface located at a distance of r (cm) from the center of A should be proportional to the concentration gradient, i.e.,

$$j_B' = 4\pi r^2 D_{AB} \frac{d[B]}{dr} \tag{6.1}$$

where the bracket [ ] represents the molar concentration (mol cm^{-3}), and D_{AB} (cm^2 s^{-1}) is the relative diffusion coefficient that is assumed to be given by the sum of the diffusion coefficients of A and B as

$$D_{AB} = D_A + D_B \tag{6.2}$$

In a diffusion-controlled reaction, when the contact of molecules A and B immediately yields the product, the concentration of B should be zero at $r = r_{AB} = r_A + r_B$ and the same as the bulk concentration at $r > r_{AB}$. Integration of equation 6.1 from $r = r_{AB}$

to $r = \infty$ under these conditions yields

$$j_B' = 4\pi r_{AB} D_{AB}[B] \tag{6.3}$$

which represents the flux of B to reach one A molecule. The total flux of B to reach all A molecules in a volume of V (cm^3) is then expressed by using the number of A molecules in V, N(A):

$$j_B = N(A)\, j_B' \tag{6.4}$$

Since the j_B is regarded as the diffusion-controlled rate, we obtain from equations (6.3) and (6.4):

$$\begin{aligned} \text{(diffusion-controlled rate)} \quad &= \frac{-\,dn_B}{dt} = j_B \\ &= 4\pi r_{AB} D_{AB}[B] N(A) \end{aligned} \tag{6.5}$$

where n_B is the mole number of B (mol) in V, and t the time (s).

The rate equation for a bimolecular second-order reaction is expressed as

$$-\frac{d[B]}{dt} = k_{hom}[A][B] \tag{6.6}$$

where k_{hom} the second-order rate constant ($cm^3\ mol^{-1}\ s^{-1}$). The concentration of A, [A], in equation (6.6) is given by

$$[A] = \frac{N(A)}{LV} \tag{6.7}$$

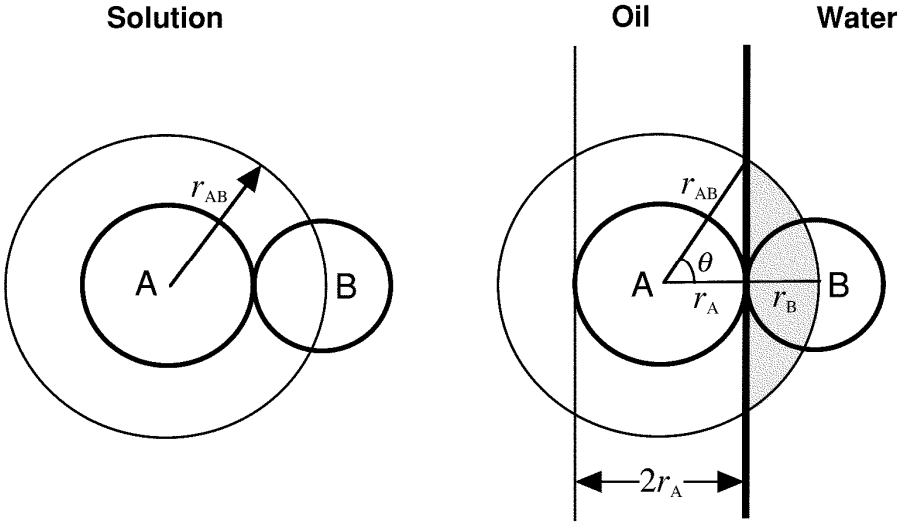

Figure 6.1. Models for diffusion-controlled bimolecular reactions (a) in homogeneous solution and (b) at an O/W interface. For details, see the text.

where L is Avogadro's number. Using equations (6.5) and (6.7) with a relation:

$$\frac{dn_B}{dt} = V\,\frac{d[B]}{dt} \tag{6.8}$$

we can obtain

$$-\frac{\mathrm{d[B]}}{\mathrm{d}t} = 4\pi r_{\mathrm{AB}} D_{\mathrm{AB}} L[\mathrm{A}][\mathrm{B}] \tag{6.9}$$

Comparison of equation (6.9) and equation (6.6) finally yields an expression for the diffusion-controlled (i.e., maximum) rate constant:

$$k_{\mathrm{D,hom}} = 4\pi r_{\mathrm{AB}} D_{\mathrm{AB}} L \tag{6.10}$$

This equation was first proposed by Smoluchowski [4] for the calculation of the rate of coagulation of colloid suspensions.

6.3 Extension to a bimolecular reaction at the O/W interface

Let us extend the diffusion-controlled rate theory in homogeneous solution to a bimolecular reaction at the O/W interface. Figure 6.1 shows models for diffusion-controlled bimolecular reactions (a) in homogeneous solution and (b) at an O/W interface. In homogeneous solution, molecule B diffuses from all directions onto the spherical surface of the radius of r_{AB} around the center of A. At the O/W interface, however, molecule B in the W phase can access molecule A staying in contact with the O-phase side of the interface, only from the W-phase side. It is here assumed that molecule B reacts with molecule A just when it reaches the "reaction surface", i.e., the part of the spherical surface of the radius of r_{AB} around the center of A which bulges out to the W phase (see the shadow part in Figure 6.1b). If the O/W interface is "rigid", this assumption is not valid, because molecule B can access the reaction surface only from the vertical direction. However, since our aim is to estimate a realizable maximum value of the rate constant, we make the reaction surface as wide as possible, upon considering the "softness" of the O/W interface. The diffusion-controlled molar flux of B toward the reaction surface may be obtained approximately by analogy of equation (6.3) as

$$j_{\mathrm{B,het}}' = 4\pi r_{\mathrm{AB}} \xi D_{\mathrm{B}}^{\mathrm{W}} [\mathrm{B}] \tag{6.11}$$

Here, ξ is defined as the ratio of the reaction surface to the surface area of the sphere with the radius of r_{AB}, i.e.,

$$\xi = \frac{2\pi r_{\mathrm{AB}}{}^2 (1 - \cos\theta)}{4\pi r_{\mathrm{AB}}{}^2} = \frac{1 - \cos\theta}{2} \tag{6.12}$$

where θ is the angle shown in Figure 6.1b and given by

$$\theta = \cos^{-1}\left(\frac{r_{\mathrm{A}}}{r_{\mathrm{AB}}}\right) = \cos^{-1}\left(\frac{r_{\mathrm{A}}}{r_{\mathrm{A}} + r_{\mathrm{B}}}\right) \tag{6.13}$$

It should also be noted in equation (6.11) that $D_{\mathrm{B}}^{\mathrm{W}}$ represents not the relative but the absolute diffusion coefficient of B in the W phase (cf. equation (6.3)). In this theory, molecule A is regarded as staying at the interface for a reaction with B.

Next, let us estimate the interfacial reaction rate in an area of S (cm^2). The total flux

of B to reach all A molecules in the area of S is expressed using the number of A in S, N'(A):

$$j_{\mathrm{B,het}} = N'(\mathrm{A})\, j_{\mathrm{B,het}}' \tag{6.14}$$

Here, it is assumed that molecules A existing at the interface are fully isolated from each other so that diffusion layers of B are not overlapped. Since the $j_{\mathrm{B,het}}$ given by equation (6.14) is regarded as the diffusion-controlled rate, we obtain from equations (6.11) and (6.14):

$$\begin{aligned}(\text{diffusion-controlled rate}) &= \frac{-\,\mathrm{d}n_{\mathrm{B}}'}{\mathrm{d}t} = j_{\mathrm{B,het}} \\ &= 4\pi r_{\mathrm{AB}} \xi D_{\mathrm{B}}^{\mathrm{W}} [\mathrm{B}] N'(\mathrm{A})\end{aligned} \tag{6.15}$$

where n_{B}' is the molar number (mol) of B existing in the area of S.

The rate equation for a bimolecular second-order reaction at an O/W interface is written as

$$\frac{1}{S}\left(-\frac{\mathrm{d}n_{\mathrm{B}}'}{\mathrm{d}t}\right) = k_{\mathrm{het}}[\mathrm{A}][\mathrm{B}] \tag{6.16}$$

where k_{het} ($\mathrm{cm}^4\ \mathrm{mol}^{-1}\ \mathrm{s}^{-1}$) is the second-order rate constant for a unit area, being different in dimension than k_{hom} ($\mathrm{cm}^3\ \mathrm{mol}^{-1}\ \mathrm{s}^{-1}$) in equation (6.6).

Although the estimate of N'(A) in equation (6.14) has a rather large uncertainty, we assume that N'(A) is the number of A existing in an interfacial layer of a thickness of $2r_{\mathrm{A}}$ (see Figure 6.1b):

$$N'(\mathrm{A}) = 2r_{\mathrm{A}} S[\mathrm{A}]L \tag{6.17}$$

Here, the concentration of A is assumed to be the same as the bulk concentration, [A], at any point in the layer. Although this assumption may lead to some overestimation of N'(A), the combination of equations (6.15)–(6.17) yields an expression of the diffusion-controlled rate constant:

$$k_{\mathrm{D,het}} = 8\pi r_{\mathrm{A}} r_{\mathrm{AB}} \xi D_{\mathrm{B}}^{\mathrm{W}} L \tag{6.18}$$

This equation has been derived by assuming that the reaction rate is limited by the diffusion of B in W. Reversely, if the diffusion of A in O is the rate-determining step, we can obtain the following equation:

$$k_{\mathrm{D,het}} = 8\pi r_{\mathrm{B}} r_{\mathrm{AB}} \zeta D_{\mathrm{A}}^{\mathrm{O}} L \tag{6.19}$$

where $D_{\mathrm{A}}^{\mathrm{O}}$ is the diffusion coefficient of A in O, and ζ is given by

$$\zeta = \frac{2\pi r_{\mathrm{AB}}{}^2 (1-\cos\omega)}{4\pi r_{\mathrm{AB}}{}^2} = \frac{1-\cos\omega}{2} \tag{6.20}$$

with

$$\omega = \cos^{-1}\left(\frac{r_B}{r_{AB}}\right) = \cos^{-1}\left(\frac{r_B}{r_A + r_B}\right) \tag{6.21}$$

6.4 Overall rate constant

The diffusion-controlled rate constant thus estimated is related to the initial step of an ET reaction at an O/W interface:

$$\text{A (O)} + \text{B (W)} \underset{k_{uni}}{\overset{\text{diffusion } k_{D,het}}{\rightleftharpoons}} \text{A}\cdots\text{B} \xrightarrow{\text{ET } k_{ET}} \text{products} \tag{6.22}$$

where A···B represents the encounter complex of A and B, which is formed at the interface; k_{uni} is the dissociation rate constant of A···B; and k_{ET} is the first-order heterogeneous rate constant of the intramolecular ET, which could be estimated using the Marcus theory. On the analogy of a bimolecular reaction in homogeneous solution [4,5], the steady-state approximation method is here used to obtain an expression of the overall rate constant (k):

$$k = \frac{k_{D,hom}k_{ET}}{k_{ET} + k_{uni}} = \frac{k_{D,hom}}{1 + (k_{uni} \,/\, k_{ET})} \tag{6.23}$$

As is evident from this equation, $k_{D,het}$ is the attainable maximum value of k; when $k_{ET} \gg k_{uni}$, the overall reaction becomes diffusion-controlled, i.e., $k = k_{D,het}$. For slow reactions where $k_{ET} \ll k_{uni}$, the first step in the reaction scheme (6.22) is in equilibrium, i.e.,

$$k = Kk_{ET} \tag{6.24}$$

with $K = k_{D,het}/k_{uni}$. Further analysis based on the present scheme is in progress.

I would like to add that in the theory described above, as well as previous theoretical treatments of ET rate constants, the effect of the molecular-level diffusion process is dealt with by including it in the overall (i.e., observed) rate constant. However, a somewhat different approach to this problem has been advanced by Senda [6], who proposed a model which includes the bimolecular-reaction effect in the voltammetric theory of ET at the O/W interface.

6.5 Theoretical estimation of the rate constant

Based on the above theoretical scheme, the overall rate constant can be estimated as follows:

In a similar treatment to that for a homogeneous reaction [4,5], k_{uni} may be related to $k_{D,het}$ as

$$k_{uni} = \left(\frac{10^{-3}}{L}\right)\frac{k_{D,het}}{\Delta V} \tag{6.25}$$

where ΔV (cm^3) is the volume of the encounter complex and can be approximated to be $(4/3)\pi r_{AB}{}^3$. The multiplier in equation (6.25), $(10^{-3}/L)$, has been introduced by considering the units of $k_{D,het}$ (M^{-1} cm s^{-1}) and k_{uni} (cm s^{-1}).

In the analogy of the transition state (activated complex) theory for electrode reactions [7–9], the first-order rate constant (k_{ET}) for the heterogeneous ET at the O/W interface is expressed by

$$k_{ET} = \kappa Z_{het} \exp\left(-\frac{\Delta G^{\ddagger}}{RT}\right) \tag{6.26}$$

where κ is the transmission coefficient ($\kappa = 1$ for a perfect adiabatic ET) and Z_{het} is the collision number of (hypothetical) uncharged species with unit area of an interface, usually being taken to be ~10^4 cm s^{-1}. The pre-exponential factor (κZ_{het}) for the first-order k_{ET} given by equation (6.26) is different from that for the second-order rate constant derived by Marcus (see equation (1.9) or (1.10)), however the free energy of activation $\Delta G^{\ddagger}$ could be estimated with the help of the Marcus theory [10–14]:

$$\Delta G^{\ddagger} = w^{r} + \frac{\lambda}{4}\left(1 + \frac{\Delta G^{\circ} + w^{p} - w^{r}}{\lambda}\right)^2 \tag{6.27}$$

Here, w_r and w_p are the work terms for bringing the reactants from d (the distance between two reactants) = ∞ and for removing the products to $d = \infty$, respectively; λ is given by the sum of the outer-sphere (λ_o) and inner-sphere (λ_i) reorganization energies; ΔG° is the standard free energy of reaction. Because ΔG° is expressed by the interfacial potential difference ($\Delta_O^W\phi$) as $\Delta G^{\circ} = -nF(\Delta_O^W\phi - \Delta_O^W\phi^{\circ})$ (n, the number of electrons; $\Delta_O^W\phi^{\circ}$, the standard redox potential), equation (6.27) is rewritten as

$$\Delta G^{\ddagger} = \Delta G^{\circ\ddagger} - \frac{1}{2}nF\left(\Delta_O^W\phi - \Delta_O^W\phi^{\circ}\right) + \frac{1}{4\lambda}\left\{n^2F^2\left(\Delta_O^W\phi - \Delta_O^W\phi^{\circ}\right)^2 - 2nF\left(\Delta_O^W\phi - \Delta_O^W\phi^{\circ}\right)\left(w^{p} - w^{r}\right)\right\} \tag{6.28}$$

where $\Delta G^{\circ\ddagger}$ is the activation free energy at $\Delta_O^W\phi = \Delta_O^W\phi^{\circ}$. If the working terms are negligible, equation (6.28) can be reduced to

$$\Delta G^{\ddagger} = \Delta G^{\circ\ddagger} - \frac{nF}{2}\left(\Delta_O^W\phi - \Delta_O^W\phi^{\circ}\right) + \frac{n^2F^2}{4\lambda}\left(\Delta_O^W\phi - \Delta_O^W\phi^{\circ}\right)^2 \tag{6.29}$$

with $\Delta G^{\circ\ddagger} = \lambda/4$ (cf. equation (6.27)). Substituting equation (6.29) to equation (6.26) yields

$$\ln k_{ET} = \ln(\kappa Z_{het}) - \frac{\lambda}{4RT} + \frac{nF}{2RT}\left(\Delta_O^W\phi - \Delta_O^W\phi^{\circ}\right) - \frac{n^2F^2}{4RT\lambda}\left(\Delta_O^W\phi - \Delta_O^W\phi^{\circ}\right)^2 \tag{6.30}$$

Thus, the plot of the logarithm of k_{ET} against $\Delta G^{\circ} = -nF(\Delta_O^W\phi - \Delta_O^W\phi^{\circ})$ should give a parabola with the apex at $\Delta G^{\circ} = \lambda$.

The values of $k_{D,het}$, k_{uni}, and k_{ET} thus estimated allow for the calculation of the overall rate constant k using equation (6.23).

6.6 Application to experimental data

Recently, Bard's group [15,16] reported the driving force dependence of rate constants for heterogeneous ETs between $ZnPor^+$ and aqueous reductants, on the basis of SECM measurements. In Figure 1.3 (in chapter 1), the second-order rate constant (k_{12}) is plotted against the driving force $\Delta E_{1/2}$ (= $\Delta G°/nF$; here, n = 1). It has then been claimed that the plot shows a trend in accordance with the Marcus prediction based on equation (6.30). However, it should be noted that the plot includes the data obtained with three different organic solvents and with some different aqueous reductants. Also note that the parabolic line is drawn using equation (6.30), i.e., by neglecting the work terms. Furthermore, the above-described diffusion process is tacitly assumed to be very fast compared with the ET process. In the following, the values of $k_{D,het}$ and k_{uni} for the present ET system are calculated and their contribution to the overall rate constant is evaluated.

Assuming that the diffusion of $ZnPor^+$ (= **A**) in O is the rate-determining step, we use equation (6.19) with parameters (r_A = 8 Å; r_B = 5 Å; $D_A^O = 2.5 \times 10^{-6}$ cm^2 s^{-1}) to obtain $k_{D,het}$ = 76 M^{-1} cm s^{-1}. The value of k_{uni} is estimated as 14 M^{-1} cm s^{-1} by using equation (6.25) with $r_{AB} = r_A + r_B$ = 13 Å and with ΔV (= $(4/3)\pi r_{AB}^3$) = 9.2×10^{-21} cm^3. The values

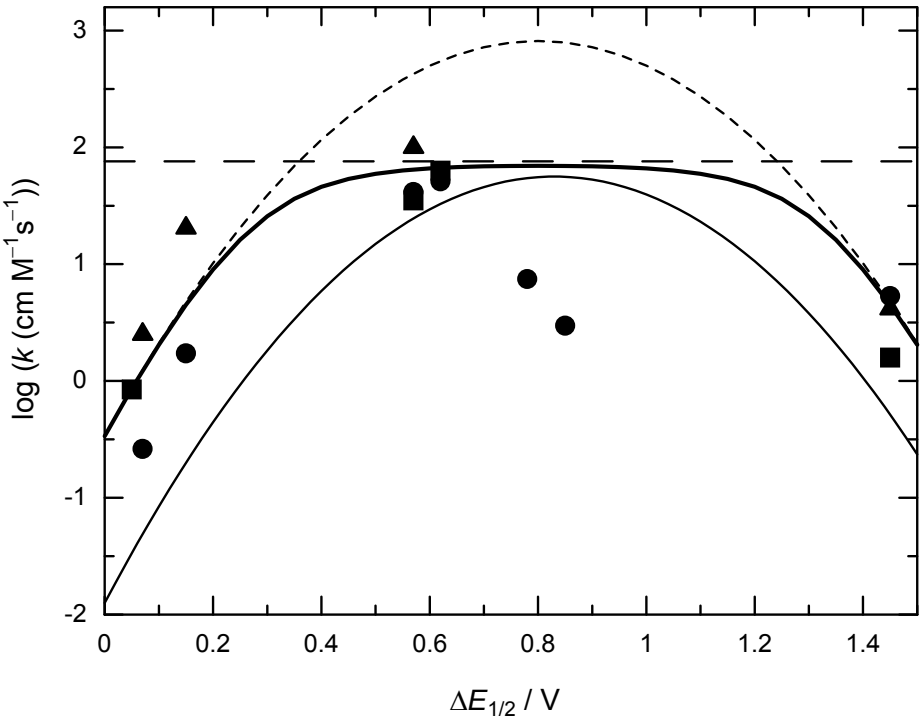

Figure 6.2. Driving force dependence of the second-order rate constant (k) for heterogeneous ETs between $ZnPor^+$ and aqueous reductants. Thick solid line: from equation (6.23) with λ (= 0.8 eV) and κZ_{het} (= 1.5×10^2 cm s^{-1}). Thin solid line: the theoretical curve by Bard et al. [12]. The plots show the experimental data for the benzonitrile/W (●), benzene/W (■), and DCE/W (▲) interfaces. For further details, see the text.

of $k_{D,het}$ and k_{uni} are employed to calculate the overall rate constant k using equation (6.23). The calculation result is shown in Figure 6.2. The thick solid line represents the driving force ($\Delta E_{1/2}$) dependence of k, which has been drawn so as to fit the experimental data [16]; the values of λ (= 0.8 eV) and κZ_{het} (= 1.5×10^2 cm s^{-1} [17]) have been used as the fitting parameters. It should here be noted that the overall rate constant is restricted by the diffusion-controlled rate constant indicated by the broken straight line (cf. the broken curve representing the Kk_{ET} value which corresponds to the k value for $k_{ET} \ll k_{uni}$). In Figure 6.2 is also shown the theoretical curve (thin solid line) by Bard et al. [16], who did not consider the contribution of the diffusion process. Neither their nor our theoretical curve, however, has an absolute advantage in fitting the experimental data showing considerable scatter. Further experimental verification is desirable.

References and note

[1] G. Geblewicz and D.J. Schiffrin, J. Electroanal. Chem. 244 (1988) 27.

[2] V.J. Cunnane, D.J. Schiffrin, C. Beltran, G. Geblewicz, and T. Solomon, J. Electroanal. Chem. 247 (1988) 203.

[3] Y. Cheng and D.J. Schiffrin, J. Electroanal. Chem. 314 (1991) 153.

[4] M. von Smoluchowski, Z. Phys. Chem. 92 (1917) 129.

[5] P. Debye, Trans. Electrochem. Soc. 82 (1942) 265.

[6] G.K. Vemulapalli; *Physical Chemistry*; Prentice-Hall, Englewood Cliffs, NJ, 1993.

[4] D. Rehm and A. Weller, Israel J. Chem. 8 (1970) 259.

[5] J.I. Steinfeld, J.S. Francisco, and W.L. Hase; *Chemical Kinetics and Dynamics*; Prentice-Hall, Englewood Cliffs, 1989; Chapter 4.

[6] M. Senda, Rev. Polarogr. (Kyoto) 49 (2003) 31.

[7] R. A. Marcus, Ann. Rev. Phys. Chem. 15 (1964) 155.

[8] R. A. Marcus, J. Chem. Phys. 43 (1965) 679.

[9] J. M. Hale; *Reactions of Molecules at Electrodes*; Ed. N. S. Hush; Wiley-Interscience, London, 1971; pp 229–257.

[10] R. A. Marcus, J. Phys. Chem. 94 (1990) 1050.

[11] R. A. Marcus, J. Phys. Chem. 94 (1990) 4152.

[12] R. A. Marcus, J. Phys. Chem. 94 (1990) 7742 (corrections).

[13] R. A. Marcus, J. Phys. Chem. 95 (1991) 2010.

[14] R. A. Marcus, J. Phys. Chem. 99 (1995) 5742 (corrections).

[15] A. L. Barker, P. R. Unwin, S. Amemiya, J. Zhou, and A. J. Bard, J. Phys. Chem. B 103 (1999) 7260.

[16] Z. Ding, B. M. Quinn, and A. J. Bard, J. Phys. Chem. B 105 (2001) 6367.

[17] This value is about two order lower than the theoretically expected value of ~10^4 cm s^{-1} (= κZ_{het} with $\kappa = 1$).

Summary

In this thesis the author has introduced some new methodologies for clarification of the reaction mechanisms of ETs at O/W interfaces. The new methodologies include the ECSOW system, the microflow cell, digital simulation of cyclic voltammograms, etc. The utilities of these methods have been demonstrated by clarifying the mechanisms of two typical ET reactions which include the Fc–$Fe(CN)_6^{3-}$ system and the Q–AH_2 system.

In the first chapter, the history of the study of ET at the O/W interface is reviewed and the basic theoretical aspects are presented.

In the second chapter, the ECSOW system has been developed as a new electrochemical device to distinguish heterogeneous and homogeneous ET processes at O/W interfaces. A comparison of cyclic voltammograms obtained with the ECSOW system and with the corresponding O/W interface gives invaluable information on the reaction mechanism of ET at the O/W interface. This has been shown by the application to the Q–AH_2 system (chapter 4) and the Fc–$Fe(CN)_6^{3-}$ system (chapter 5).

Another novel device, i.e., the microflow electrolytic cell, has been developed in chapter 3. This microflow cell is available not only for absolute quantitative analysis of ions but also for determination of the number of electrons required for an interfacial ET reaction, as shown in the subsequent chapter.

In chapter 4, the Q–AH_2 system as a biomimetic ET system has been studied using several techniques including cyclic voltammetry, polarography with an ascending water electrode, coulometry with a microflow cell, the ECSOW system, etc. The results have shown that two electrons participate in the oxidation of one molecule of AH_2 by Q and that the IT of the semiquinone radical anion ($Q^{\bullet -}$) as the reaction product is responsible for the current flowing through the interface. Based on these findings, an IT mechanism as shown in Figure 4.10 could be proposed. The validity of this mechanism has also been supported by a spectrophotometric detection of $Q^{\bullet -}$ without electrochemical control.

In chapter 5, the Fc–$Fe(CN)_6^{3-}$ system has been studied in some detail. It has been revealed that the concentration dependence of the cyclic voltammogram observed with the O/W interface has different features from that obtained with the ECSOW system, especially for lower Fc concentrations. This comparison has allowed us to identify the existence of a kinetically controlled process for the O/W interface. The kinetic data have been analyzed by means of a digital simulation technique. Then, it has been shown that the reaction mechanism can be elucidated in terms of the IT mechanism shown in Figure 5.5. Furthermore, the validity of the mechanism has been confirmed by spectrophotometric detections of Fc^+ in the W phase with and without electrochemical control.

In the above two ET systems, it has been showed that homogeneous ET (i.e., IT

mechanism) is easier to occur than heterogeneous ET (i.e., ET mechanism). One of the reasons is in the difference in the volume of reaction field between the ET and IT mechanisms. In the ET mechanism, the reaction field should be restricted to an interfacial layer as thin as several Angstroms, whereas in the IT mechanism, the reaction layer in the W phase is much thicker (sub-mm). Such a large difference in the volume of reaction field leads to the most crucial advantage of the IT mechanism.

Nevertheless, it can be expected that the use of an extremely hydrophobic redox species in the O phase makes the heterogeneous ET occur more favorably. In chapter 6, the rate of the heterogeneous ET at the O/W interface has been discussed theoretically. The diffusion controlled rate constant ($k_{D,het}$) of ET at the O/W interface has been derived by the analogy of the Smoluchowski–Debye theory for a bimolecular reaction in a homogeneous medium. It has been claimed that if the heterogeneous ET is very fast, the overall ET process should be limited by diffusion, i.e., the overall rate constant, $k = k_{D,het}$.

In recent years, many efforts, including this study, have been focused on the kinetics of ET at O/W interfaces. However, the experiment seems to have not caught up with the theory. The experimental data is still insufficient for the verification of the Marcus theory. Further experimental approaches as well as theoretical advances seem to be needed.

Acknowledgements

The author wishes to express his sincere gratitude to Dr. Toshiyuki Osakai of Kobe University for his appropriate guidance and encouragement throughout not only this study but also author's life. The author also wishes to express his sincere thanks to all members of Osakai laboratory (both present and past) for their helpful assistance and encouragement.

The author is grateful to Dr. Sadayuki Himeno, Professor of Kobe University, for his appropriate advice. The author is also grateful to Dr. Noriyuki Sotani, and Dr. Keisuke Tominaga for their valuable suggestion and discussion.

Finally, the author would like to express his cordial gratitude to his family for their encouragement.

List of publications

Publications Relevant to the present study

1. Toshiyuki Osakai, Naoki Akagi, Hiroki Hotta, Shigeo Sawada, Mechanistic study of the oxidation of L-ascorbic acid by chloranil at the nitrobenzene | water interface, J. Electroanal. Chem., 490 (2000) 85.

2. Hiroki Hotta, Naoki Akagi, Takayasu Sugihara, Seiko Ichikawa, and Toshiyuki Osakai, Electron-Conductor Separating Oil-Water (ECSOW) system: a new strategy for characterizing electron-transfer processes at the Oil/Water interface, Electrochem. Commun., 4 (2002) 472.

3. Shigeo Sawada, Masaru Taguma, Takashi Kimoto, Hiroki Hotta, and Toshiyuki Osakai, Complete electrolysis using a microflow cell with an Oil/Water interface, Anal. Chem., 74 (2002) 1177.

4. Shigeo, Aoyagi, Masaaki Matsudaira, Takahiro Suzuki, Hajime Katano, Shigeo Sawada, Hiroki Hotta, Seiko Ichikawa, Takayasu Sugihara, and Toshiyuki Osakai, Performance Evaluation of the Four-Electrode Type Measurement System for Ion-Transfer Voltammetry, Electrochemistry, 70 (2002) 329.

5. Hiroki Hotta, and Toshiyuki Osakai, Mechanistic Study of Electron Transfer at the Oil/Water Interface, Rev. Polarogr., 49 (2003) 15. (Review)

6. Hiroki Hotta, Seiko Ichikawa, Takayasu, Sugihara, and Toshiyuki Osakai, Clarification of the mechanism of the interfacial electron-transfer reaction between ferrocene and hexacyanoferrate(III), J. Phys. Chem. B, in press.

7. Takayasu Sugihara, Hiroki Hotta, and Toshiyuki Osakai, Mechanistic Study of the Electron Transfer of L-Ascorbic Acid at the Oil/Water Interface by Digital Simulation of Cyclic Voltammograms, Bunseki Kagaku, 52 (2003) in press.

Chapter 1 is described in reference 5.
Chapter 2 is described in reference 2.
Chapter 3 is described in reference 3.
Chapter 4 is described in reference 1.
Chapter 5 is described in reference 6.

Related papers

1. Hiroki Hotta, Harumi Sakamoto, Satomi Nagano, Toshiyuki Osakai, Yoshio Tsujino, Unusually large numbers of electrons for the oxidation of polyphenolic antioxidants, Biochim. Biophys. Acta (general subject), 1526 (2001) 159.

2. Jie Ding, Hiroki Hotta, Toshiyuki Osakai, Ion transfer of heteropolytungstate anions at the nitrobenzene | water interface and its relevance to their antiviral activities, J. Electroanal. Chem., 505 (2001) 133.

3. Junko Koyama, Izumi Morita, Kiyoshi Tagahara, Toshiyuki Osakai, Hiroki Hotta, Mou Xiao Yang, Teruo Mukainaka, Hoyoku Nishino, and Harukuni Tokuda, Correlation with redox potentials and inhibitory effects on Epstein-Barr Virus activation of azaanthraquinones, Chem. Pharm. Bull., 49 (2001) 1214.

4. Hiroki Hotta, Masashi Ueda, Satomi Nagano, Yoshio Tsujino, Junko Koyama, and Toshiyuki Osakai, Mechanistic study of the oxidation of caffeic acid by digital simulation of cyclic voltammograms, Anal. Biochem. 303 (2002) 66.

5. Hiroki Hotta, Satomi Nagano, Masashi Ueda, Yoshio Tsujino, Junko Koyama, and Toshiyuki Osakai, Higher radical scavenging activities of polyphenolic antioxidants can be ascribed to chemical reactions following their oxidation, Biochim. Biophys. Acta (general subject) 1572 (2002) 123.